Order Number 9521308

New magnetically uniaxial phases in the Sm, Fe binary system

Rani, Raj, Ph.D.

City University of New York, 1995

U·M·I
300 N. Zeeb Rd.
Ann Arbor, MI 48106

NEW MAGNETICALLY UNIAXIAL PHASES IN THE Sm, Fe BINARY SYSTEM

by

RAJ RANI

A dissertation submitted to the Graduate Faculty in Physics in partial fulfillment of the requirements for the degree of Doctor of Philosophy, The City University of New York.

1995

This manuscript has been read and accepted for the Graduate Faculty in Physics in satisfaction of the dissertation requirement for the degree of Doctor of Philosophy.

12/16/94
Date

Fred J. Cadieu
Chairman of Examining Committee

1/17/95
Date

Joseph B. Kriegh
Executive Officer

Fred J. Cadieu
Professor F. J. Cadieu

Jacob Neuberger
Professor J. Neuberger

L. A. Ferrari
Professor L. A. Ferrari

Professor V. Sahni

M. Miksic
Professor M. Miksic

Supervisory Committee

THE CITY UNIVERSITY OF NEW YORK

ABSTRACT

NEW MAGNETICALLY UNIAXIAL PHASES IN THE Sm, Fe BINARY SYSTEM

by

Raj Rani

Adviser: Professor F. J. Cadieu

For the first time, films magnets of binary Sm_5Fe_{17}, and $SmFe_{12}$, magnetically uniaxial phases have been sputter synthesized without any addition of a phase stabilizing third element. Perpendicular to the film plane, the room temperature saturation magnetization for highly (002) aligned film samples of $SmFe_{12}$ phase were measured to be 14.3 ± 0.5 kG and the estimated anisotropy field was 130 ± 10 kOe. X-ray diffraction studies, hysterisis loop measurements, composition measurements, and projection of moment calculations allowed to identify the $SmFe_{12}$ phase as $ThMn_{12}$ type tetragonal structure with a = 8.438 ± 0.006 Å, and c = 4.805 ± 0.006 Å. Film samples of this phase were synthesized by depositing the material on preheated substrates. For Sm_5Fe_{17} phase, the material was first deposited in amorphous form and subsequently crystallized. Sm_5Fe_{17} film samples were synthesized with record high room temperature coercivity of 14.1 kOe for the two element Sm, Fe system. On nitriding Sm_2Fe_{17}, profound changes in magnetic properties have occurred, room temperature inplane coercivity rose from 0.75 kOe to 23 kOe. The $Sm_2Fe_{17}N_x$ compound retained its parent structure with the cell volume increase of ≈ 7 %. The room temperature coercivity as a function of the Sm concentration reached a maximum value of ≈ 23 kOe at a slightly richer than stoichiometric Sm

High anisotropy (002) textured film samples of $Pr(Fe_{12-y-z},Co_y,Mo_z)N_x$, where y = 0-2.5, and z = 0.4-1.0 compounds were synthesized with so far the highest coercivity of 9.4 kOe. X-ray diffraction data showed that the $ThMn_{12}$ type tetragonal structure was retained with a saturation increase in the cell volume over the first 15 minutes of nitriding time at 750 K. The coercivity reached a maximum for nitriding time of 25 minutes of nitriding time. For $Pr_{1.04}Fe_{10.36}$ $Co_{1.16}Mo_{0.44}N_x$ sample measured at 293 K, perpendicular to the film plane saturation magnetization, coercivity, and energy product were 11.6 ± 0.5 kG, 9.4 kOe, and 23.6 Million Gauss-Orested, respectively. These film magnets find their applications in storage media, microwave devices, and small film-scale permanent magnet geometries, etc.

ACKNOWLEDGMENTS

I express my deep sense of gratitude and indebtedness to Professor F. J. Cadieu for his generous support, patient and painstaking guidance, timely advice, and encouragement which were indispensable for the successful accomplishment of this work. Invaluable help rendered by Research Associate Dr. H. Hegde in various stages of this thesis work is gratefully acknowledged. I am thankful to a former colleague Dr. K. Chen, and to my fellow researchers Mr. A. Navarathna, and Mr. P. Samarsekara for their co-operation in the laboratory.

I am thankful to Professor L. A. Ferrari, Professor M. Miksic, Professor V. Sahni, and Professor J. Neuberger, members of the Supervisory Committee, for their suggestions.

It is my pleasure to extend my thanks to all the members of the faculty and staff, and colleagues at Physics Department of Queens college. I am sincerely grateful to Professor J. Neuberger for his encouragement throughout my PhD program. My special thanks to Mrs. Susan Wasserman, and Mrs. Shirley Allen for their wholehearted assistance.

I am extremely indebted to my parents and family members for providing me the most needed moral support, congenial atmosphere, and encouragement during the entire course of my educational career.

My thesis is part of the research program, studying the magnetic properties of rare earth transition metal permanent film magnets, principally funded by grants awarded to Professor Cadieu. The early stages of this work was supported by U. S. Department of Energy Grant No. DE-FG02-86-ER45265. The later stages of this work was supported by U. S. Army Research Office Grant No. DAAH04-94-G-0079.

Raj Rani

(RAJ RANI)

TABLE OF CONTENTS

LIST OF TABLES

LIST OF FIGURES

CHAPTER 1

INTRODUCTION

Widespread interest in RE-TM intermetallics kindled from 1966, when Hoffer and Strnat reported that YCo_5 had an anisotropy constant of 5.5×10^7 ergs/cm^3, by far the largest value for any material then known;[1, 2] by then, it was understood that a good permanent magnet must have a large saturation magnetization, high Curie temperature, and large magnetic anisotropy for high coercivity. Transition metals, TM's, namely, Fe and Co have large magnetic moments [$\mu(Fe) = 2.1\ \mu_B$, $\mu(Co) = 1.56\ \mu_B$], and high Curie temperatures [$T_c(Fe) = 1043$ K, $T_c(Co) = 1388$ K] but very low coercivities. On the other hand, many Rare Earth metals, RE's, have large magnetic moment and single ion anisotropy but very low Curie temperature. High anisotropy of the light rare earth sublattice and its ferromagnetic coupling to transition metal sublattice provides the bulk magnetization. The direction of easy magnetization in the RE-TM compounds is determined by the competition between the TM sublattice anisotropy and the RE sublattice anisotropy. Researchers have been trying to optimize the magnetic properties of these intermetallics to fabricate high quality permanent magnets possessing uniaxial anisotropy. In uniaxial compounds, the easy magnetization axis points parallel to the crystallographic c-axis. As a result, a large applied field is required to rotate the magnetization vector away from the c-axis. In easy plane materials, the magnetic easy axis lies in the plane perpendicular to crystallographic c-axis, and the magnetization

vector can easily be rotated in the basal plane.

Intermetallic compounds of Fe combining a high value of saturation magnetization and reasonably high Curie temperature with a large easy axis anisotropy are extremely rare. On the other hand the Sm, Co binary system is known to have many stable compounds such as $SmCo_2$, $SmCo_3$, $SmCo_5$, Sm_2Co_{17}, and $SmCo_{12}$, etc.[3] On the Co rich side, $SmCo_5$ is found to be very useful as a permanent magnet due to its high saturation moment, high anisotropy field, and considerably high Curie temperature. Sm_2Co_{17} has a high saturation moment and high Curie temperature as compared to $SmCo_5$ but low magnetocrystalline anisotropy. In pure form Sm_2Co_{17} cannot be fabricated into a permanent magnet because of its low coercivity ${}_iH_c$ = 2 kOe. A compromise between the high saturation magnetization of Sm_2Co_{17} and the high coercivity of $SmCo_5$ has been achieved for $SmCo_{7.5}$ type compounds. The precipitation results in a cellular arrangement of Sm_2Co_{17} based phase surrounded by $SmCo_5$ type phase at the grain boundaries. Coercivities greater than 12 kOe were reported for TDK $Sm(CoFeCuZr)_{7.5}$, and the high coercivity was attributed to domain wall pinning.[4]

Curie temperatures of iron compounds are substantially lower than those of the corresponding cobalt compounds. There is no iron counterpart of technologically significant $SmCo_5$ system. Sm_2Fe_{17} is an easy plane material with a fairly low Curie temperature of 385 K, thus rendering itself useless as a permanent magnet material. Low Curie temperatures of RE_2Fe_{17} compounds have often been attributed to short Fe-Fe

distance as well as to the negative exchange interaction among the Fe atoms. It presumably is due to the high degree of localization of Fe moment as compared to the Co moment. For RE-Fe compounds, the magnetic properties are mainly determined by Fe-Fe inter atomic distances and the number of nearest neighbors whereas for RE-Co compounds, the magnetic properties are determined by the conduction electron transfer from the RE to the 3d band of cobalt. The tetragonal ternary compound $Sm_2Fe_{14}B$, with specific lattice sites for boron, is also an easy plane material whereas $Nd_2Fe_{14}B$ has extremely good magnetic properties with room temperature energy product $(BH)_{max}$ = 45 Million Gauss-Orested, MG-Oe, even though its Curie temperature is 573 K.[5, 6] However, highly oriented sputter synthesized film samples of $Nd(Fe,Co,Mo)_{12}N$ exhibited highest room temperature energy product of 46.3 MG-Oe, perpendicular to the film plane.[7, 8]

Film magnets have been synthesized through R. F. glow discharge deposition on the polycrystalline Al_2O_3 substrates. Two distinct modes of crystallization, namely, direct crystallization and subsequent crystallization were employed. In the first approach, atoms are deposited onto a heated substrate whereas in the later method atoms are deposited onto a water-cooled substrate and later on the amorphous deposits subjected to heat treatment. In the direct crystallization process, thermallization of sputtering gas atoms play an important role.[9, 10] The deposition is carried out at a relatively high sputtering gas pressure so that the kinetic energy of the deposition atoms is greatly reduced as they arrive at the substrate to prevent the disruptive growth.

Direct crystallization synthesis allows highly textured films with high remanent magnetization, whereas the subsequent crystallization permits only the synthesis of magnetically isotropic microstructures often permitting high coercivities with random alignment of easy axis of the crystallite easy axes.

In the last decade, intensive research and technological development of $R_2Fe_{14}B$ based magnets has occurred.[5, 11] In parallel, $RFe_{12-x}M_x$ series, where R = Sm, Pr, Nd, and M = Ti, V, Mo, etc. have been investigated in the film form as well as in the bulk.[12, 15] The objective of this thesis work is also aimed at the search for a new Fe-based compound in the pure Sm, Fe system exhibiting uniaxial properties.

Before this work, there was no compound synthesized with just Fe, and Sm alone that exhibited uniaxial magnetic properties. This thesis is directed towards the film synthesis of new phases, namely $SmFe_{12}$, $Sm_2Fe_{17}N_x$, and Sm_5Fe_{17} observed in the pure Sm, Fe system. The phases observed in the synthesized films are new and different from those evidenced in the x-ray pattern for the targets. To substantiate the proof for the existence of $ThMn_{12}$ type phase in the pure Sm, Fe system, the magnetic properties, and crystal structures have been correlated through a "projection of moments model". At one end of the continuum, a systematic research has been conducted to establish a spectrum of sputter conditions for the formation of new phases. At the other extreme, for each phase, the magnetic properties were optimized with a thoughtful variation of control parameters such as sputtering gas pressure, substrate temperature, and deposition rate.

An attempt has been made to explain some of the observed facts such as change in the crystalline anisotropy on nitriding. The magnetic properties and crystal structure have been correlated to the sputter deposition changes.

This thesis is organized as follows: Chapter 2 provides an overall view of fundamental aspects such as crystal structure, magnetization, and crystal anisotropy in RE-TM systems. Chapter 3 reveals all the experimental details from the film synthesis procedure to the microstructure of the film magnets. Investigations on the synthesis of a new Sm, Fe binary phase having uniaxial magnetic properties and tetragonal $ThMn_{12}$-type structure is carried out in chapter 4. Chapter 5 is devoted to interstitial modification of the Sm_2Fe_{17} phase in the film form, with special emphasis on change in magnetic properties on nitrogen absorption. Chapter 6 covers film synthesis of another new magnetic phase namely the Sm_5Fe_{17}, and includes a discussion of crystallization time effects on Sm_5Fe_{17} phase. Chapter 7 mainly discusses the highly (002) aligned $Pr(Fe, Mo)_{12}$ film samples with a focus on the minimum nitriding time requirements. Chapter 8 furnishes the summarized report of this thesis work.

CHAPTER 2

INTERMETALLIC COMPOUNDS OF RARE-EARTH TRANSITION METAL SYSTEMS

2.1 Introduction

The Rare Earth-Transition Metal, RE-TM, intermetallics benefit from the intrinsic properties of both components, i. e., from the high magnetic moment, and high magnetic coupling strength of the TM partner and strong single-ion magnetocrystalline anisotropy of the RE partner. Three types of exchange interactions are known to occur in RE-TM compounds: RE-RE, RE-TM, and TM-TM interactions. RE-RE interactions are weakest of all due to the smaller spatial extent of the 4f wave functions. The magnetic coupling has to proceed indirectly possibly through the spin polarization of the conduction electrons. Localized 4f spin moments located elsewhere in the crystal lattice will feel this polarization and orient themselves accordingly. This type of indirect mechanism is generally referred to as Ruderman, Kittel, Kasuya, and Yosida, RKKY, interaction.[16] It plays an important role in the magnetic spin-order of RE-TM compounds. TM-TM interaction is a direct consequence of the much larger spatial extent of the 3d wave functions as compared to the 4f wave functions. The large spatial extent of the 3d wave function in TM's leads to substantially large overlap of the neighboring 3d orbitals that results in the formation of 3d-electron energy bands rather than 3d-levels. RE-TM

interaction between the RE-TM moments has a strength intermediate between the two type of interactions. It was originally proposed by Campbell that the exchange interaction involving RE-TM and RE-RE could be described through an indirect exchange mechanism. So, conceptually there are only two kind of interactions involved in the RE-TM compounds i. e., TM-TM, and RE-RE interactions.

2.2 Magnetism in RE-TM Systems

The magnetic behavior of the RE-TM intermetallics can be interpreted in terms of a two sublattice model. TM-sublattice plays a decisive role in determination of the Curie temperature in RE-TM systems because of the much larger strength of the 3d-3d (TM-TM) interaction as compared to that of the 3d-4f (TM-RE) and 4f-4f (RE-RE) interaction. Magnetization in the transition metals, TM's, is due to the unfilled 3d bands and is caused by direct exchange splitting of the 3d electrons.

In Rare-Earth metals, magnetization arises exclusively by the spin and orbital motion of 4f electrons. The orbital motion of these localized electrons is influenced by the perturbing effect of electrostatic potential originating from the neighboring ions in the environment. It leads to an indirect exchange splitting of the largely localized 4f shell electrons. So, these elements show strong single ion anisotropy but low ordering temperatures. The indirect exchange interaction between 4f electrons and itinerant conduction electrons (6s) unbalances the spin. The imbalance is large in the vicinity of

Rare Earth ion with spatial dependence as R^{-3} for large R, is known as RKKY interaction. This RKKY interaction extends over a long range, an oscillatory function of the type:

$$F(x) = \frac{x\cos x - \sin x}{x^4} \qquad \text{------ (1)}$$

In the Campbell model, the 4f electron spin of the RE induces a positive local 5d spin moment through the ordinary intra-atomic 4f-5d exchange with subsequent direct 5d-nd interactions with any other neighboring nd spin moment. Because of the localized nature of the 4f electron shell, the interaction between the 4f spin and itinerant electron spin can occur only through the local exchange interaction on the RE atom described by the intera-atomic exchange integrals $J_{4f\text{-}5d}$, $J_{4f\text{-}6s}$, and $J_{4f\text{-}6p}$. Among these exchange integrals, $J_{4f\text{-}5d}$ (short range) is dominant according to the Campbell's model.[17] On the other hand, in the originally formulated RKKY model, $J_{4f\text{-}6s}$ (long range) was considered to be dominant.

In RE-TM compounds , for light rare earth, LRE, with atomic number smaller than Gadolinium, Gd, the spin and orbital angular momentum oppose each other and the total angular momentum J = L-S. The total rare earth moment ($gJ\mu_B$) couples ferromagnetically to the 3d (TM) spin moment. For Gd and RE's with higher atomic number i. e., heavy rare earths, HRE, and the total angular momentum J = L+S, the total RE moment couples antiferromagnetically to the 3d (TM) moment. This coupling scheme can be understood in terms of the 3d(TM)-4d(RE) hybridization.[18]

In the formation of the RE-TM compounds, large difference in the electronegativity of two partners is responsible for the hybridization of the 3d (TM), and the 5d (RE) orbitals. Hybridization results in the transfer of charge from the 5d (RE) band to the 3d(TM) band such that the occupation numbers are $n_{3d}+n_{5d} = n'_{3d}$, after hybridization. Consequently, 5d electrons from RE transfer and fill the low-lying 3d states in TM. The gap between the unhybridized spin-down bands is smaller than between the unhybridized spin-up bands, hence the hybridization and the electron transfer are greater for the spin down bands that result antiferromagnetic interaction between the 3d(TM) and 5d (RE) moments. The 5d (RE) spins ferromagnetically align the 4f (RE) spins through contact interactions described by atomic exchange integral $J_{4f\text{-}5d}$. Indirect exchange interaction between 4f electrons of RE and 3d electrons of TM allows linking of the high ordering temperature of TM, and the high magnetocrystalline anisotropy of RE in RE-TM system.

2.3 The Crystal Structure of RE-TM Compounds

There are numerous RE-TM intermetallic compounds presumably due to the large electronegativity difference between RE and TM atoms. Various structures observed in the RE-TM systems are summarized in Table 1. Most of these structures are related and originate from the hexagonal lattice of the $CaCu_5$ type through some simple substitutions accompanied by layer shifts.[19, 20] Substitution of one RE atom by a pair of TM atoms is called dumb-bell substitution. Rhombohedral Th_2Zn_{17}-type, and hexagonal Th_2Ni_{17}-type

structures can be obtained by replacing one-third of all RE atoms by a dumb-bell pair of TM atoms. There are two ways in which these substitutions can lead to ordered structures. If the planes containing RE atoms and TM dumb-bells are stacked in the c-direction in the sequence ABCABC..., one obtains rhombohedral Th_2Zn_{17}-type structure shown in the Fig. 1. One unit cell comprises of three formula units of 2-17 structure. If the stacking involves the sequence BCBCBC..., the Th_2Ni_{17}-type hexagonal structure is obtained. Layer B consists of one Th(RE) atom and two Ni(TM) atoms whereas layer C consists of three Ni(TM) atoms. Both these structures give rise to x-ray diffraction patterns similar to those of the basic $RETM_5$ structure but containing additional superstructure reflections characterizing either the hexagonal or the rhombohedral type of stacking.

The $ThMn_{12}$ structure, like the Th_2Zn_{17} and Th_2Ni_{17} structures can be derived from the hexagonal $CaCu_5$ structure. Schematic representation of the unit cell of the tetragonal $ThMn_{12}$ structure with space group I4/mmm is shown in Fig. 1. The rare earth occupies the single 2a thorium site (point symmetry 4/mmm) while the transition elements are distributed over the three manganese sites namely 8i, 8f, and 8j.

On the TM richer side, RE-TM (TM = Fe, Co, Ni) systems are marked by a series of structures e. g., RE_2TM_{17} , $RETM_{12}$, etc. derived from the $CaCu_5$-type structure by systematic dumb-bell substitution for each TM atom. Whereas on the RE richer side, RE-TM systems namely $RETM_2$, $RETM_3$, RE_2TM_7, etc. are derived from $CaCu_5$ structure by

one to one replacement of Cu(TM) by Ca(RE) atom. Powder diffraction patterns of $SmFe_2$, $SmFe_3$, and Sm_2Fe_{17} are given in Tables 2, 3, and 4 respectively.

As the dumb-bell axis is parallel to the c-axis of the 1-5 structure, contraction is expected along the a-axis from 1-5 to 2-17 and 2-17 to 1-12 transformations as these structures are obtained through dumb-bell substitution.

$$3 \cdot RE\,TM_5 \Rightarrow RE_2(RE)\,TM_{15} \Rightarrow RE_2(TM_2)\,TM_{15} \Rightarrow RE_2\,TM_{17}$$

$$4 \cdot RE\,TM_5 \Rightarrow RE_2(RE)(RE)\,TM_{20} \Rightarrow RE_2(TM_2)(TM_2)\,TM_{20} \Rightarrow 2 \cdot (RE\,TM_{12})$$

In RE-TM systems, saturation magnetization is generally found to increase monotonically with the TM concentration in going from RE-rich compounds to TM-rich compounds.

Experimentally it has been found that when RE = HRE (where HRE = Heavy Rare Earth such as Er, Ho, etc.) RE-TM compounds showed ferrimagnetic behavior. The observed decrease in magnetic moment for HRE-TM compounds could be explained by assuming that the moment of RE and TM sublattices subtract. On the other hand, when RE = LRE, the ferromagnetism behavior was manifested by RE-TM compounds which implies that moment of RE and TM sublattices should add as described earlier.

2.4 Anisotropy in RE-TM Compounds

Magnetic anisotropy seems to be an important factor in determining the shape of the hysteresis loop of magnetic materials. RE-TM permanent magnet materials are known to possess the highest value of magnetic anisotropy, and also the highest room temperature coercivity values. There are several kinds of anisotropy: magnetocrystalline or crystal; shape, stress or strain, induced; and exchange anisotropy. Of these, only magnetocrystalline anisotropy is an intrinsic property of the materials and allows preferred orientation for the magnetization vector. The energy required to rotate the magnetization vector from the easy to the hard direction of magnetization is a measure of magnetocrystalline anisotropy.

In RE-TM intermetallics, magnetocrystalline anisotropy is determined by using the two sublattice model. According to this model, the total magnetization is contributed both by the RE sublattice as well as the TM sublattice. The contribution of the TM-sublattice can be estimated from the experimental data available for the compounds in which RE component consists of the non-magnetic element such as La, Y, or Lu.

Magnetocrystalline anisotropy of RE's is primarily a consequence of the spin-orbit interaction and/or the crystal field effect. When an applied field tries to reorient the spin of an electron, the orbit of that electron also tends to be reoriented. But the orbit is strongly coupled to the lattice (crystal field effect) and therefore it resists the attempt to

rotate the spin axis. This interaction can be explained by using point-charge ionic model, according to which the 4f electrons are confined to the immediate vicinity of the RE nucleus and the surrounding ions are treated as point charges. The strong 4f spin-orbit coupling leads to a well defined total angular momentum J. As a result, the free-ion wavefunction used to obtain the energy eigenvalues can be described by $| L,S,J,J_z>$.

The electrostatic potential at a point $P(r,\Theta,\Phi)$ near the origin due to the surrounding j ions is,

$$V(r,\Theta,\Phi) = \sum_j \frac{q_j}{\vec{R}_j - \vec{r}} \qquad \text{------ (2)}$$

If the RE ion has a charge of q_i, then its potential energy due to the perturbing potential V is given by,

$$W_c = \sum_i \sum_j \frac{q_i q_j}{\vec{R}_j - \vec{r}_i} \qquad \text{------ (3)}$$

where the summation is confined to the unfilled shell electrons in the first order perturbation. Since spin-orbit coupling is stronger as compared to coulomb interactions in RE-TM compounds, the wave function for 4f (RE) electrons is completely described by $| L,S,J,J_z>$. In Stevens equivalent operator formulism, the general expression for the crystal field hamiltonian with the same transformation properties under rotation as the potential can be written as

$$H_{cf} = \sum_n \sum_m B_n^m O_n^m \qquad \text{------ (4)}$$

where O_n^m, called the Stevens operators, are the polynomials of order n of angular momentum operators J and Jz. Crystal field coefficients B_n^m represent the symmetry and strength of the crystal field surrounding the 4f electron system. These coefficients are determined in part by the surrounding ions and in part by the radial extent of the RE ion.

$$B_n^m = \langle J \| \Theta_n \| J \rangle \langle r^n \rangle (1-\sigma_n) K_n^m A_n^m(J) \qquad \text{------ (5)}$$

where $\langle J \| \theta_n \| J \rangle$ = reduced matrix element ($=\alpha_j$, and β_j) and $(1-\sigma_n)$ is the shielding factor. $A_n^m(J)$ is controlled by electrostatic potential generated by the surrounding ions. $\langle r^n \rangle$ is the radial matrix element for the 4f shell.

The total hamiltonian for a given RE site can be written as

$$H_{RE} = \sum_n \sum_m B_n^m O_n^m - 2 \sum_{n.n.} J_{RT} \, \vec{S}_R \cdot \vec{S}_T - 2 \sum_{n.n.} J_{RR} \, \vec{S}_R \cdot \vec{S}_R \qquad \text{------ (6)}$$

where the summation n. n. is carried out over the nearest neighbor spins, J_{RT} and J_{RR} are the RE-TM and RE-RE magnetic coupling constants respectively. The total free energy, F_{RE} of the RE sublattice at a given temperature is obtained by diagonalization of H_{RE} and using energy eigenvalues to calculate the partition function Z_{RE} by means of the relation

$$F_{RE} = -k_B T \ln Z_{RE} \qquad \text{------ (7)}$$

Then, the total energy of the two-sublattice system is determined by adding the energies of both the sublattices.

The number of terms in the hamiltonian equation seem to be rather large. However for high symmetry systems, most of the $B_n^{m'}s$ vanish. For $ThMn_{12}$ type structure, the crystal field hamiltonian can be written as

$$H_{cf} = B_2^0 O_2^0 + B_4^0 O_4^0 + B_6^0 O_6^0, \qquad \text{------ (8)}$$

where,

$$B_2^0 = \alpha_j \langle r^2 \rangle (1-\sigma_2) A_2^0 \qquad \text{------ (9)}$$

expresses the contribution of second order crystal field term. α_j are called Stevens coefficients of RE, and A_2^0 is the electric field gradient at the RE site. At room temperature, $B_2^0 O_2^0$ is the most dominant term. As a result, the total hamiltonian for RE takes the form

$$H_{RE} = B_2^0 O_2^0(J) + g\mu_B \vec{J} \cdot \vec{H}_{ex} \quad . \qquad \text{------ (10)}$$

The sign of the term B_2^0 determines whether the compound has easy axis or easy plane or cone structure. The sign of A_2^0 is frequently obtained from rare earth Mossbauer spectroscopy but that of α_j depends on the shape of 4f charge distribution. For instance, in $Sm(Fe,Ti,V)_{12}$, A_2^0 is negative and $\alpha_j(Sm)>0$ which orient EMD along c-axis.[21] Below room temperature, higher order terms cannot be neglected as the spin reorientation takes place. To sum up, spin reorientation is a manifestation of competing anisotropies with different temperature dependence of RE, and TM sublattices.

Magnetocrystalline anisotropy for RE sublattice can also be described by a phenomenological relation:

$$E_a(RE) = K_1 \sin^2\theta + (K_2 + K_2^1 \cos 4\Phi)\sin^4\theta + (K_3 + K_3^1 \cos 4\Phi)\sin^6\theta \text{ - - - - - (11)}$$

where θ, and Φ are the polar angles of magnetization relative to the crystallographic axis. At room temperature, the RE sublattice anisotropy energy is determined from

$$K_{1,RE} \approx -\frac{3}{2} B_2^0 \langle O_2^0 \rangle \qquad \text{- - - - - - (12)}$$

The preferred direction of magnetization can be determined experimentally from the knowledge of anisotropy energy on highly aligned samples and the above equation.

The anisotropy energy in the RE-TM compounds is due to the contribution from both the RE, and TM sublattices. At temperatures higher than that compared to the crystal field splitting, the contribution of TM lattice would be dominant. As a result, the competing anisotropies of RE and TM, and their dependence on temperature could lead to the switching of anisotropy from easy axis to easy plane or easy cone for the same compound. The occurrence of spin reorientation from axial to planar or a conical behavior in some $R_2Fe_{14}B$, and $RTiFe_{11}$ systems has been explained using Second Order Crystal Field Theory.[22] This kind of temperature dependence is observed in $DyTiFe_{11}$ where the high temperature easy axis anisotropy changes into basal plane anisotropy at lower temperatures. (axial @ T= 295 K, planar @ T = 77K).[23]

2.5 Realization of Coercivity in terms of Anisotropy

It is an experimental fact that for certain ranges of particle size, the coercive force of a ferromagnetic material increases as the particle size increases and on reaching a maximum value it start decreasing with further increase of the particle size. Presumably, the maxima in the coercivity value correspond to the single domain sized crystallites. In addition, it also depends strongly on the microstructure of the compound and the phases present in the grain boundaries. Presence of pinning sites such as magnetic separation of grains by an additional non-magnetic element seem to favor the high coercivity values. However, it seems almost impossible to realize completely all the crystal anisotropy in terms of coercivity, possibly due to presence of unavoidable soft magnetic phases acting as nucleation centers. The nucleation of reversed domains at surface defects is also an important factor in limiting the coercivity of RE-TM magnets.

CHAPTER 3

EXPERIMENT

3.1 Introduction

There is a considerable research interest in permanent magnet materials because of their applications in widely varying areas ranging from computer peripherals to medical appliances. Thin film magnets find their potential utilization in storage media, small scale electromechanical devices, microwave devices and small film-scale permanent magnet geometries.

Fabrication of bulk magnets is a multi-step process involving alloy preparation, milling and composition control, particle alignment, sintering, heat treatment, machining and magnetizing. Film synthesis procedure is single-step process that also allows extreme texturing in the directly crystallized films without subjecting to extremely high temperatures which are necessary for the bulk preparation techniques.

3.2 Synthesis of Film Magnet

Sputtering is most - widely used technique for the deposition of magnetic films because it offers an advantage of obtaining uniform composition films from multi -

component targets with better adherence properties. In this study, each multi - element target consisted of two or more of the elements such as Sm, Pr, Co, and Fe, etc that differ greatly in melting points, and vapor pressures. The target is water cooled to prevent melting of the target or diffusion of atoms within the target. Details of the sputtering technique can be found well cited in literature.[24, 25]

Trisputtering is used as a means of gaining control over film composition. The button shaped alloy targets used in this study were made through arc melting in water - cooled copper crucible using tungsten electrode in a 99.99% pure argon atmosphere. The details of this specially designed arc melter were reported earlier by Cadieu et al.[26] Each ingot was melted at least four times, flipped the sides after each melting; in order to ensure homogeneity. The inert gas Ar was cycled through the melting chamber at a rate of 25 CFH in order to provide the cleaner environment for the melting species. The purity of elements used is at least 99.9% by weight.

The film magnets were synthesized in an ultra-high vacuum system (base pressure $< 10^{-7}$ torr) by R. F. sputtering in Ar at pressures from 75 mTorr to 150 mTorr. In order to maintain system purity, the Ar gas is cycled during the deposition process. The gas flow and pressure is controlled by an MKS mass flow controller and an exhaust valve controller during deposition.

The film synthesis procedure involves two methods differing in the process of

crystallization.[27] First method is direct crystallization: the binary samples were directly crystallized by sputter deposition onto substrates maintained at proper high temperatures. The second method is subsequent crystallization: the film magnets were sputter synthesized in the amorphous form and then crystallized through post deposition thermal treatment.

Deposition rates were easily controlled and highly reproducible provided the substrate and target assembly is not displaced. In addition the deposition rate remains fairly uniform with time if the R. F. input power and gas pressure do not change appreciably. For film under study, the deposition rates ranged from about 0.005Å/s to 2 Å/s.

In the direct crystallization approach, during deposition process, substrate temperature is observed to be about 50° C higher as compared to the prior substrate temperature. This increase is primarily due to the plasma heating caused by the electron bombardment.

Films were deposited on polycrystalline Al_2O_3 corundum substrates which were heated by a quartz heater lamp. The temperature of the substrate can be controlled in the range from room temperature to above 700° C. The quartz lamp assembly is also water-cooled to prevent it from melting or demagnetizing the magnet. At high temperatures, for directly crystallized Sm, Fe films, Sm composition in the target had to be much higher

as compared to the amount of Sm in the phase formed, as Sm is extremely volatile. For instance, (002) textured films of $SmFe_{12}$ could be synthesized only through direct crystallization whereas Sm_2Fe_{17} and Sm_5Fe_{17} phases could only be synthesized by the subsequently crystallization technique.

3.3 Magnetic Measurements

The magnetic measurements were performed at room temperature using two Princeton Applied Research (PAR) Vibrating Sample Magnetometers (VSM), one equipped with 90 kOe Nb-Ti superconducting solenoid and a cryogenic system that provides stable temperature control from 4.2 K to 300 K, and the other with a low field of 20 kOe electromagnet, shown in Fig. 2, and a furnace that allows measurements over the temperature range 300 - 1000 K. Automated scanning and data acquisition procedures were employed for hysterisis loop measurements, as well as for the x-ray diffraction experiments.[28]

For low field measurements up to 20 kOe, the sample holder and sample sized substrate piece has a diamagnetic contribution in the order of 10^{-6} emu/g. For the film samples measured at 90 kOe of applied fields, usually the raw data, measured perpendicular to the film plane, exhibited negative slope. This is because the sample holder was found to be diamagnetic, and this contribution becomes very large at higher fields. So, the sample holder and substrate piece, approximately of the same size as

various samples, were also measured at room temperature as well as at lower temperatures. The combined correction for the sample sized substrate piece and the holder was diamagnetic for perpendicular to the film plane holder and paramagnetic for the inplane holder. All the hysterisis loops measured at higher as well as lower fields were corrected w.r.t. the respective holder contributions.

The typical signal to noise ratio was about 3%. For most of the phases synthesized, it was not possible to saturate the samples fully in the film plane, or out of the film plane, or both. The thermo-magnetic measurements were made by the low field VSM in a field of 2-5 kOe in the temperature range of 300 - 900 K.

3.4 Film Thickness and Composition Measurements

Quantitative analysis of the elemental composition was done through the Hitachi Scanning Electron Microscope model S-570 coupled with an energy dispersive X-ray spectrometer. Details of the Scanning Electron Microscopy procedures can be obtained from literature.[29] The film thickness was measured with Scanning Electron Microscope, SEM, at ultra high magnifications by directly viewing an edgewise mounted freshly cut sample of the film under study. However, a quick estimation of average film thickness was made by weighing the substrate before, and after the film deposition, and using the suitable density for the phase synthesized. The later method is useful only for the non-porous and void-free films, otherwise it underestimates the actual film thickness.

3.5 Study of Crystal Structure

The crystal structure and crystallite orientation were determined by x-ray diffraction measurements using $Cu_{K\alpha}$ radiation and a liquid nitrogen cooled Si(Li) detector. Automated data acquisition, and angle scanning control was achieved with a personal computer coupled to an MCA. X-ray diffraction experiments were performed on various film samples in order to investigate the crystal structure of the compound. The increased background existing at the lower angles in the x-ray diffraction traces for almost all the samples is due to the glass holder on which the samples were mounted during the data collection. X-ray data, and hence the mounting of the sample is cross checked from the presence of the substrate lines in about 2 μm thick samples. $Cu_{K\alpha 1}$ radiation were used for diffraction analysis. Precise lattice parameters were determined by using a fitting routine developed in the laboratory. This program determines the weighted root mean square angular deviation between the observed and calculated Bragg angle based on a given structure and lattice parameters. Details of the x-ray diffraction can be obtained from a number of existing references.[30-33]

CHAPTER 4

A NEW PHASE IN THE DIRECTLY CRYSTALLIZED Sm, Fe BINARY FILMS

4.1 Introduction

The pure Sm-Fe system is known to exhibit $MgCu_2$, $PuNi_3$, and Th_2Zn_{17} type phases in the bulk form.[34] Since Fe is more abundant and economical as compared to Co and carries considerably larger free ion magnetic moment, therefore, the interest was to study the possible synthesis of the binary Sm-Fe compounds. Unfortunately, the $SmFe_5$ compound is not known to exist. On the other hand, Sm_2Fe_{17} is a stable compound exhibiting easy plane anisotropy, so, it does not exhibit hard magnetic properties.

A few years ago, it was discovered that the Fe rich pseudobinary compounds $SmFe_{12-x}T_x$ (T = Ti, V, Si, etc., x > 1 of the $ThMn_{12}$ tetragonal structure exhibit very strong uniaxial magnetic anisotropy.[35-37] In this system, the presence of the nonmagnetic third element was presumed to be essential as a phase stabilizing agent. However, the addition of these nonmagnetic elements was found to be highly detrimental to the saturation moment and the contribution of these third elements to the magnetocrystalline anisotropy of the 1-12 system was found to be negligible.

4.2 Synthesis of a New Phase

In an attempt to form nitrided 2-17 phase, a set of three targets of pure Sm, and Fe were made with a small gradient across the length of the substrate. Films of about 2 μm thick were synthesized by direct crystallization method at various substrate temperatures. From 450-600 K, the compound showed soft magnetic properties for the samples in the composition range of 8.5 atomic percentage, at.%, of Sm to 10.5 at% Sm as shown in Fig. 3. From the x-ray diffraction studies on these samples, only α-Fe peak was observed in the background of a broad hump. It implies the presence of a two phase mixture of amorphous Sm-Fe and α-Fe as indicated by the x-ray diffraction trace in Fig. 4. In this substrate temperature range, the material showed soft magnetic properties. At 675 K, the diffraction lines were well defined and coercivity also increased from less than 1 kOe to 3.5 kOe. Scanning Electron Micrographs of these samples showed two distinct phases, globules of one phase in the matrix of another phase. Composition of these two phases was measured by running EDXS at ultrahigh magnification. The composition of Sm-rich globules was Sm=33 at% Fe=67 at% and that of iron enriched phase found to be Sm=7.8 at% Fe=92.2 at%. these compositions relate to the stochiometeric 1-2 and 1-12 phases respectively. Sputtering conditions varied in controlled manner allowed to synthesize various samples of single phase except for a little amount of α-Fe coexistence as found by x-ray examination. In all these samples, magnetization perpendicular to the plane of this unidentified phase was much higher than the in plane magnetization. Figure 5 shows hysterisis loops for a typical sample of this new phase in the Sm, Fe system.

4.3 Identification of $SmFe_{12}$ Phase

It has been found that this new binary phase forms readily in the directly crystallized films in the temperature range of 400-550° C. Identification of the 1-12 phase is carried out as follow:

The 1-12 and 2-17 structures are superstructures of the disordered $CaCu_5$ structure with certain RE atoms in the 1-5 structure being replaced by pairs of TM atoms generally called dumb-bell atoms. So, the basic unit cells are related by the transformations: $a_{1-12} \Rightarrow 2 \cdot c_{1-5}$, $c_{1-12} \Rightarrow a_{1-5}$. The deviation from the ideal case are driven by the transition metal composition and leads to the high density of lines observed in the 1-12 phase as compared to the 1-5 structure.

The c-axis of 2-17 is along 1-5 c-axis while the 1-12 c-axis is along the basal plane of the parent 1-5. So the x-ray diffraction powder patterns of these compounds are marked by the presence of the strong fundamental lines arising from the parent 1-5 structure and the weak superstructure lines unique to the given superstructure. In the x-ray diffraction trace of $SmFe_{12}$ films with weak texturing, Fig. 6, we observed a total number of 10 lines. All of these lines were fitted to the 1-12 cell with a = 8.438 Å and c = 4.805 Å, while most of these lines can also be fitted to Th_2Zn_{17} cell with a = 8.351 Å, and c = 12.652 Å. In that case, the (002) reflection of 1-12 cell transforms to the (300) reflection of the rhombohedral 2-17 phase. The corresponding 2-17 indexing

implies that most of the crystallites have c-axis of magnetization in the film plane. Therefore, the in plane magnetization should be larger than the magnetization perpendicular to the film plane, which is contrary to what has been observed in the hysterisis loops. The observed magnetic properties were very different from those expected on the basis of the 2-17 structure with (300) texture. On the other hand, these magnetic properties are well explained in terms of 1-12 cell with the above cited (002) texture. Comparing these "2-17" parameters a = 8.351 Å, c = 12.651 Å with the well established lattice parameters a = 8.555 Å, c = 12.445 Å of Sm_2Fe_{17} phase, we see an expansion along the c direction and contraction along the a direction. This suggested the presence of additional dumbbell sites as is the case in the $ThMn_{12}$ structure. The lattice parameters for $ThMn_{12}$ type structure yielded approximately 2% lower volume for the binary phase than that for the pseudobinary compounds like $SmFe_{11}Ti_1$ again supporting the formation of 1-12 phase.[38-40]

The $ThMn_{12}$ and Th_2Zn_{17} structures are superstructures of $CaCu_5/TbCu_7$ structure. For 2θ range 25° - 60° one observes seven lines in the 1-5 structure as compared to about twenty lines for 2-17 or 1-12 structures. All the indices of 1-5 could be indexed in terms of 2-17 or 1-12 superstructures are related through the following matrix relationships.

3 $SmCo_5$ + 1 dumbbell subst.=> Sm_2Co_{17}.

$$\begin{pmatrix} h \\ k \\ l \end{pmatrix}_{2-17} = \begin{pmatrix} 1 & -1 & 0 \\ 1 & 2 & 0 \\ 0 & 0 & 3 \end{pmatrix} \begin{pmatrix} h \\ k \\ l \end{pmatrix}_{1-5} \qquad \text{------ (13)}$$

2 $SmCo_5$ + 1 Dumbbell subst.=> $SmCo_{12}$

$$\begin{pmatrix} h \\ k \\ l \end{pmatrix}_{1\text{-}12} = \begin{pmatrix} -1 & 1 & 0 \\ 0 & 0 & 2 \\ 1 & 1 & 0 \end{pmatrix} \begin{pmatrix} h \\ k \\ l \end{pmatrix}_{1\text{-}5} \qquad \text{------ (14)}$$

The lattice parameters are related as:

$$a_{2\text{-}17} => \sqrt{3}\, a_{1\text{-}5} \qquad a_{1\text{-}12} => 2\, c_{1\text{-}5}$$

$$c_{2\text{-}17} => 3\, c_{1\text{-}5} \qquad c_{1\text{-}12} => a_{1\text{-}5}$$

It is important to note that for every diffraction line of 1-5 structure, a corresponding fundamental line of rhombohedral 2-17 and tetragonal 1-12 structure can be found. From the formula for d spacing and the relation between a and c axes, one can easily obtain the following transformation formula:

$$1 \cdot (Th_2Zn_{17} \text{ type}) = 3 \cdot (CaCu_5 \text{ type}) \qquad \text{------ (15)}$$

$$(h^2+hk+k^2)(Th_2Zn_{17} \text{ type}) = 3 \cdot (h^2+hk+k^2)\ (CaCu_5 \text{ type}) \text{------ (16)}$$

In addition to these transformation related lines, the superstructure exhibited a higher density of lines. These superstructure lines help to distinguish the closely related structures from one another.

The experimental 2θ angles for the SmFe binary sample are shown in the Table 5. The indexing for various structures was obtained through a fitting procedure developed in the laboratory.[40] Possible fittings based upon a hexagonal $CaCu_5$ cell, the

rhombohedral Th_2Zn_{17} cell, and the tetragonal $ThMn_{12}$ cell are given in the Table 5.

On the basis of various structure fittings, the respective lattice parameters are given below:

$$a_{1\text{-}5} = 4.821 \text{ A} \quad c_{1\text{-}5} = 4.218 \text{ A}$$

$$a_{2\text{-}17} = 8.351 \text{ A} \quad c_{2\text{-}17} = 12.652 \text{ A}$$

$$a_{1\text{-}12} = 8.438 \text{ A} \quad c_{1\text{-}12} = 4.805 \text{ A}$$

Ratio of in plane remanence to the perpendicular to the plane remanence as observed experimentally is ≈ 0.5. This ratio has also been calculated through projection of moments model for the observed reflections corresponding to various expected structures.

In general, $Mr = Ms < | \cos\theta | >$ where θ is the angle between the easy axis and the applied field. For random orientation of the particles, $Mr = 0.5$ Ms for any direction of the applied field. Special cases for a variety of different orientations have been derived [41] and its direct verification for real system has also been discussed.[42]

For crystallites c-axis oriented with angle θ, and continuously distributed over all Φ, the z component of magnetization, $M_z = M \cos\theta$, and the x component of magnetization $M_x = M \sin\theta \cos\Phi$. Therefore the ratio of in plane to perpendicular to the plane remanent magnetization can be expressed as:

$$\left(\frac{\textit{Inplane remanent moment}}{\perp \textit{ plane remanent moment}}\right)_{cal.} = \frac{\int_{-\pi/2}^{\pi/2} \int_{-\pi/2}^{\pi/2} \sin\theta \cos\Phi \, d\theta \, d\Phi}{\int_{\pi/2}^{\pi/2} \cos\theta \, d\theta} \quad \text{- - - - - (17)}$$

For a discrete distribution of crystallites, we sum over the orientations present in the film.

$$\left(\frac{\textit{Inplane remanent moment}}{\perp \textit{ plane remanent moment}}\right)_{cal.} = \frac{0.64 \sum_i I_i \sin\theta_i}{\sum_i I_i \cos\theta_i} \quad \text{- - - - - - (18)}$$

$$\text{where, } I_i = \frac{I_{observed}}{I_{Powderpattern}} \quad \text{- - - - - - (19)}$$

For the hypothesized Th_2Zn_{17},

$$\left(\frac{\textit{Inplane remanent moment}}{\perp \textit{ plane remanent moment}}\right)_{cal.} \approx 1.29 \quad \text{- - - - - - (20)}$$

In $ThMn_{12}$ type structure,

$$\left(\frac{\textit{Inplane remanent moment}}{\perp \textit{ plane remanent moment}}\right)_{cal.} \approx 0.54 \quad \text{- - - - - - (21)}$$

$I_{\text{Powder pattern}}$ for this case was calculated by Cadieu et.al.[33]

The ratio of remanent moment in plane and perpendicular to the plane calculated for the 1-12 structure was very close to the experimentally observed value, supporting formation of 1-12 phase rather than 1-5 or 2-17 structures. For 1-5 to 2-17 transformation

$(\Delta V/V) = -3.8\%$, and $(\Delta\rho/\rho) = 1.4\%$ as presented in Table 6, where as the respective changes for 2-17 to 1-12 transformations, Table 7, were $(\Delta V/V) = -2.3\%$, and $(\Delta\rho/\rho) = 0.8\%$. The above calculations for the 2-17 to 1-12 transformations suggested the presence of additional dumbell sites in 1-12 structure as compared to 2-17. The presence of dumbbell sites lead to a decrease in the volume as a-axis contracted and c-axis expanded while accommodating additional dumbbells during the process of transformation.

A ^{57}Fe Mossbauer spectroscopy analysis of the data obtained at room temperature on highly (002) textured samples is shown in Fig. 7. The near absence of second and fifth lines lead to the result that c-axis is parallel to the direction of propagation i.e., perpendicular to the film plane as the film sample was mounted perpendicular to the direction of propagation. An average hyperfine field of 269.8 kOe was obtained that corresponds to an average moment of 1.8 μ_B/Fe atom using a hyperfine interaction constant of α-Fe i. e., 150 kOe/μ_B, in agreement with the value obtained from the hysterisis loops.

For the first time, strongly uniaxial $SmFe_{12}$ binary phase was synthesized. The measured magnetic properties, diffraction measurements, projection of moment calculation, Mossbauer experiments, density calculations and composition studies allowed to definitively identify the phase as $ThMn_{12}$ type. Lattice parameters of this $ThMn_{12}$-type structure are a = 8.438 Å and c = 4.805 Å

Curie temperature measurements were made on highly (002) textured film samples using low field VMS firstly by pumping down the sample chamber and then maintaining the He gas flow at 300 CC/min to prevent oxidation of the sample. The projected value of Curie temperature, as seen in the Fig. 8, for $SmFe_{12}$ is about 375°C. So, the $SmFe_{12}$ phase was synthesized well above its Curie temperature.

The ability to form the 1-12 binary phase without the addition of third element made it possible to maximize the magnetic moment in the 1-12 Sm, Fe system. The deposition temperatures were generally higher than the Curie temperature of the 1-12 phase. Therefore , the alignment of crystallites is not due to demagnetization energy but essentially due to the thermal energy supplied by the heating through the quartz lamp. So, the thermal energy helps the crystallites to grow perpendicular to the film plane. Once, the seed crystallites are nucleated, the replication of the successive layers takes place.

The preceding sections discussed the synthesis and identification of a $ThMn_{12}$ type new phase in the Sm, Fe system. The following sections deals with the affect of various deposition parameters that influence the microstructural orientation of crystallites in the synthesized films. There are three most important control parameters that influence the microstructural orientation of crystallites in the synthesis of Sm, Fe films. These control parameters are the deposition rate, substrate temperature, and sputtering gas pressure during deposition process.

Films were synthesized for a wide range of sputtering rates from 0.005 Å/s to 1 Å/s. For rates from 0.005 Å/s to 0.01 Å/s, $SmFe_{12}$ does not form even though the film composition was 8.5 at%, and 91.5 at% of Sm and Fe respectively. At these deposition rates, samarium does not lock into the $SmFe_{12}$ phase. At rates of 0.026 Å/s to 0.037 Å/s, $SmFe_{12}$ phase does form, but accompanied by a significant amount of α-Fe as observed in the x-ray diffraction traces for such samples. However, for rates higher than 0.065 Å/s to 1 Å/s, a very small proportion of α-Fe was observed in the $SmFe_{12}$ phase. The directly synthesized $ThMn_{12}$ type films are strongly (222) textured at higher rates. This corresponds to the shortest stacking repeat distance in the $ThMn_{12}$ type tetragonal cell. Mobility of the surface atoms is greatly reduced by the incoming flux of the depositing atoms.

4.4 Effect of Temperature on the Crystallite Orientation

The films were synthesized in one step through the deposition of Sm-Fe material onto the heated substrate under proper sputtering conditions. The texture of these sputter synthesized films is build up during the deposition process without any initial texture. Thus, the texture of the film is strongly dependent on the sputter process parameters. The texture changes in the $ThMn_{12}$ type sputter synthesized films with sputter gas pressure and deposition temperature were studied. The study was carried out for substrate temperature in the range 650 K to 900 K, and sputtering gas pressure of 75 to 150 mTorr of Ar. These pressures were high enough to thermalize the sputtered atoms before their arrival

at the substrate.

Figure 9 shows the $Cu_{K\alpha}$ diffraction trace of SmFe films synthesized at 100 mTorr of Ar at various substrate temperatures. It is seen that the growth of crystallites with perpendicular to film plane c-axis orientation becomes favorable at higher temperatures. At higher substrate temperature, the surface mobility of the deposited atoms is increased and they can diffuse through a larger distance, thereby, favoring the longest stacking (002) texture. It is seen through the increased (002) texturing of the films with rising substrate temperatures.

4.5 Variation of Texture with Pressure

To understand how to synthesize reproducible thin films with desired magnetic properties, and crystal texturing, it is important to understand the factors that influence the microstructural orientation of the films. For films of similar composition, the (002) texture is dominant at relatively lower pressure as seen in Fig. 10. During the sputter deposition, variation of various control parameters allowed the preferential crystallographic texturing of the films with the same phase. To a large degree, the mode of texture change with lowering of the gas pressure corresponds to that of increasing substrate temperature. This could be attributed to the higher energy of the depositing sputtered atoms at lower gas pressures. In the binary $SmFe_{12}$ films, the (002) texture could only be obtained at substrate temperature of 900 K and gas pressure of 75 mTorr.

The texturing achieved does not depend on any substrate epitaxy, but because the magnetic easy axis of 1-12 system is along the crystal c-axis.

4.6 Change in Properties on Nitriding

Recently, it has been shown that in bulk processed Sm_2Fe_{17} phase, interstitial nitrogen changes the easy plane anisotropy of the Sm_2Fe_{17} to easy axis anisotropy. In sputter deposited films, incorporation of impurity gas phases are known to change the magnetic and crystalline properties.

On nitriding, the x-ray diffraction lines corresponding to 1-12 phase samples at 800 K for 2 hours became very broad with an intense α-Fe peak as seen in Fig. 11. It seems that as this compound tries to absorb N_2 interstitially, it breaks up into α-Fe and amorphous SmFe. As a result, the easy axis properties switched to easy plane behavior. The structure of $RETM_{12}$ phase is tetragonal, I4/mmm. There are three sites populated by the transition metal atoms (x, 1/2, 0) x $\approx$ 1/4 (x, 0, 0) x $\approx$ 1/3, and (1/4, 1/4, 1/4). Each of these sites with eight atoms in the crystallographic cell that contains two formula units per cell. The largest interstitial site in this compound is the base center (1/2, 1/2, 1/2) (0, 0, 1/2).[43] On nitriding, the inplane magnetization is higher than the perpendicular to the plane magnetization, and the coercivity decreased to less than one kOe. In other words, the easy axis anisotropy changed to easy plane anisotropy.

4.7 Conclusion

Films of binary $SmFe_{12}$ compound exhibiting $ThMn_{12}$ type crystal structure were successfully synthesized without the addition of a phase stabilizing third element. These films were crystallized by R. F. sputter deposition on Al_2O_3 substrates preheated to 400-500° C. Through x-ray diffraction, the lattice parameters of the tetragonal structure were determined to be a = 8.431 ± 0.008 Å and c = 4.815 ± 0.005 Å. The binary $SmFe_{12}$ samples has been found to be magnetically uniaxial as the polycrystalline films showed a perpendicular to the film plane magnetic anisotropy and the x-ray diffraction trace showed perpendicular to the film plane c-axis texturing. For (222) textured samples, room temperature magnetization values of 10.4 ± 0.5 kG and 13.0 ± 0.5 kG respectively were obtained for magnetization measurements parallel and perpendicular to film plane at applied fields of 18 kOe. The maximum room temperature coercivity of 3.0 kOe was observed for these (222) textured samples. So, it has been possible to increase the coercivity of $SmFe_{12}$ by synthesizing in (222) texture, at the expense of decrease in remanence.

The hysteresis loops of these films exhibited a slight dip on entering the second quadrant due to the presence of trace amounts of magnetically soft impurity phases and α-Fe. So far, the 1-12 phase has not been observed in films that were subsequently crystallized. Such films could be formed in either the magnetically soft 2-17 phase or the high anisotropy 5-17 phase.[44-48]

Through high field magnetic measurements on (002) textured films, it was found that this $SmFe_{12}$ binary phase has room temperature saturation moments of 14.3 ± 0.5 kG and uniaxial anisotropy field of 130 ± 10 kOe. The average iron moment in the $ThMn_{12}$ is rather small for a compound containing so much amount of iron. At T = 0 K, the average iron moment for $YFe_{11}Ti$ is 1.73 μ_B.[56] As the three different Fe sites namely 8i, 8f, and 8j have different number of nearest neighbors, and different Fe-Fe distance, their moments are also different. The Fe moments for 8i, 8f, and 8j sites are 1.99 μ_B, 1.51 μ_B, and 1.76 μ_B respectively. The corresponding average Fe-Fe distances for the respective sites are 2.69 Å, 2.49 Å, and 2.57 Å. The small iron moment may be consequence of the nearest neighbors for the 8f sites. In addition, Slater Pauling idea of short antiferromagnetic versus long ferromagnetic bonds may be a useful pointer in the case of $RETM_{12}$ phase. As the three different Fe sites have different environments, and one of these bonds is significantly shorter than the other two, the net magnetization decreases. For $SmFe_{11}Ti$, the Fe moments at 8i, 8f, and 8j sites are 2.08 μ_B, 1.59 μ_B, and 1.84 μ_B respectively. If similar moments are assumed for the $SmFe_{12}$ phase sites, the average moment is about 1.84 μ_B that corresponds to a saturation magnetization of 14.6 kG at 0 K which is in fair agreement with the measured value of 14.3 ± 0.5 kG at room temperature.

This leads to the hope that this 1-12 binary phase shall prove to be an attractive candidate for permanent magnet film applications, provided it is possible to synthesize it in the single phase form, with isolated grains of optimal size.

CHAPTER 5

SYNTHESIS OF $Sm_2Fe_{17}N_x$ PHASE

5.1 Introduction

Recently, much attention has been paid to the research for new intermetallic phases richer in Fe which might have a potential for permanent magnet applications. The outstanding intrinsic magnetic properties of tetragonal $Nd_2Fe_{14}B$, high saturation magnetization and anisotropy field can be attributed to the high amount of iron, the presence of light rare earth (LRE), and to the complex non cubic structure of the phase. This thesis is aimed at the development of new Fe-based compounds having low cost, high saturation magnetization and magnetic hardness. When Coey and Sun reported that nitrogen converted easy plane Sm_2Fe_{17} to a high anisotropy uniaxial system, $Sm_2Fe_{17}N_x$ became the third high anisotropy ordered Sm-Fe phase.[49, 50] Isotropic $Sm_2Fe_{17}N_x$ bulk magnets with room temperature coercivities of 18 kOe by rapid solidification [51] 23 kOe by melt spinning [52] and 30 kOe by mechanical alloying [53] were reported. So far, there are no reports about the bulk magnets of $Sm_2Fe_{17}N_x$ prepared by normal sintering method.

In general, gas phase interstitial modification is possible if the binding energy of interstitial atoms in the lattice exceeds the molecular binding energy in the gaseous phase. Interstitial atoms of smaller size with moderate electronegativity require much lower

energy to deform the lattice around interstices as compared to the larger sized ones. This energy can be provided if the electronegativity between interstitial atoms and lattice atoms is sufficiently strong [54]. The large electronegativity difference sometimes leads to disproportioning of the lattice and formation of an entirely different compound as Sm_2O_3 (Chapter 6 Fig. 21.) appeared in Sm_5Fe_{17} on longer heat treatments. The gas phase interstitial modification can also be viewed as gas solid reaction since the N_2 gas enters into the lattice after the Sm_2Fe_{17} phase is formed. The gas-solid reaction energy

$$\frac{x}{2} N_2(g) + Sm_2Fe_{17}(s) \rightleftharpoons Sm_2Fe_{17}N_x(s) \qquad \text{- - - - - - (22)}$$

basically consists of three parts: the energy to dissociate the gas molecules, to expand the lattice in order to accommodate the gas atoms, and for the gas-lattice interactions. The gas solid reaction takes place only if the reaction enthalpy for the above process is sufficiently negative. R_2Fe_{17} compound can absorb N_2 gas once the temperature has been raised sufficiently high to overcome the activation energy for the absorption process. Apart from relation (22), one has to consider the following reaction:

$$N_2(g) + R_2Fe_{17}(s) \rightleftharpoons 2\,RN + 17\,Fe(s) \qquad \text{- - - - - - (23)}$$

Fortunately, the activation energy for this process is higher as compared to that required for reaction (22), since it involves phase separation of $R_2Fe_{17}N_x$ into grains consisting of RN and grains of Fe metal. This phase separation is limited by the metal atom diffusion which makes it possible to synthesize $R_2Fe_{17}N_x$. Otherwise, $R_2Fe_{17}N_x$ is metastable as compared to RN and Fe metal. It implies that RN and Fe metal will be formed if the charging process is carried out at very high temperatures that is exactly what has been

observed experimentally.[55]

The Curie temperature enhancement is very strong in $RE_2Fe_{17}N_x$ compounds. On comparing the single crystal data for Y_2Fe_{17} i.e., a = 8.466 Å, c = 8.300 Å, T_c = 324 K, M_s = 35.2 μ_B/f.u., [56] with high field data for $Y_2Fe_{17}N_x$ a = 8.637 Å, c = 8.465 Å, T_c = 690 K M_s = 38.5 μ_B/f.u., the nitrogen induced enhancement of Fe moment ≈ 9%, in agreement with the results obtained through Mossbauer experiments by Gubbens et. al.[56] This moment enhancement is too small to account for the strong increase observed in the Curie temperature of $Y_2Fe_{17}N_x$.

From the comparison between the molecular field coefficients, obtained through the phenomenological theory, of pure Sm_2Fe_{17}, and $Sm_2Fe_{17}N_x$ [57], RE-Fe exchange interaction is found to weaken a little, whereas the Fe-Fe exchange interaction got almost tripled. The effect of nitriding is essentially to expand the unit cell without changing the crystal symmetry. Moreover, the interstitial occupation of N-atoms in $Sm_2Fe_{17}N_x$ could increase the Fe-Fe distance, thereby enhancing the exchange interaction and leading to increased Curie temperature. In other words, the large increase in T_c can be attributed to the volume dependence of Fe-Fe exchange interactions.

Jaswal et. al [58] theoretically explained the increase in Curie temperature upon nitriding using Mohn and Wohlfarth model [59] according to which the Curie temperature, T_c, is proportional to (M_0^2/χ) Where M_0 is magnetic moment per atom at 0 K, and the

enhanced susceptibility $(1/\chi_0)$ is given by

$$\frac{1}{\chi_0} = \frac{\left(\frac{1}{2N_{\uparrow}(E_f)} + \frac{1}{2N_{\downarrow}(E_f)} - I\right)}{2\mu_B} \qquad \text{------ (24)}$$

where $N_{\uparrow}(E_f)$ and $N_{\downarrow}(E_f)$ are the up- and down-spin density of states at the fermi level and I is the Stoner parameter that does not alter much on nitriding. An increase in M_0 and a substantial decrease in $N_{\uparrow}(E_f)$ upon nitriding are responsible for almost doubling the Curie temperature. These changes are due to the overall narrowing of the Fe d-band caused by the reduction in the overlap upon lattice expansion. Moreover, as nitrogen has strong electronegativity, it is an electron acceptor. The charge transfer occurs between nitrogen and surrounding metallic iron atoms. Strong inter-atomic interactions of nitrogen and iron atoms result in a substantial change in the density of states of Fe atoms that explains the rise in T_c upon nitriding. In other words, the large increase in T_c can be attributed to the volume dependence of Fe-Fe exchange interaction. A further interesting feature of the $Sm_2Fe_{17}N_x$ compound is the large magnetocrystalline anisotropy.

5.2 Origin of Changing Anisotropy on Nitriding

Sm-sublattice in the Sm_2Fe_{17} compound has an easy c-axis anisotropy, however, the planar anisotropy of the Fe-sublattice overcomes the axial anisotropy of the Sm-sublattice.[60] The change in anisotropy on nitriding is mainly due to the change of Sm local environment as the magnetic measurements on Y_2Fe_{17} showed that the Fe-sublattice

anisotropy is not much changed on nitriding.[61]

On the basis of geometrical considerations , nitrogen atoms occupy the 9e octahedral interstitial sites in the c-planes. As can be seen from the Fig. 12 for each Sm ion, there are three nitrogen neighbors located in the same c-plane [62]. The excess basal-plane electron charge density will enhance the electric field gradient at the 4f electron charge cloud leading to a shift of second order crystal-field coefficient and A_2^0 towards more negative values. Each nitrogen atom has two rare earths as nearest neighbors. The modified basal plane electronic charge density in $Sm_2Fe_{17}N_x$ enhances the electric field gradient at Sm ions. As a result, the N-atoms located very close to the RE atoms are expected to enhance strongly crystal field induced anisotropy of the RE lattice in $RE_2TM_{17}N_x$ system. The modification of crystal field is much more pronounced in the case of $Sm_2Fe_{17}N_x$. This further suggests that the crystal field interaction in $Sm_2Fe_{17}N_x$ is vastly different from its binary counterpart, pure Sm_2Fe_{17}. From x-ray diffraction data, on magnetically oriented powder samples of $RE_2Fe_{17}N_x$ with RE = Ce, Pr, Nd, Sm, Gd, Tb, Dy, Ho, Er, Tm, Lu, and Y, Sun et. al [57] have established that only the nitride with R = Sm has easy c-axis anisotropy at room temperature. The crystal field anisotropy on compressed, and aligned Sm_2Fe_{17} bulk samples is reported to be altered from planar to axial upon nitriding with an anisotropy field greater than 100 kOe.[63]

Coehoorn et. al [57] calculated the crystal field parameter to study Gd-Fe compound and found that it is the interstitial occupation of the nitrogen atom and not just the volume

expansion that changes the single-ion anisotropy in the 2-17 compounds on nitriding.

5.3 Synthesis of Sm_2Fe_{17} Phase

Magnetically isotropic Sm_2Fe_{17} films were crystallized from amorphous deposits obtained by R. F. sputter deposition, at 100 mTorr Ar gas, onto water-cooled polycrystalline Al_2O_3 substrates. The samples were sputtered and crystallized in situ in an all stainless steel sputtering system. These Sm_2Fe_{17} phase samples were then nitrided (in situ) in the N_2 atmosphere (570 Torr) by heating the film deposited substrate to various temperatures. The recent discovery of the strong enhancement of T_c motivated us to investigate the effect of nitriding in the sputtered films of Sm_2Fe_{17} phase.

5.4 Effect of Nitriding on Crystal Structure.

Figure 13 shows x-ray diffractometer traces, $Cu_{K\alpha}$ radiation, of the Sm_2Fe_{17} samples before and after nitriding. Before nitriding all 14 reflections observed between $2\theta = 28°$ and $73°$ were fit to the 2-17 rhombohedral structure with a = 8.555 Å, and c = 12.445 Å, with a weighted root mean square deviation in 2θ equal to 0.01°. On nitriding treatment in N_2 atmosphere, film samples of Sm_2Fe_{17} phase absorbed nitrogen in a gas solid reaction at temperatures in excess of 625 K to form $Sm_2Fe_{17}N_x$. After nitriding, the $Sm_2Fe_{17}N_x$ film samples maintained their original structure but with increased lattice parameters, which was shown by the shifting of peak positions to lower

diffraction angles. The relative volume increase w. r. t. the parent compound (pure Sm_2Fe_{17} phase) was ≈ 7 %. Due to film substrate stress effects, this was slightly higher than the reported bulk values. The nitrogen atom radius is smaller than that of the samarium and iron atoms. So, the lattice dilating and smaller size of nitrogen atoms suggest that the nitrogen atoms should enter into the lattice interstitially rather than substitutionally.

In order to accurately assess the potential of $Sm_2Fe_{17}N_x$ system as permanent magnet material, an understanding of its fundamental magnetic properties is essential.

5.5 Nitriding Effect on Magnetic Properties

The best $Sm_2Fe_{17}N_x$ film samples were synthesized by crystallizing the originally ≈ 5-6 micron thick R. F. sputtered deposits and then nitriding in 570 Torr of N_2 gas at temperature of 675 K. Hysteresis loops measured at 293 K of the subsequently in situ crystallized film samples shown in Fig. 14 (dashed curve) exhibited a low coercivity consistent with the predominance of the magnetically soft easy plane Sm_2Fe_{17} phase. After nitriding at 675 K for 2 hours (solid curve) samples exhibited room temperature in plane coercivity, ${}_iH_c$, of 22.7 kOe. The small step in the demagnetization curve near zero field was attributed to pure Sm_2Fe_{17}, $SmFe_3$, and probably to small amounts of α-Fe in the film samples.

For 12.2 at% Sm film sample, the in plane room temperature coercivity values to 22.7 kOe with a smooth rise to 35.2 kOe at 10 K as shown in the Fig. 15. Bulk reported data reveals a substantial increase 130°C to 475°C in the Curie temperature, and change in anisotropy from in plane to easy axis with anisotropy field H_a = 100 kOe of Sm_2Fe_{17} phase on nitriding. The large increase in Curie temperature can be attributed to the volume dependence of the Fe-Fe exchange interactions. The $(BH)_{max}$ for the zinc bonded magnets is = 10.5 MG-Oe [65].

5.6 Effect of at% Sm on Magnetic Properties

Sm_2Fe_{17} - An ordered phase:

Several un-nitrided films were synthesized under same sputter conditions. Film samples were chosen with different at% of Sm. The phases present as a function of the Sm concentration were studied by x-ray diffraction. Samples with less than stoichiometric Sm exhibited α-Fe diffraction peaks. This is shown in Fig. 16(a) for a sample with 9 at.% Sm, 91 at.% Fe. The $SmFe_3$ phase was clearly seen for higher than stoichiometric Sm concentrations as in Fig. 16(c) for a sample containing 14 at.% Sm.

The effect of Sm concentration on the magnetic properties of the $Sm_2Fe_{17}N_x$ film samples was also studied. The highest in plane room temperature coercivity, 22.7 kOe has been observed for the samples with 12.2 at.% Sm which corresponds to a slightly

richer Sm concentration than the stoichiometric ratio. This is as expected since some Sm oxide is generally present. The room temperature coercivity decreased for higher, as well as for lower, Sm concentrations. This is indicated in Fig. 17. After nitriding, the x-ray diffraction lines were broader and it was relatively difficult to distinguish the various impurity phases as there seemed to be some Sm_2Fe_{17} phase still present in addition to $Sm_2Fe_{17}N_x$.

5.7 Coercivity Dependence on Nitriding Temperature

The effect of nitriding temperature on the subsequently crystallized Sm_2Fe_{17} samples is shown in Fig. 18. The tailing in the loop at 625 K shows the onset of nitriding in the Sm_2Fe_{17} film samples. However, the optimum intake of nitrogen occurred at 675 K. The optimum range of the nitriding temperatures corresponded to 675-725 K as seen in Fig. 18. At 780 K the ${}_iH_c$ dropped to about 4 kOe, and α-Fe precipitated which strongly degraded the film properties.

5.8 Depth Profile of α-Fe Concentration

Nitrogen absorption possibly caused the mechanical stress in the film which is likely to intensify the precipitation α-Fe from the compound. In order to see if α-Fe were concentrated more in the film surface than in the bulk, the outermost 1.5 μm of the $Sm_2Fe_{17}N_x$ film samples was removed by sputter etching. The relative intensity of the α-

Fe was substantially lower after the surface was removed as shown in Fig. 19. The corrected α-Fe to integrated 2-17 intensities ratio decreased from 7.3 %, before the sputter etching, to 2.4 % after sputter etching. This decrease in the intensity ratio inferred that α-Fe was more in the film surface than in the bulk of the film samples.

Before sputter etching, from the hysterisis loop measurements, $(B_r/4\pi M)$ = 86.9 %, and room temperature coercivity, ${}_iH_c$ = 22.76 kOe whereas after sputter etching $(B_r/4\pi M)$ = 83.2 %, and ${}_iH_c$ = 22.08 kOe. Remanence to saturation flux density ratio was higher for the original sample as compared to that of the sputter etched sample. Moreover, x-ray diffraction traces before and after sputter etching, show the reduced amount of α-Fe in the film in agreement with the composition measurements. So, it leads to the possibility of slightly increased un-nitrided phase in the film surface as a result of the ionic bombardment during sputter etching, which was extremely difficult to be detected in the x-ray diffraction patterns. It may be due to an increase in the nucleation centers (or dislocations) at the surface due to ion bombardment during sputter etching. If the precipitation is mostly due to the stress in the film, then it implies that the stress is more near the film surface than in the bulk of the film.

Repeated attempts to form textured Sm_2Fe_{17} film samples by direct crystallization invariably resulted in the formation of disordered related phases. The disordered phases were fitted to the $CaCu_5$ type cell. Nitriding of these disordered phases did not increase the coercivity in contrast to the observed change for the ordered Sm_2Fe_{17} film samples.

5.9 Conclusion

$Sm_2Fe_{17}N_x$ film samples 5 to 6 μm thick with in plane room temperature coercivities up to ≈ 23 kOe at 293 K, ≈ 35 kOe at 10 K, were synthesized. The nitrided $Sm_2Fe_{17}N_x$ system was thus confirmed to remain uniaxial to low temperatures. The best film samples corresponded to a slightly richer Sm concentration than stoichiometric. Sputter etching was used to show that the α-Fe present after nitriding was concentrated in the film surface regions. At low temperatures, the nitriding process takes longer time to reach equilibrium state because the diffusion kinetics are slow. On the other extreme, at very high temperatures, the 2-17 compound dissociates into SmN, and Fe. So, the nitriding of the ordered 2-17 films had to be performed in a very narrow temperature range to optimize the magnetic properties. Best results were obtained by subsequently crystallizing the as deposited film samples in situ at 900 K for 1 hour in Ar and then nitriding at 675 K in 0.75 atmosphere of N_2 gas.

Because of the low x-ray scattering factor for nitrogen, it is almost impossible to determine the atomic locations in the compounds from the x-ray data. However, neutron diffraction studies [67, 68] have shown that the nitrogen atoms occupy the 9e sites or 6h sites in the rhombohedral (Th_2Zn_{17}) and hexagonal (Th_2Ni_{17}) compounds respectively, and the composition of nitride is close to $R_2Fe_{17}N_3$. The 9e octahedral interstice lies in the c-planes that contain the rare earths coordinated by two RE atoms and four TM atoms. Nitrogen atoms located very close to RE atoms enhance strongly the crystal field-induced

anisotropy of the RE sublattice in the $R_2Fe_{17}N_x$. Interstitial proximity of nitrogen atoms to RE atoms in $Sm_2Fe_{17}N_x$ leads to a drastic enhancement in the RE sublattice anisotropy. As nitrogen atoms enter the interstitial sites in $Sm_2Fe_{17}N_x$, they are expected to modify the crystal structure, exchange interactions, and anisotropy constant. It seems that this atomic scale perturbation is very helpful in modifying the microstructure itself that increased the coercivity.

The maximum coercivity of the $Sm_2Fe_{17}N_x$ film samples depends on volume percentage of the nitrided phase present. For pure Sm_2Fe_{17}, K1 is negative (easy plane), but as the nitrogen enters the 9e sites it creates a strong electric field gradient at the Sm 4f shell. As a result the crystal field coefficients are modified and K1 increases. For the un-nitrided "soft centers", K1 remains negative and these centers will act as nucleation centers to aid the domain reversal and therefore decrease the coercivity.

New high performance permanent film magnets were synthesized as a result of nitriding (in situ) of subsequently crystallized 2-17 phase. Peak positions shifted significantly toward the lower diffraction angles, indicating increased cell volume. Peak widths were also increased upon nitriding. Sputter process parameters such as crystallization temperature, crystallization time, nitrogen pressure, nitriding temperature, and nitriding time must be adjusted in order to obtain the optimum magnetic properties in $Sm_2Fe_{17}N_x$ system. The material seemed to be thermodynamically metastable w.r.t. SmN and α-Fe at ambient temperatures. It certainly disproportionate at elevated

temperatures. Moreover nitriding at high temperature presumably introduced relatively higher stress in the film as the films synthesized at high nitriding temperatures peeled off. Therefore, the nitriding should be performed below the dissociation temperature for the optimized times in order to obtain the optimum magnetic properties . Impurities in the starting phase may also play a role in the rate and degree of nitriding ultimately achieved. Nitriding profoundly changes the magnetic properties and substantially improved the Curie temperature and room temperature saturation magnetization. High Curie temperature, high saturation magnetization and strong uniaxial anisotropy makes $Sm_2Fe_{17}N_x$ an attractive candidate for permanent magnet applications. Unfortunately, the precipitation of α-Fe and limited thermal stability of $Sm_2Fe_{17}N_3$ have so far restricted the application of the compound. Samples show no tendency to degrade in air up to two years after preparation at room temperatures.

In bulk processing of RE-TM compounds, hydrogen has been known to occupy two fairly large interstitial sites namely 9e, and 3b. At the temperatures of about 250° C, hydrogen gas easily reacts with Sm_2Fe_{17}, but the hydride remains easy plane with much less increase in Curie temperature.[69] As the results of $Sm_2Fe_{17}H_x$ were not very convincing, so the project of hydrogenation of Sm_2Fe_{17} compounds was not persuaded. To summarize, the strong uniaxial anisotropy in $Sm_2Fe_{17}N_x$ and its high Curie temperature and room temperature magnetization make this compound a promising material for permanent magnet applications.

CHAPTER 6

ANOTHER NEW HIGH COERCIVITY, $_iH_c$, Sm_5Fe_{17} PHASE

6.1 Introduction

The quest of non cobalt containing magnets was stimulated by the discovery of $Nd_2Fe_{14}B$ and lead to the evolution of numerous stable as well as metastable phases. In order to synthesize the extremely textured (002) films, the Sm rich targets were used as highly (002) texture of $ThMn_{12}$-type phase could be formed only at very high temperatures. With these Sm rich targets ($\approx$ 20 at% Sm), instead of directly crystallizing, the subsequently crystallization technique was used. On measuring the hysterisis loops, another high coercivity SmFe binary phase was discovered. This new phase with extremely high room temperature coercivity has been identified as Sm_5Fe_{17} with hexagonal structure, a = 20.061 Å c = 12.282 Å.

Sputtered films of $Sm_5(Fe_{1-x}Ti_x)_{17}$ deposited onto room temperature substrates and then subsequently crystallized were reported to exhibit room temperature in plane coercivities of 38.5 kOe. Highest in plane room temperature coercivities about 46 kOe were reported for sputter synthesized samples corresponding to intermediate compositions of Ti, and V. However, mechanically alloyed samples of $Sm_5(Fe_{1-x}Ti_x)_{17}$ at compositions similar to sputter synthesized samples showed room temperature coercivities of slightly

more than 50 kOe. For these bulk samples, the remanence B_r values were reported to be about 3 kG that yielded extrapolated saturation $4\pi M_s$ values of 6 kG substantially decreasing the energy product values.

The Sm_5Fe_{17} phase was presumed [74] to exist only for ternary compounds $Sm_5(Fe_{1-x}T_x)_{17}$ where T = Ti, V, etc. However, as a permanent magnet, the addition of a nonmagnetic third element is detrimental to the saturation moment that reduces the available energy product considerably. In addition, the third element T is presumed to be passive in its contribution to the magnetocrystalline anisotropy. The 5-17 structure type was first associated with the high $_iH_c$ Sm-Fe-Ti as an analog of the low coercivity Nd_5Fe_{17} phase first reported by Schneider et. al.[70, 71, 72] X-ray diffraction data analysis on single crystals were reported to have hexagonal space group P63/mcm. Schneider et. al also established that the Nd_5Fe_{17} structure is built up of layers which are a tessellation of triangles, pentagons, hexagons, and heptagons such that the unit cell consists of 12 formula units. Stadelmaier et al [73] gave a comparison of indexing of SmFeTi high coercive phase with Nd_5Fe_{17}. At that time, formation of Sm_5Fe_{17} had not been reported.

For the first time, magnetically hard two element Sm_5Fe_{17} phase have been successfully synthesized in the sputtered films without the addition of a phase stabilizing third element. These films were synthesized by at first making an amorphous 2-3 μm thick deposits of desired composition and then crystallizing these deposits by heating in situ. This method of crystallization produced fine grained crystallites 300 to 600 Å in the

diameter. The orientation of c-axis in such crystallites was found to be random.

6.2 Magnetic Properties

High field magnetic hysterisis loops were measured for the temperature range of 15 K to room temperature as shown in Fig. 21. The shape of initial magnetization suggest that the magnetization process is a combination of both the pinning and nucleation type. The samples were magnetically isotropic as demonstrated by the identical shapes of the hysterisis loops measured in the film plane and perpendicular to the film plane. The room temperature ${}_iH_c$ was 14.7 kOe with a smooth rise to 31.1 kOe at 15 K. These values were far higher than any previously reported values for a two element Sm-Fe compound. For this entire range of temperature, it was not possible to saturate the magnetization up to an applied field of 90 kOe. The room temperature remanent magnetization values measured for this binary phase were about 5 kG, that yielded saturation moment of approximately 10 kG, which is significantly larger than the estimated value, 8 kG, for the ternary 5-17 sputter synthesized phase.

6.3 Crystal Structure of Sm_5Fe_{17} Phase

The as-deposited films were found to be amorphous as evidenced by a weak shoulder in the x-ray diffraction pattern obtained by using $Cu_{K\alpha}$ radiation. X-ray

diffraction traces, $Cu_{K\alpha}$, for samples crystallized at 720 K for 30-75 minutes exhibit only 5-17 lines. In the 2θ range of 25 - 55 , thirty seven reflections were observed as summarized in Table 8. All the thirty seven lines can be fitted, for fitting tolerance on $2\theta \leq 0.05$, to a hexagonal structure with a = 20.06 ± 0.01 Å, and c = 12.28 ± 0.01 Å., about 2% smaller than Ti stabilized $Sm_5(Fe, Ti)_{17}$ compound as shown in the Table 9. Since the a lattice parameter is so large, only a few of the diffraction lines are uniquely indexed. The most intense line at 2θ = 34.47 is assigned to the possible indices (314), (333), and (432). In the 5-17 films, the crystallite c-axis distribution was found to be random, there being no preferred c - axes orientation of crystallites. A sample crystallized for 75 minutes at 720 K is shown in the Fig. 22(a). All the thirty seven observed lines in this x-ray diffraction pattern could be fitted to a hexagonal cell with lattice parameters a = 20.06 ± 0.01 Å, and c = 12.28 ± 0.01 Å as seen in the Table 9.

6.4 Effect of Crystallization Time, C.T., on Composition of Sm_5Fe_{17} Phase

Figures, 22(b) and 22(c) show similar sample crystallized at 720 K for successively longer crystallization times, 360 and 990 minutes. The 5-17 phase is being gradually replaced by a mixture of (5-17) + (2-17) + (α-Fe) + Sm_2O_3, as shown in the Fig. 22(b), and then to a same phase mix with α-Fe becoming the dominant phase. Fig. 23(c) shows a similar base composition film heated to 600 K for 75 minutes. The deposit was not crystallized at this lower temperature. The lack of any developed lines indicated that the deposit was still amorphous. The only sharp line observable at higher angle was

from the substrate.

Samples crystallized for shorter and longer times exhibited lower coercivities as shown in the Fig. 24. The partial loop shown in this Fig. (a), crystallized for 30 minutes, was obtained by high field measurements. Fig.s 24(b), and 24(c) show similar samples for successively longer crystallization times, 360 minutes and 990 minutes.

There was a systematic increase and then reduction in the width to height ratio of hysterisis loops as the 5-17 phase initially forms over the first 30 minutes and then decomposes.

Towards the higher end of crystallization temperature range x-ray diffraction studies showed the presence of soft magnetic phases like α-Fe and Th_2Zn_{17} type phases alongside the magnetically hard 5-17 phase. As a measure of fraction of the 5-17 phase in the multi-phase films a concentration "F" factor was determined from hysterisis loops as given below:

$$F = \left(\frac{Width\ at\ 4\pi M{=}0}{Height\ 2\cdot(4\pi M_s)}\right)\cdot\left(\frac{1}{N_{30\,\mathrm{min.}}}\right) \qquad \text{------ (25)}$$

where $N_{30\,\mathrm{min.}}$ is

$$N_{30\,\mathrm{min.}} = \frac{Width\ at\ 4\pi M{=}0\ for\ 30\ \mathrm{min.}}{Height\ 2\cdot(4\pi M_s)\ for\ 30\ \mathrm{min.}} \qquad \text{------ (26)}$$

Figure 25 shows a plot of this Sm_5Fe_{17} phase concentration indicator, F, versus crystallization time. The F concentrations have been normalized using the properties as measured for samples crystallized for 30 minutes. No second phase can be detected in the sample used as the normalization base. The exact correspondence between the percentage of Sm_5Fe_{17} concentration in the samples and the F function has not been precisely determined. The longer crystallization times as well as higher temperatures drastically degrade the film properties. The overall samarium concentration in the film decreased from an initial 24 at% to about 12 at% at the end of 990 minutes as seen from the data summarized in Table 10.

The range of temperature for obtaining optimum magnetic properties were determined to be 700 K - 750 K for the crystallization time of 70 minutes. However, the range of crystallization temperature may depend on the crystallization time.

Minimum crystallization time for obtaining the optimized magnetic properties was found to be 30 minutes at crystallization temperatures of 720 K. Again, the minimum crystallization time may be different for different crystallization temperatures. There was a systematic increase and then reduction in the width to height ratio of hysterisis loops as the 5-17 phase initially formed over the first 30 minutes and then decomposed.

6.5 Thermal Stability of Sm_5Fe_{17} Phase

Figure 26 shows the high temperature hysterisis loops for the 5-17 phase measured at low applied fields of ≈ 18 kOe for the temperature range of 300 K to 725 K. During the measurements, sample was protected from oxidation by maintaining constant flow of purified Ar gas. There were systematic decreases in the in-plane coercivity, remanence, and magnetization with temperature for these film samples as seen in Table 11. However it was not possible to determine the Curie temperature of this compound as this 5-17 phase was not stable enough at the crystallization temperatures to prevent continuous evaporation of samarium from the film.

Figure 27 shows temperature dependence of magnetic properties such as remanence, coercivity, and magnetization, for Sm_5Fe_{17} phase as measured by VSM applying the magnetic fields up to 18 kOe in the temperature range of 25° C to 450° C. The reversible temperature coefficients from 25° C to 100° C for Sm_5Fe_{17} phase were $\alpha(B_r)$=-0.105%/° C, $\beta({}_iH_c)$=-0.032%/° C, and $\gamma(4\pi M @ 15\ kOe)$=-0.155%/° C.

The remanence decreased slowly from 25° C to 100° C, while quite rapidly in the temperature range of 250° C - 350° C and reduced to zero at 400° C and at 450° C does not show paramagnetic behavior because of α-Fe precipitation. Irreversible reduction in the remanence with temperature were related to the metastable character of the 5-17 phase as evidenced by the x-ray diffraction pattern.

Coercivity did not change appreciably in the temperature range of 25° C to 100° C , started dropping slowly from 100° C to 175° C, however quite rapidly in the temperature range of 175° C - 300° C. Its value at 300° C was 300 Oe and dropped to 100 Oe at 400° C. The temperature dependence of the coercivity curve is shown in Fig. 27. However, the best film samples with the least amount of impurity phases showed room temperature coercivity of 14.7 kOe as seen in the Fig. 20.

For $T \geq To$, ${}_iH_c$ decreases with temperature because higher activation energy is available for the particles or domain walls in order to overcome the energy barriers. On the other hand, as T is lowered below To, $T \leq To$, the available activation energy decreases, thereby requiring much higher applied fields for the domain reversal.

Magnetization ($4\pi M$) @ 15.5 kOe of applied field showed quite different behavior. It decreased at a rate of 0.155%/° C from 25° C to 100° C and relatively slowly from 100° C to 250° C. After 400° C, it started increasing indicating the precipitation of α-Fe from the Sm_5Fe_{17} phase.

Fig. 28 shows the x-ray diffraction trace obtained from the sample cooled down to room temperature after subjecting to high temperature. It showed decrease in the intensity of Bragg lines and increase in the diffused background. Intensity of low G(hkl) was affected less than the reflections of high G(hkl). Figure 29 shows the hysterisis loops measured at room temperature after cooling down the sample to room temperature. The

tailing of the hysterisis curve in the third quadrant indicates the persistence of 1-5 phase even on subjecting the sample to high temperatures.

Figures 30, and 31 show the hysterisis loop and x-ray diffraction trace of a 5-17 sample on nitriding. It showed soft magnetic properties with easy plane behavior consistent with the precipitation of α-Fe. The intensity of α-Fe peak increased with longer nitriding times for a given temperature.

6.6 Conclusion

Development of the high ${}_iH_c$ phase for strictly two element Sm, Fe system were studied. Single phase Sm_5Fe_{17} film samples were synthesized with a record high coercivities of 14.1 kOe for this two element Sm, Fe system. Optimum sputter conditions were determined in order to obtain good permanent magnet properties. Attempts were made to elucidate the origin of magnetic hardening by correlating the magnetic properties to the crystal structure and the microstructure of the synthesized 5-17 films. Coercivity increased at low temperatures and reached the value of 31.1 kOe at 15 K. This was the highest value reported for two element Sm-Fe phase at the cryogenic temperatures

The synthesis of binary Sm_5Fe_{17} phase provides basis to determine the volume expansion on adding the third element like Ti, V, etc. Addition of third element lead to a systematic increase in the cell volume. This implies that the Ti and V are actually

acting as replacement elements for Fe in the primary magnetic phase.[44, 48, 74, 75]

The somewhat high temperature and long time exposure has resulted in the formation of 1-3, and 2-17 phases with only traces of 5-17 phase. Short diffusion heat treatment seems to favor the formation of Sm_5Fe_{17} phase. The longer crystallization time have significant effect on the kinetics of amorphization and disproportion. The subsequent crystallization method lead to reasonable coercivities but with the restriction that the material is magnetically isotropic. The coercivity of Sm_5Fe_{17} samples is comparable to 2-14-1 type materials. However technical applications are not evident because of the high Sm content. Attempts to nitride Sm_5Fe_{17} resulted in the decomposition into Fe and amorphous Sm. It has not been possible to directly crystallize the Sm_5Fe_{17} phase onto heated substrates.

However temperature about 700 K is found to be an optimum temperature in order to obtain the best magnetic properties as shown in the Fig. 20. It shows in plane hysterisis loops for a sample crystallized at T = 720 K for 30 minutes. The room temperature ${}_iH_c$ was 14.7 kOe with a smooth rise to 31.1 kOe at 15 K. These values are far higher than any value reported for two element Sm-Fe compound.

CHAPTER 7

ALIGNED HIGH ANISOTROPY $Pr(Fe,Co,Mo)_{12}N_x$ PHASE

7.1 Introduction

In chapter 5, it has been discussed that the RE-TM intermetallics of the type RE_2Fe_{17} can absorb moderate quantities of nitrogen at 450° C giving the approximate composition $RE_2Fe_{17}N_3$ at 570 Torr of N_2. X-ray diffraction showed that the rhombohedral structure is retained but with increased lattice parameters. The increase in lattice parameters clearly indicates that nitrogen atom occupy the interstitial sites. Furthermore, profound changes in magnetic properties have occurred on nitriding. More significantly, the anisotropy of the compound changed from easy plane to easy axis, and Curie temperature increased by about 50%. As the film samples of $Sm_2Fe_{17}N_3$ could be obtained only through the subsequent crystallization technique, it was not possible to synthesize in the textured form, thereby severely limiting the remanence and energy product for these film magnets.

High anisotropy oriented sputtered film samples of $Pr(Fe_{12-y-z}Co_yMo_z)N_x$, where y = 0-2.5, and z = 0.4-1.0, compounds were synthesized. The nitrided film samples with room temperature coercivity of 9.4 kOe were synthesized for as low as twenty five minutes of in situ nitriding times. Work done elsewhere [76, 77] reported the formation of

arc melted $PrMo_{1.5}Fe_{10.5}$ compounds and their nitrides, with 2 kOe coercivities at room temperature for the nitrides. Before nitriding, the films exhibited non uniaxial soft magnetic properties with room temperature coercivities of ≈ 0.70 kOe. The film synthesis procedure is similar to those discussed previously for the synthesis of other highly aligned $ThMn_{12}$ type systems.[78, 13]

7.2 Experiment

Oriented films of approximately 2 to 3 μm thickness were synthesized by the direct crystallization of the desired compositions through R. F. sputtering onto heated polycrystalline Al_2O_3 substrates in the temperature range of 675 K to 800 K. The sputtering targets used in these studies were made by arc melting in an inert atmosphere from pure elements of at least 99.9% pure. The sputtering deposition chamber had a base pressure of $5 \cdot 10^{-8}$ mTorr. The sputtering gas pressure was 75 mTorr of Argon. The deposition rate was ≈ 1.2 Å/s. These films were nitrided in situ at 570 Torr of N_2 for times ranging from 5 minutes to 150 minutes. The nitriding temperatures were varied from 700 K to 850 K. The magnetic data reported were measured using vibrating sample magnetometers. The x-ray diffraction data was collected with a digital system using $Cu_{K\alpha}$ radiation.

7.3 Results and Discussion

Figure 32 shows hysterisis loops for an un-nitrided $Pr_{1.03}Fe_{10.44}Co_{1.13}Mo_{0.40}$ sample synthesized under similar sputter conditions before nitriding. It exhibited soft magnetic properties consistent with easy plane anisotropy. The room temperature flux density was higher in the film plane as compared to that perpendicular to the film plane. The field required to obtain saturation in the direction perpendicular to the film plane, obtained by extrapolation, was 34.8 kOe. The atomic percentage of Pr was slightly higher as compared to the stochiometric composition for $Pr(Fe,Mo,Co)_{12}$ films.

Figures 33 and 34 respectively show T = 293 K, and T = 10 K, demagnetization curves for a $Pr_{1.04}Fe_{10.36}Co_{1.16}Mo_{0.44}N_x$ sample. This film exhibited an extreme degree of texturing such that the c-axes of the grains were aligned perpendicular to the film plane. For T = 293 K, the perpendicular to the film plane saturation flux density, $4\pi M_s$ = 11.6 ± 0.5 kG, intrinsic coercivity ${}_iH_c$ = 9.40 kOe, and maximum energy product BH_{max} = 23.6 MG-Oe. For the T = 10 K curve, $4\pi M_s$ = 12.5 ± 0.5 kG, ${}_iH_c$ = 22.0 kOe, and BH_{max} = 32.8 MG-Oe. As will be discussed shortly this film was in situ nitrided for a time long enough to maximize the coercivity. Such samples were taken as fully nitrided with ≈ 1N per $ThMn_{12}$ formula unit. The nitrided tetragonal lattice cell parameters were a = 8.78 Å, and c = 4.87 Å.

Figures 34 (a) and (b) show the magnetization curves measured in the film plane

and perpendicular to the film plane at 10 K and 293 K respectively. Note that measurements perpendicular to the film plane correspond to measurements parallel to the crystallite c-axes. From these curves, the anisotropy field of $Pr_{1.04}Fe_{10.36}Co_{1.16}Mo_{0.44}N_x$ sample was estimated to be 144 kOe and 96.5 kOe at 10 K and 293 K respectively. The anisotropy field for $Pr(Fe,Mo,Co)_{12}N_x$ film samples did not differ significantly over a wide range of cobalt compositions i.e., from 2.8 at% to 15.0 at% metallic composition of the 1-12 phase.

Figure 36 shows the X-ray diffraction traces, $Cu_{K\alpha}$ radiation, before and after nitriding. The direct synthesis of Pr-Fe-Mo-Co films into $ThMn_{12}$ phase with systematic control of deposition conditions allowed us to obtain an extreme degree of crystallographic texturing upon deposition. Figure 37 shows cell volume as a function of nitriding time. Following in situ nitriding the $ThMn_{12}$ type tetragonal structure was retained with ≈ 4% increase in cell volume which saturated for a nitriding temperature of 750 K after about the first 15 minutes of nitriding time at 6.9%. This behavior is shown in Fig. 37 by smooth increase of cell volume from ≈ 4% to 6.9% in fifteen minutes of nitriding time. The observed cell volume increase is larger than that observed in bulk samples because of the film strain effects. The Full Width at Half Maxima, FWHM, of the x-ray diffraction lines was unchanged after nitriding. The lines were fairly sharp before and after nitriding even for samples with very short nitriding times.

The variation of ${}_iH_c$ was studied as a function of nitriding time. Series of film

samples were sputter synthesized under similar sputter conditions except for the nitriding time. As shown in Fig. 38, the maximum room temperature coercivity, ${}_iH_c$, perpendicular to the film plane was 9.4 kOe, for the film sample directly crystallized at 725 K and 75 mTorr of Argon and nitrided at 750 K and 570 Torr of N_2 for 25 minutes. An attempt was made to determine the minimum nitriding time at various nitriding temperatures for optimized magnetic properties. At room temperatures, the saturation flux density measured perpendicular to the film plane for high field measurements up to 90 kOe of applied fields was 10.5 ± 0.5 kG for $Pr_{1.05}Fe_{11.17}Mo_{0.78}N_x$, and 11.6 ± 0.5 kG for $Pr_{1.04}Fe_{10.36}Co_{1.16}Mo_{0.44}N_x$ samples. For measurements perpendicular to the film plane, the room temperature static energy product was 23.6 MG-Oe which increased to 32.8 MG-Oe at 10 K. This is the highest value ever reported for $Pr(Fe,Mo,Co)_{12}N_x$ $ThMn_{12}$ type samples. The nitriding time for the $Pr_{1.04}Fe_{10.36}Co_{1.16}Mo_{0.44}N_x$ sample was 25 minutes, however the minimum nitriding time was 10 minutes at 850 K, and the room temperature coercivity measured following low field magnetization to 18 kOe perpendicular to the film plane was 6.4 kOe for a similar composition sample.

The films offer a unique advantage of studying the shortest possible nitriding times of the order of a few minutes as compared to that of several hours needed for the bulk samples to nitride. Moreover even after several hours of nitriding time, it is not possible to nitride the inner core of the bigger sized grains in the bulk samples.

7.4 Conclusion

Sputter deposition with systematic control of the deposition parameters allowed us to achieve an extremely high degree of c-axes texturing perpendicular to the film plane. For each nitriding temperature, the minimum nitriding time was determined for optimized magnetic properties.

It should be noted that perpendicular to the plane coercivity reached a maximum after the volume increase upon nitriding had saturated. Upon partial site filling the volume has to assume that saturated volume or else the cell would need to be distorted which is inconsistent with the x-ray data. The magnetic anisotropy and coercivity, however, continued to change until the N sites were filled. The maximum in coercivity was taken as the indicator of full site occupancy rather than the cell volume saturation time for that reason. Longer than necessary nitriding times resulted in some phase deterioration with a lower than optimal coercivity. For higher nitriding temperatures, less nitriding time was required to optimize the coercivity. For 850 K, the optimum nitriding time was found to be 10 minutes.

The room-temperature easy plane anisotropy field of $Pr_{1.05}Fe_{11.20}Mo_{0.76}$, and $Pr_{1.03}Fe_{10.44}Co_{1.13}Mo_{0.40}$ samples, were 30 kOe and 34.8 kOe respectively. On nitriding a profound change of magnetocrystalline anisotropy occurred, the easy plane anisotropy switched to easy axis anisotropy. The highest room temperature coercivity and energy

product were obtained for a $Pr_{1.04}Fe_{10.36}Co_{1.16}Mo_{0.44}N_x$ sample. For this film at 293 K, the perpendicular to the film plane saturation flux density, $4\pi M_s$ = 11.6 ± 0.5 kG, the intrinsic coercivity ${}_iH_c$ = 9.40 kOe, and maximum energy product BH_{max} = 23.6 MG-Oe. At 10 K, the corresponding $4\pi M_s$, ${}_iH_c$, and BH_{max}, were 12.5 ± 0.5 kG, 22.0 kOe, and BH_{max} = 32.8 MGOe respectively.

CHAPTER 8

CONCLUSIONS

This thesis work has elucidated a systematic study of synthesis processes and magnetic properties for Sm-Fe film system. The sputter parameters were varied in a controlled fashion firstly to study the formation conditions for new phases, and secondly to optimize the magnetic properties, and obtain strong crystal texturing, specifically in $ThMn_{12}$ type phase, as a function of sputtering gas pressure and substrate temperature. Two highly uniaxial new magnetic phases were discovered, for the first time, in the Sm-Fe binary system namely $SmFe_{12}$, and Sm_5Fe_{17}, in film form, by sputtering using arc melted targets made from pure constituents.[79] There are two important features associated with the search for these uniaxial magnetic phase, firstly these are Fe-based, secondly these are synthesized without adding any third non magnetic element such as Ti or V that decreases the remanent magnetization of the compound. Neither of these phases have been synthesized as two element compounds by any bulk processing methods.

Films magnets were sputter synthesized by direct crystallization as well as subsequent crystallization process. It is quite interesting to note that the phases observed in the sputtered films were a sensitive function of the sputter mode employed. The control of deposition conditions allowed the preparation of stochiometric films of multi-

component alloys and compounds. The atomistic growth process with systematic control over deposition parameters yielded highly aligned $ThMn_{12}$ type samples on one hand and randomly oriented crystallites in Sm_5Fe_{17}-type samples on the other hand in the same system. These metastable phases have not been stabilized by any bulk processing methods without at least 10 at% of TM metal substitution by a non magnetic third element such as Ti, or Mo. Generally, bulk magnet processing is carried out at temperatures exceeding 800° C. So, the phases that are stable at high temperatures get locked onto. Such high temperature processing is not conducive to the formation of $SmFe_{12}$ phase which is known to be unstable at temperature of 800° C and above.

Films directly crystallized at almost all sputter conditions, above the crystallization temperature, exhibited $SmFe_{12}$ phase with texture that depend on the sputter conditions. An attempt has been made to explore the possible reasons for the texturing in the $SmFe_{12}$ structure as a function of sputter process parameters.

After sputter synthesizing, binary $SmFe_{12}$ films, the films were nitrided to see the effect of N_2 on the properties of $SmFe_{12}$ phase. The easy axis behavior changed to easy plane behavior accompanied by the intense precipitation of α-Fe.

Attempts to nitride 1-12 magnets in bulk form resulted the switching of easy axis behavior to easy plane behavior. However nitriding of strictly two element 1-12 films resulted in the precipitation of α-Fe. However interstitial sites in the 1-12 structure

could be occupied by smaller radius atoms such as hydrogen.[80-82] Reports about the hydrogenation of the 1-12 bulk samples showed that the easy axis behavior switched to easy plane behavior, thereby, rendering it as a useless compound.

The Sm_5Fe_{17} and Sm_2Fe_{17} phases have only been observed to form in the samples that were deposited by the direct crystallization technique. The hard magnetic phase, Sm_5Fe_{17}, is formed during a short diffusion heat treatment of 30 - 70 minutes at a temperature between 700 K - 750 K at 100 mTorr of Argon. The temperature dependence of saturation moment and anisotropy field in Sm_5Fe_{17} samples have been studied. Remanence, B_r, for subsequently crystallized 5-17 phase is lower than 1-12 phase due to a) low saturation magnetization of the compound (higher Sm content), and b) Samples were magnetically isotropic.

Film samples of $Sm_2Fe_{17}N_x$ with high coercivity were also synthesized with extremely high inplane room temperature coercivity. On nitriding, the Sm_2Fe_{17} phase, the easy plane behavior changed to easy axis behavior accompanied by a substantial increase in Curie temperature, and drastic change in the crystal anisotropy. The expansion-induced increase of Curie temperature, therefore, reflects the volume dependence of the exchange interactions.[82] The hard magnetic properties of nitrided Sm_2Fe_{17} films were studied and compared with those of 1-12. In the bulk form, no metallurgical process has so far succeeded in producing alignment of the crystallites of nitrided 2-17 magnets, thus severely limiting the energy products in these magnets. Generally, strongly textured films

have been obtained through direct crystallization techniques by R. F. sputtering. Unfortunately, it was not possible to synthesize textured 2-17 type films in the course of these studies using direct crystallization technique.

In order to synthesize high energy product permanent film magnets, highly aligned (002) textured sputtered films of $Pr(Fe_{12-y-z}Co_yMo_z)N_x$, where y = 0-2.5, and z = 0.4-1.0 compounds were synthesized. X-ray diffraction traces showed that the $ThMn_{12}$ type tetragonal structure was retained with ≈ 4-6.9% increase in cell volume. Fortunately, there is a strong increase of the lattice parameters upon nitrogen uptake, which has been used as a guide for the nitrogen concentration. The magnetic properties specifically coercivity in nitrided compounds differ slightly owing to the different absorption content of nitrogen. The samples slightly richer in Pr showed somewhat higher coercivity perpendicular to the film plane as compared to stochiometric $Pr(Fe,Co,Mo)_{12}N_x$ films. From high field measurements to 80 kOe, the maximum room temperature coercivity perpendicular to the film plane was 9.4 kOe, which rose to 22.0 kOe at 10 K which is higher than any values reported for bulk samples. The $4\pi M_s$ value at 80 kOe measured perpendicular to the film plane was 11.6 ± 0.5 kG for $Pr_{1.04}Fe_{10.36}Co_{1.16}Mo_{0.44}N_x$ samples, and 10.5 ± 0.5 kG for $Pr_{1.05}Fe_{11.17}Mo_{0.78}N_x$ samples. After high field magnetization to 80 kOe, for measurements perpendicular to the film plane, the static energy product was 23.6 and 32.9 MGOe at 293 K, and at 10 K, respectively. The estimated anisotropy fields were 96 kOe and 144 kOe at 293 K, and 10 K, respectively for low cobalt film samples.[83]

Table 1. General Data on Various Structures Observed in RE-TM System

Compound	Structure type	Symmetry	RE Site	TM Site
$RE\text{-}TM_2$	$MgCu_2$	Cubic	8(a)	16(d)
	$MgZn_2$	Hexagonal	4(f)	2(a), 6(h)
$RE\text{-}TM_3$	$PuNi_3$	Rhombohedral	3(a), 6(c)	3(b), 6(c), 18(h)
	$CeNi_3$	Hexagonal	2(c), 4(f)	2(a), 2(b), 2(d), 12(k)
$RE_2\text{-}TM_7$	Ce_2Ni_{17}	Hexagonal	4(f1), 4(f2) 6(c1), 6(c2)	2(a), 4(e), 4(f) 6(h), 12(k)
	$GdCo_7$	Rhombohedral		3(b), 6(c) 9(e), 12(h)
$RE_6\text{-}TM_{23}$	Th_6Mn_{23}	Tetragonal	24(e)	4(b), 24(d) 32(f1), 32(f2)
$RE\text{-}TM_5$	$CaCu_5$	Hexagonal	1(a)	2(c), 3(g)
$RE_2\text{-}TM_{17}$	Th_2Zn_{17}	Hexagonal	2(b), 2(d)	6(g), 12(j)
	Th_2Ni_{17}	Rhombohedral	6(c)	6(c), 9(d) 18(f), 18(h)
$RETM_{12}$	$ThMn_{12}$	Tetragonal	2(a)	8(f), 8(i), 8(j)

Table 2. Powder Diffraction Pattern of $SmFe_2$ Cubic $MgCu_2$ Type Structure
($Cu_{K\alpha}$ = 1.5418 Å) a = 7.417 Å

2θ $Cu_{K\alpha}$	d(Å)	(hkl)	(I/I_0)
34.19	2.622	(220)	70
40.33	2.236	(311)	100
42.21	2.141	(222)	15
61.22	1.514	(422)	20
65.38	1.427	(511)	25
72.02	1.311	(440)	15

Table 3. Powder Diffraction Pattern of $SmFe_3$ Rhombohedral $PuNi_3$ Type Structure ($Cu_{K\alpha}$ = 1.5418 Å) a = 5.187 Å, c = 24.91 Å

2θ $Cu_{K\alpha}$	d(Å)	(hkl)	(I/I_0)
32.09	2.789	(107)	40
34.58	2.593	(110)	50
35.06	2.559	(018)	50
40.32	2.237	(021)	50
40.82	2.210	(202)	100
42.80	2.113	(024)	20
43.60	2.076	(0,0,12)	40
44.23	2.048	(2,0,5)	50
44.82	2.022	(0,1,11)	40
47.89	1.899	(0,2,7)	20
55.32	1.714	(0,0,15)	10
55.55	1.654	(0,0,14)	10

Table 4. Powder Diffraction Pattern of Sm_2Fe_{17} Rhombohedral Th_2Zn_{17} Type Structure ($Cu_{K\alpha}$ = 1.5418 Å) a = 8.553 Å, c = 12.443 Å

2θ $Cu_{K\alpha}$	d(Å)	(hkl)	(I/I_0)
30.01	2.977	(1,1,3)	50
31.18	2.868	(1,0,4)	20
36.39	2.469	(3,0,0)	60
37.77	2.382	(0,2,4)	50
42.26	2.138	(2,2,0)	100
42.61	2.122	(3,0,3)	100
43.49	2.081	(2,1,4)	40
43.64	2.074	(0,0,6)	20
47.86	1.901	(2,2,3)	60
48.80	1.886	(1,1,6)	50
49.45	1.714	(1,3,4)	20

Table 5. Possible Structure Fittings to the Observed Diffraction Lines in a Weakly Textured Sample of $SmFe_{12}$ Obtained by Using $Cu_{K\alpha}$ Radiations

2θ $Cu_{K\alpha}$	Hex. 1-5 h k l	Rhom. 2-17 h k l	Tetra. 1-12 h k l
30.10	1 0 1	1 1 3	2 1 1
37.33	1 1 0	3 0 0	0 0 2
43.30	2 0 0	2 2 0	2 0 2
48.58	2 0 1	2 2 3	2 2 2
51.13	- - -	- - -	3 1 2
60.34	- - -	- - -	3 3 2
62.56	2 0 2	2 2 6	4 2 2
63.01	- - -	- - -	2 1 3
67.21	3 0 0	3 3 0	3 0 3
71.29	3 0 1	3 3 3	3 2 3

Note: Based on the above fittings the respective lattice parameters are given below:

$a_{1\text{-}5}$ = 4.821 A $c_{1\text{-}5}$= 4.218 A

$a_{2\text{-}17}$= 8.351 A $c_{2\text{-}17}$=12.652 A

$a_{1\text{-}12}$= 8.438 A $c_{1\text{-}12}$= 4.805 A

Table 6. Volume and Density Changes in 1-5 to 2-17 Transformation

Hexagonal 1-5	Rhombohedral 2-17
a = 4.995 Å	a = 8.402 Å
c = 3.978 Å	c = 12.172 Å
$V_{1\text{-}5}$ = 85.954 Å^3	$V_{2\text{-}17}$ = 8.954 Å^3
$\rho_{1\text{-}5}$ = 8.599 g/cc	$\rho_{2\text{-}17}$ = 8.722 g/cc
For 1-5 to 2-17 trans.	$(\Delta V/V) = -3.8\,\%$
For 1-5 to 2-17 trans.	$(\Delta\rho/\rho) = 1.4\,\%$

Table 7. Volume and Density Changes in 2-17 to 1-12 Transformation

Rhombohedral 2-17	Tetragonal 1-12
a = 8.553 Å	a = 8.438 Å
c = 12.443 Å	c = 4.805 Å
$V_{2\text{-}17}$ = 788.30 Å^3	$V_{1\text{-}12}$ = 342.12 Å^3
$\rho_{2\text{-}17}$ = 7.902 g/cc	$\rho_{1\text{-}12}$ = 7.968 g/cc

Note: For 2-17 to 1-12 transformation the percent change in volume, x-ray density, and dumbell sites:

$(\Delta V/V) = -2.3\%$ (w.r.to 2-17)

$(\Delta V/V) = 0.8\%$ (w.r.to 2-17)

Increase in dumbell sites = 50%

Table 8. Observed Diffraction Pattern of Binary Sm_5Fe_{17} Phase, Hexagonal Structure
a = 20.061 Å c = 12.282 Å

2θ $Cu_{K\alpha}$	(hkl)	2θ $Cu_{K\alpha}$	(hkl)	2θ $Cu_{K\alpha}$	(hkl)
26.65	(330)	35.77	(440)	41.95	(631)
26.65	(322)	35.77	(404)	41.95	(712)
28.15	(421)	36.22	(530)	42.58	(720)
28.15	(223)	36.22	(513)	42.58	(533)
29.56	(104)	36.24	(531)	43.27	(542)
30.43	(332)	37.72	(414)	43.27	(325)
30.85	(600)	38.44	(433)	43.93	(524)
31.30	(323)	39.13	(523)	43.93	(415)
32.20	(520)	39.13	(504)	44.68	α-Fe
33.83	(610)	39.85	(711)	45.82	(335)
34.24	(224)	39.85	(334)	46.45	(730)
34.63	(314)	40.24	(622)	46.45	(543)
34.63	(432)	40.24	(424)	46.45	(216)
34.63	(611)	40.57	(613)	47.08	(633
35.44	(522)	41.17	(541)	48.01	(226)

Table 9. Percentage Increase in Volume and Change in X-ray Density on Substituting Ti, and V in Two Element Sm_5Fe_{17} Phase

Compound	a(Å)	c(Å)	V(Å^3)	% V	ρ(g/cc)
Sm_5Fe_{17}	20.061	12.282	4280.60	--	7.922
$Sm_5(Fe,V)_{17}$	20.115	12.318	4316.29	0.83	7.818
$Sm_5(Fe,Ti)_{17}$	20.169	12.354	4352.18	1.67	7.724
$Sm_5(Fe,V,Ti)_{17}$	20.142	12.336	4334.21	1.25	7.769

Note : V denotes the percent increase in the volme of Ti, and or V substituted compound w.r.t. pure Sm_5Fe_{17}.

Table 10. At% Sm Versus the Crystallization Time in a Sm_5Fe_{17} Sample

Time(min.)	At% Sm	Sample I.D.
15.0	4.81	FM612R2
21.5	24.44	FM613R2
26.0	24.35	FM614R2
30.0	24.22	FM610R2
60.0	22.99	FM611R2
75.0	22.02	FM604R2
240.0	18.86	FM608R2
360.0	13.49	FM609R2
990.0	11.67	FM616R2

Table 11. Thermo-Magnetic Data on Sm_5Fe_{17} Sample

Temperature T(°C)	Remanence B_r(kG)	Coercivity $_iH_c$(kOe)	Magnetization $4\pi M$ @ 15.5kOe
25	3.69	4.19	6.53
50	3.55	4.10	6.02
100	3.40	4.09	5.77
150	3.07	3.58	5.69
175	2.85	3.19	5.63
200	2.69	2.43	5.58
250	2.23	1.22	5.55
300	0.76	0.30	4.57
350	0.13	0.11	4.03
400	0.00	0.27	3.95
450	0.00	0.27	4.52

Table 12. Change in Cell Volume with N_2 Absorption for $Pr_{1.04}Fe_{10.36}Co_{1.16}Mo_{0.44}N_x$ Sample

Nitriding t(min.)	Lattice a(Å)	Parameters c(Å)	Volume V(Å^3)	%(ΔV/V)
0	8.58	4.77	351.9	-
5	8.66	4.83	362.5	3.01
10	8.74	4.87	372.3	5.78
15	8.78	4.87	376.4	6.96
35	8.79	4.87	376.4	6.96

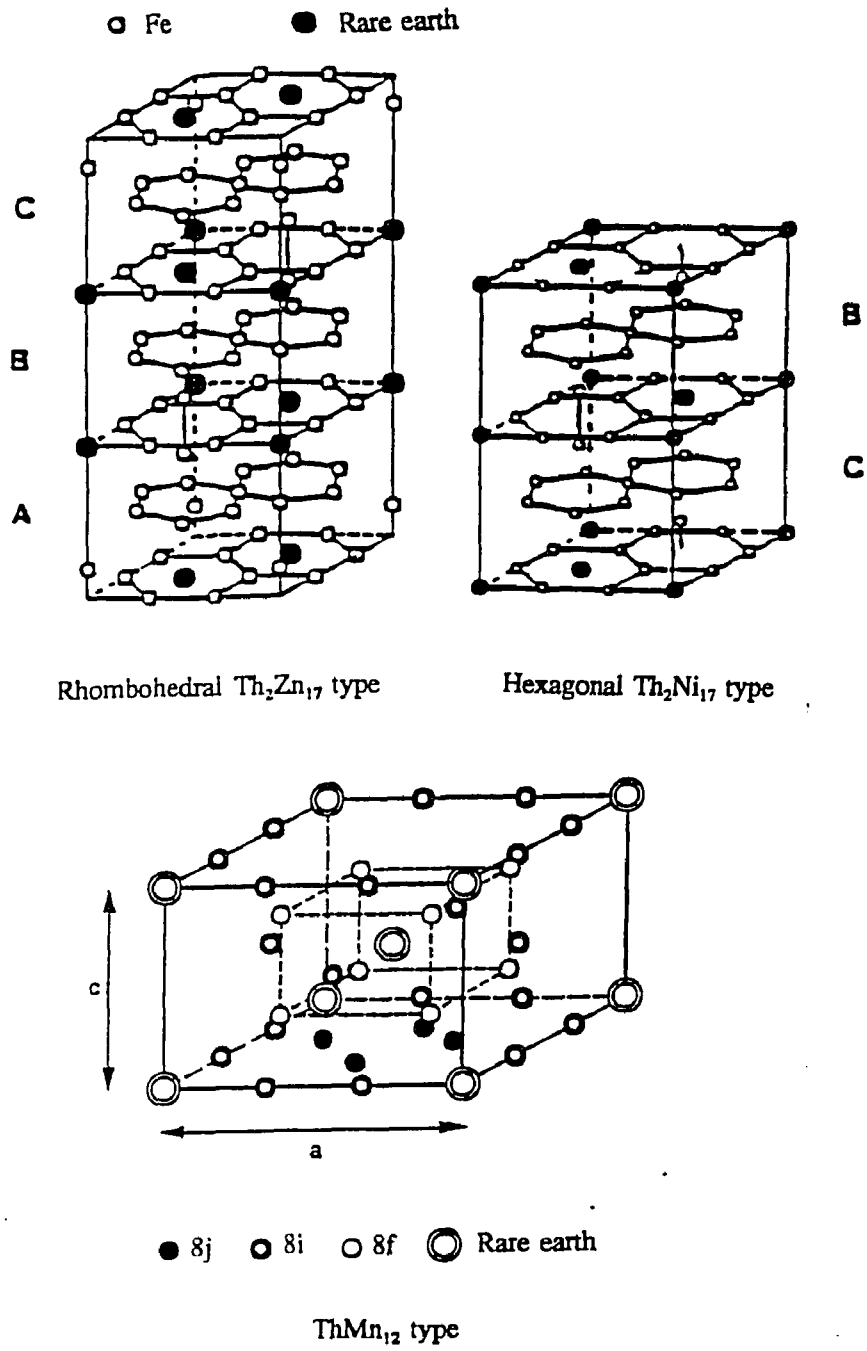

Fig. 1. Schematics of the crystal structure of Th_2Zn_{17}, Th_2Ni_{17}, and $ThMn_{12}$ type structures.

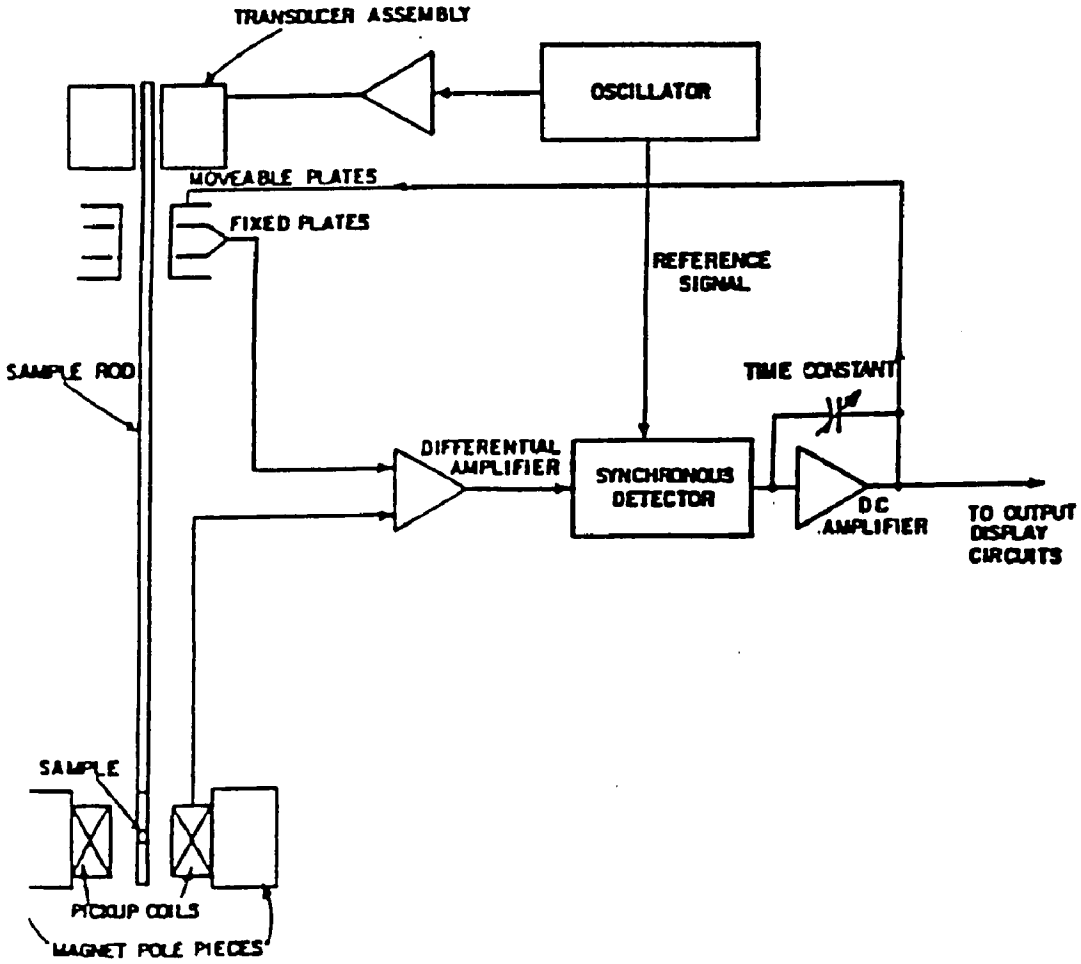

Fig. 2. Block diagram of a vibrating sample magnetometer.

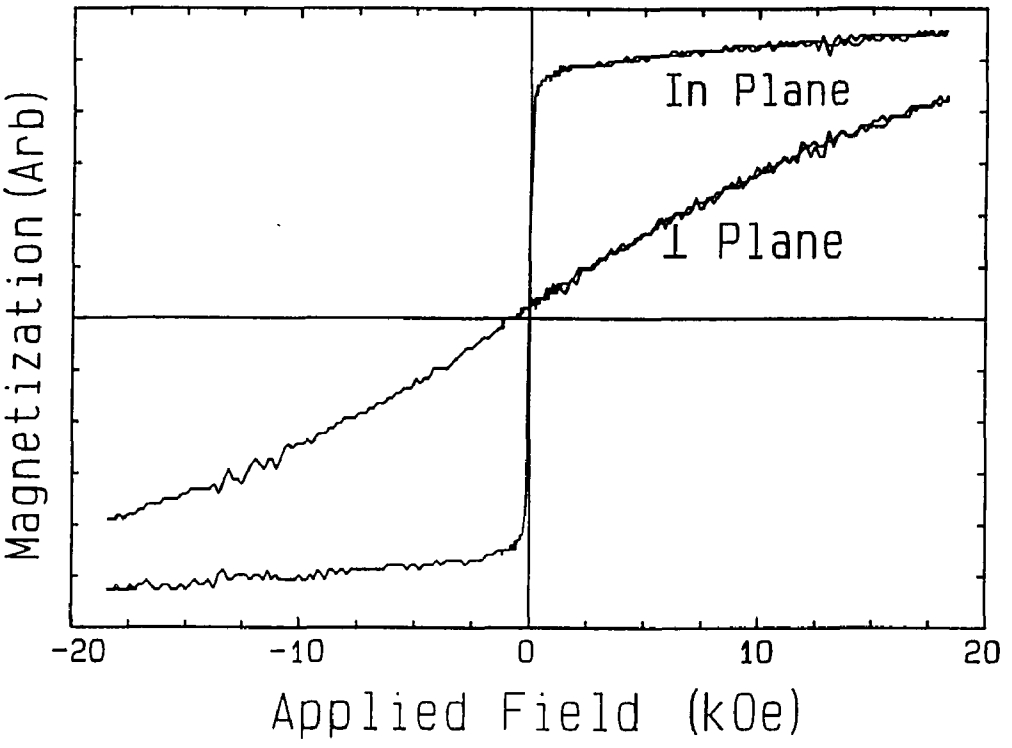

Fig. 3. Room temperature hysterisis loops representative of Sm, Fe binary samples with at% Sm = 8.5-10.5, directly synthesized in the temperature range of 450-600 K.

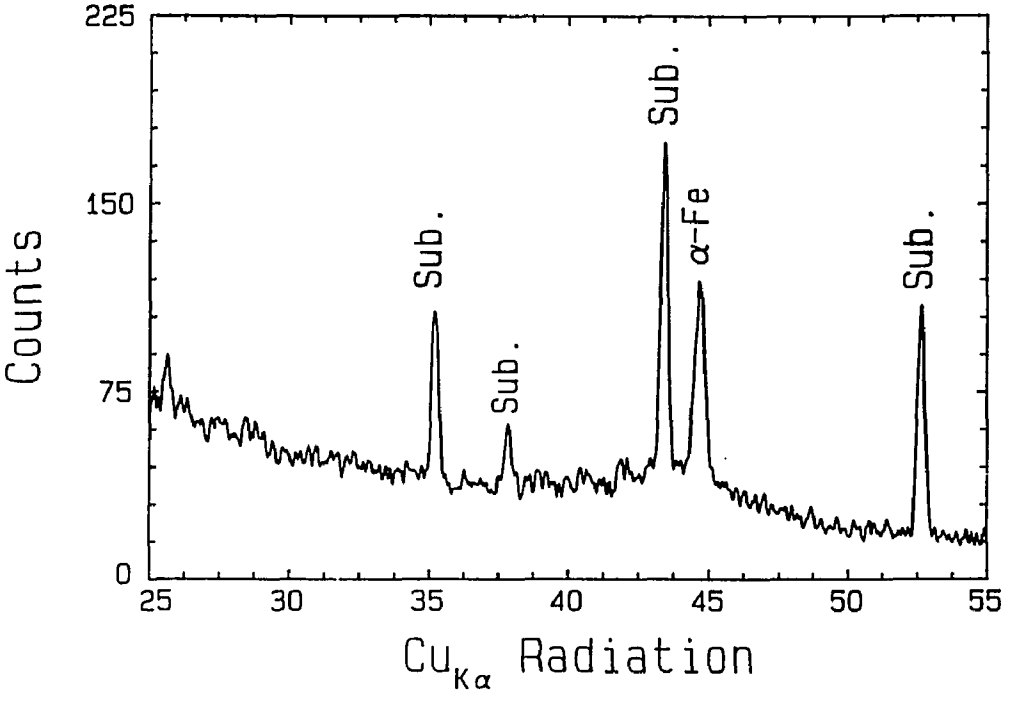

Fig. 4. $Cu_{K\alpha}$ x-ray diffractometer trace characteristic of Sm, Fe samples of Fig. 3.

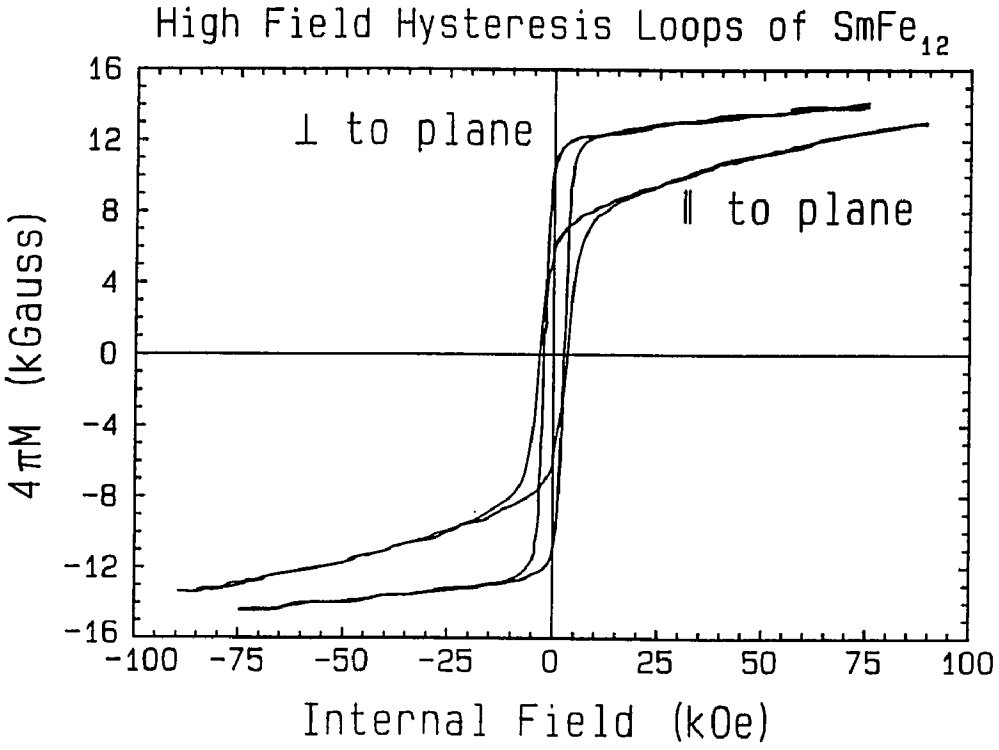

Fig. 5. Hysterisis loops for a strictly two element $SmFe_{12}$ sample measured in plane and perpendicular to the film plane. The coercivities equal 2.5 kOe perpendicular to the plane, and 3.3 kOe in plane. This sample was strongly (222) textured that tends to maximize the coercivity, but does sacrifice some remanence.

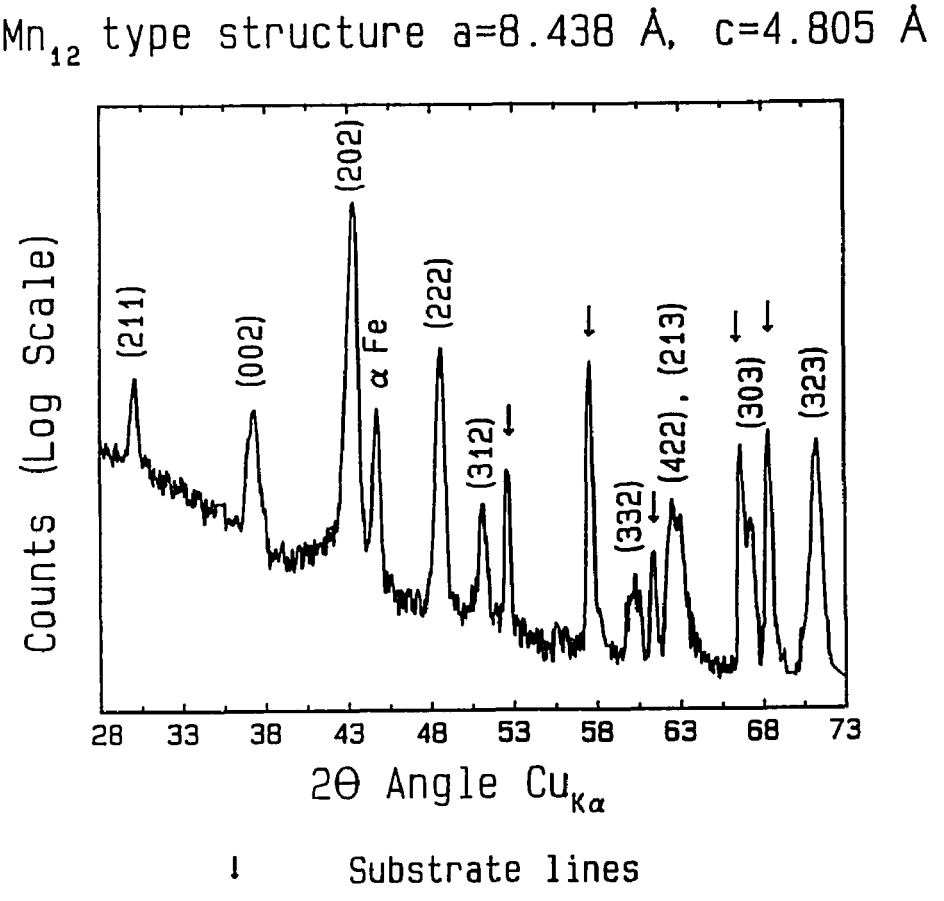

Fig. 6. $Cu_{K\alpha}$ x-ray diffraction trace of $SmFe_{12}$ film sputter deposited on the heated substrate. Y-axis is given in the log scale to accentuate the small peaks. A small quantity of impurity α-Fe phase was detected. 2θ calibration was aided by reflections from the substrate indicated by arrows. Indices shown are for tetragonal 1-12 structure with a = 8.438 Å, c = 4.805 Å.

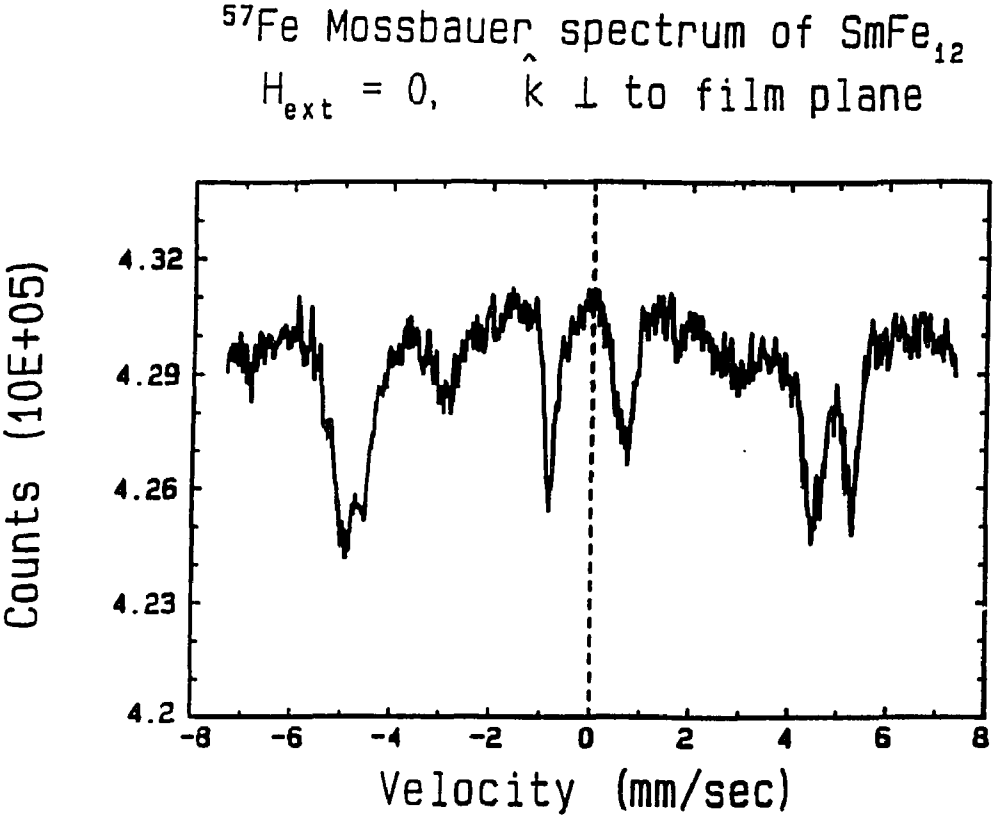

Fig. 7. Zero field ^{57}Fe Mossbauer spectrum of the $SmFe_{12}$ film $4\pi M=0$ transitions are nearly absent, indicating parallelism between propagation vector and hyperfine field.

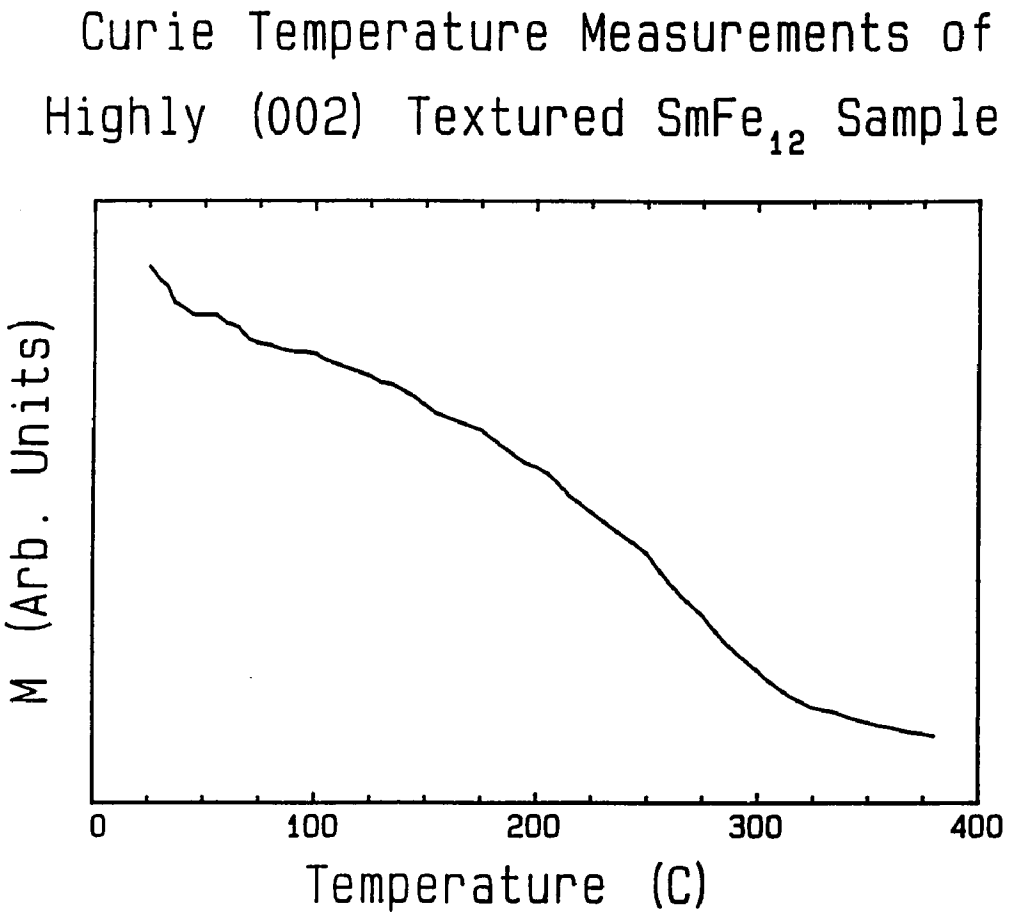

Fig. 8. Thermomagnetic data for a two element $SmFe_{12}$ sample.

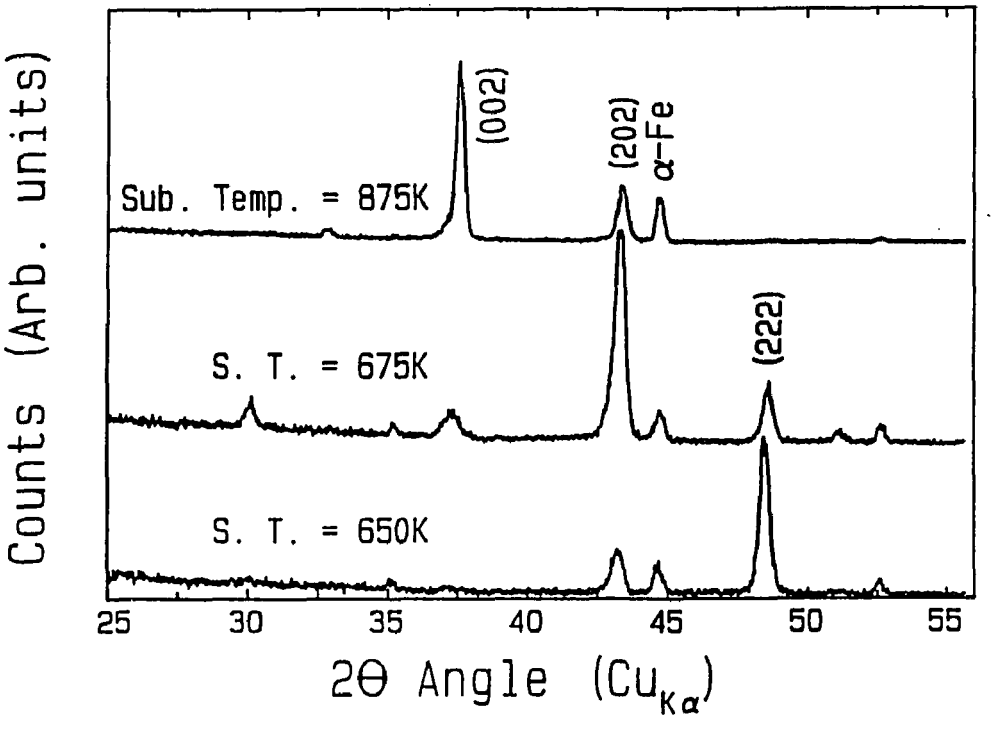

Fig. 9. X-ray diffraction traces, $Cu_{K\alpha}$, of $SmFe_{12}$ films synthesized at various substrate temperatures. The sputtering gas pressure was held constant at 100 mTorr of Argon. The crystal structure of the film is tetragonal $ThMn_{12}$ a = 8.50 Å, c = 4.79 Å.

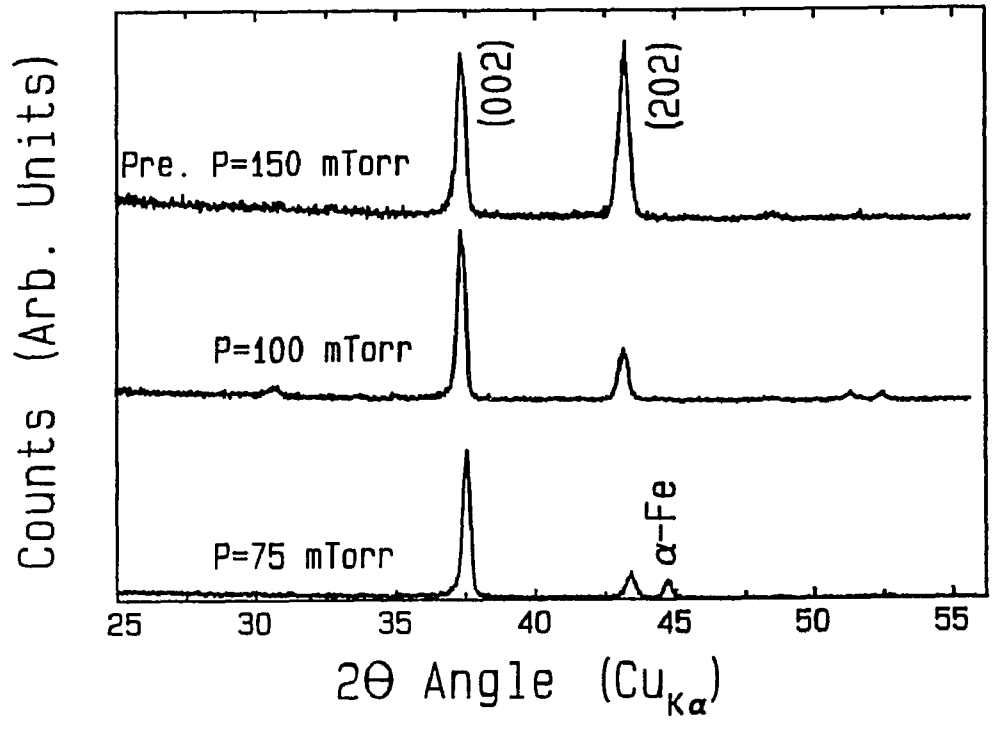

Fig. 10. X-ray diffraction trace, $Cu_{K\alpha}$, of $SmFe_{12}$ films made at various sputtering gas pressures of Argon. The substrate temperature was the same at 645 K.

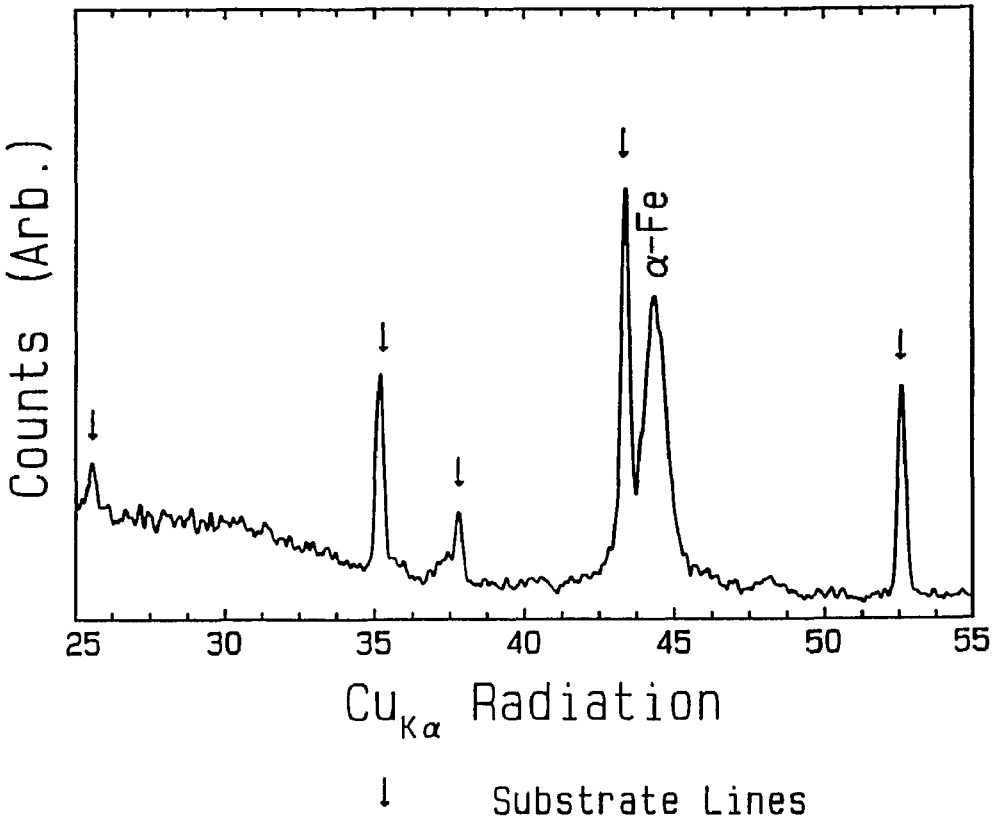

Fig. 11. X-ray diffraction trace of nitrided $SmFe_{12}$ sample. The film sample was synthesized by direct crystallization method and then nitrided in 570 Torr of N_2 for two hours.

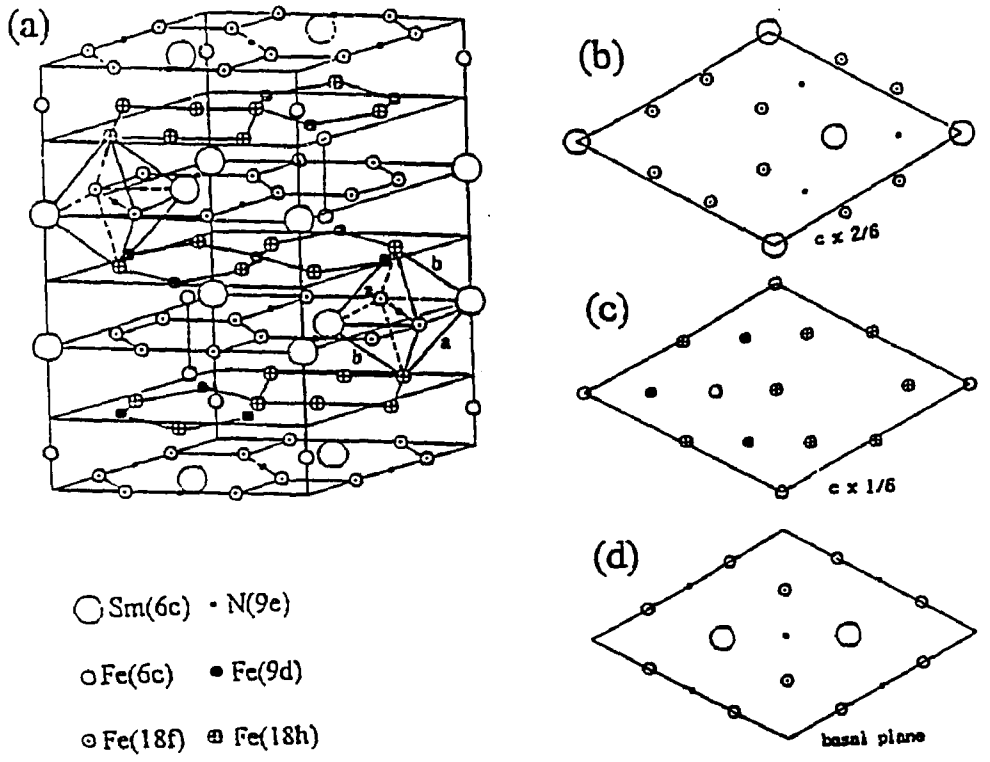

Fig. 12. Crystal structure of $Sm_2Fe_{17}N_3$, rhombohedral, Th_2Zn_{17}-type structure.

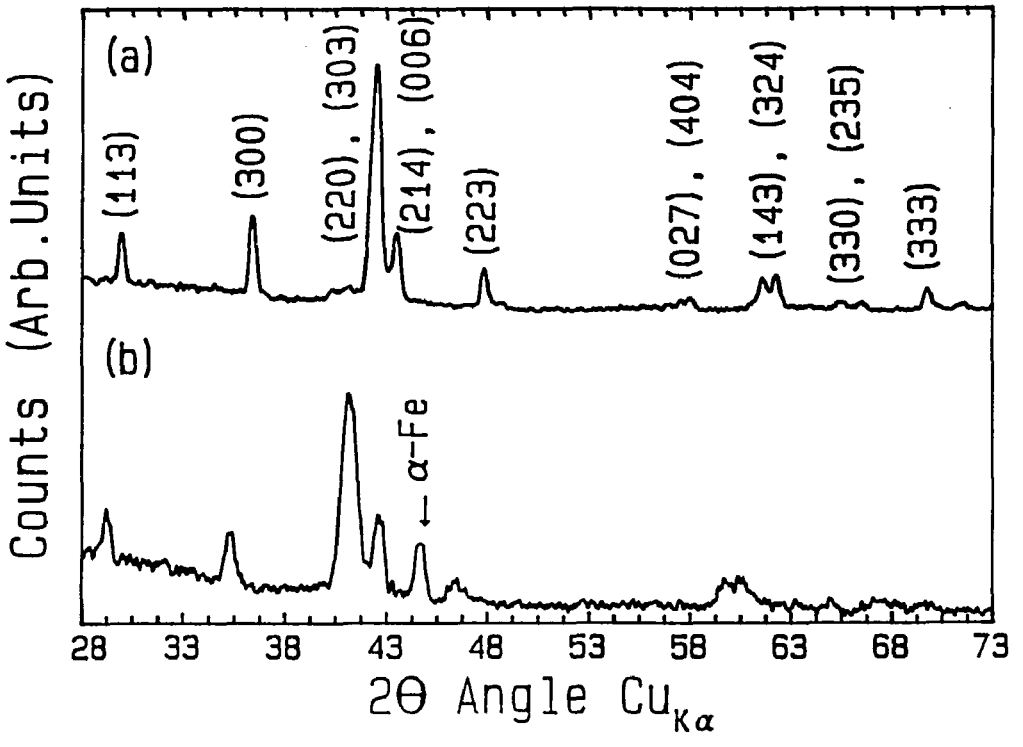

Fig. 13. X-ray diffractometer traces, $Cu_{K\alpha}$ radiation, are shown for Sm_2Fe_{17} film samples (a) before, and (b) after nitriding. The Sm content was 12.2 at % for both samples.

Figure 14

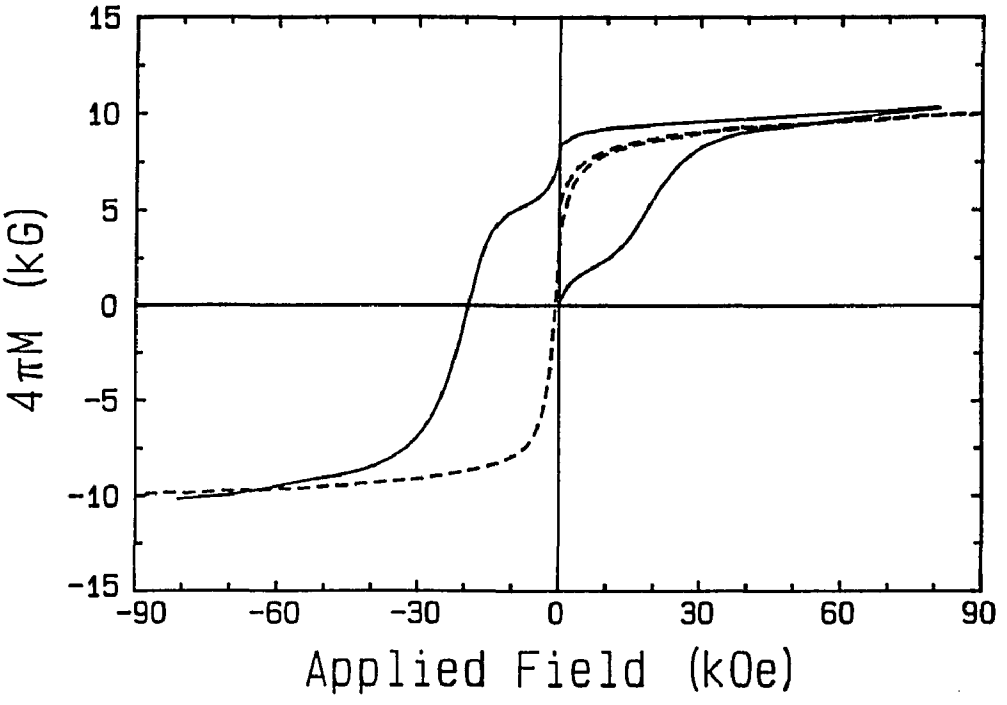

Fig. 14. Demagnetization curves for subsequently crystallized Sm_2Fe_{17} film samples (dashed curve) and after nitriding (solid curve).

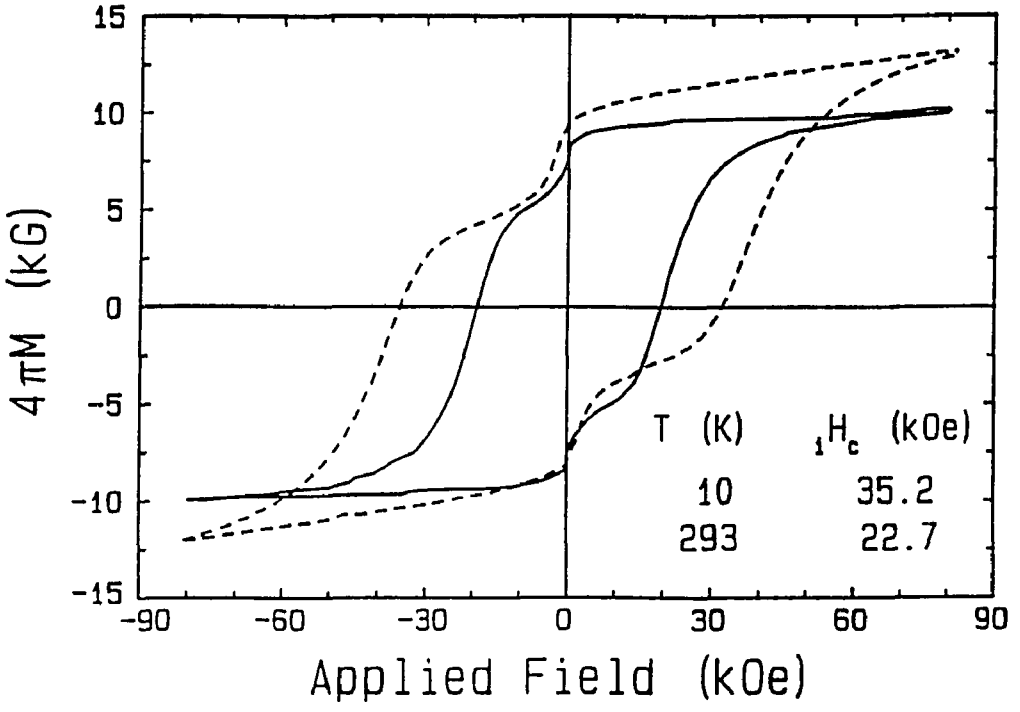

Fig. 15. In plane hysteresis loops are shown for $Sm_2Fe_{17}N_x$ film samples at 293 K, room temperature, and at 10 K.

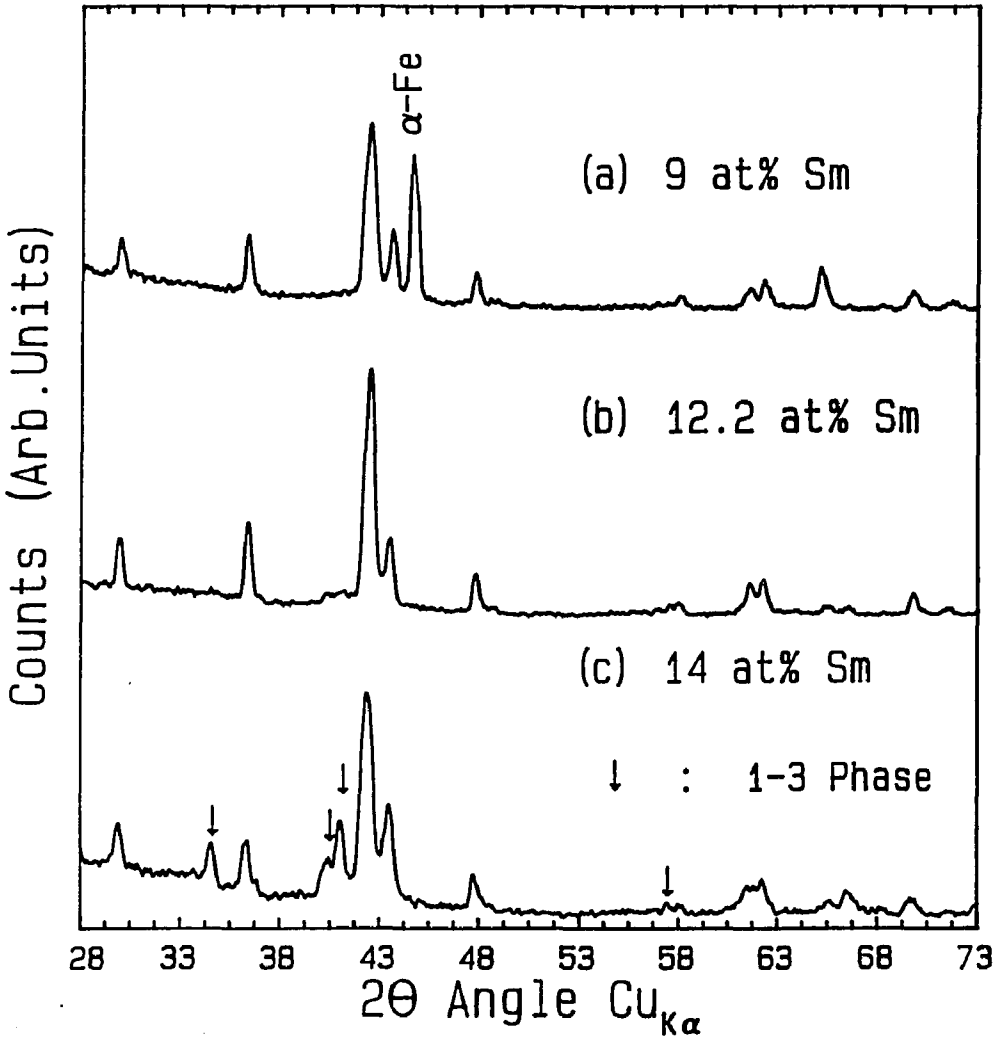

Fig. 16. X-ray diffractometer traces, $Cu_{K\alpha}$ radiation, are shown for Sm_2Fe_{17} film samples with different samarium concentrations. At 12.2 at% Sm, the film samples were nearly single phase without any noticeable amount of impurity phases. However α-Fe appears at low Sm concentrations and 1-3 phase can be clearly seen for higher Sm content in the film samples of Figures (a) and (c) respectively.

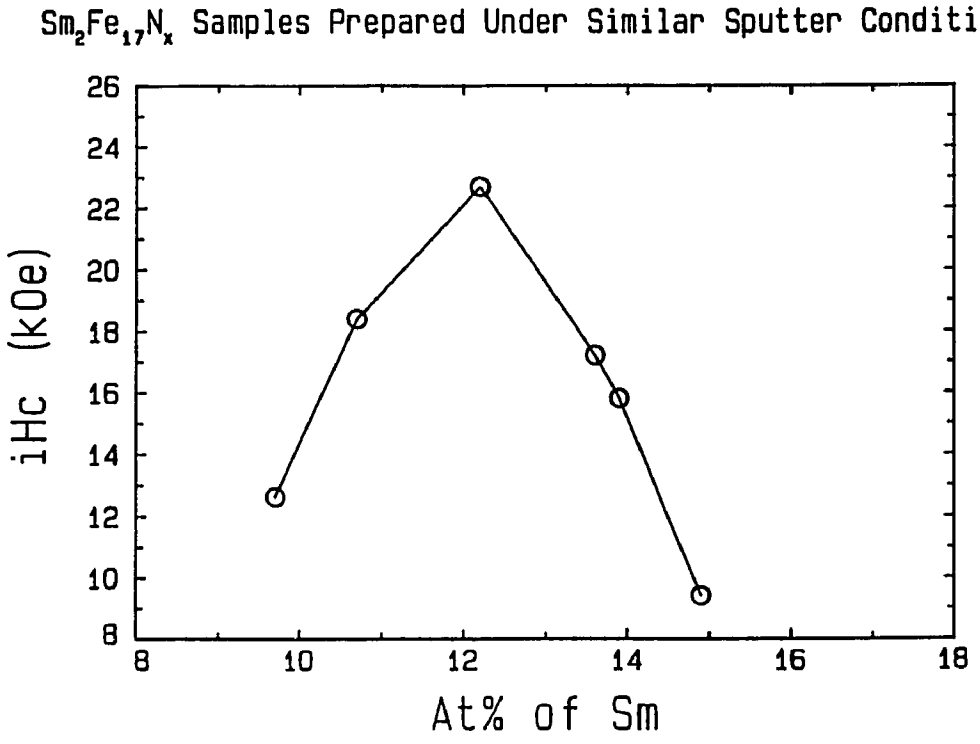

Fig. 17. The coercivity, ${}_iH_c$, versus at% Sm for $Sm_2Fe_{17}N_x$ film samples synthesized under the same sputtering conditions is shown. The highest room temperature coercivity was obtained for 12.2 at% Sm, these films were nearly single phase as seen from x-ray trace Fig. 16(b).

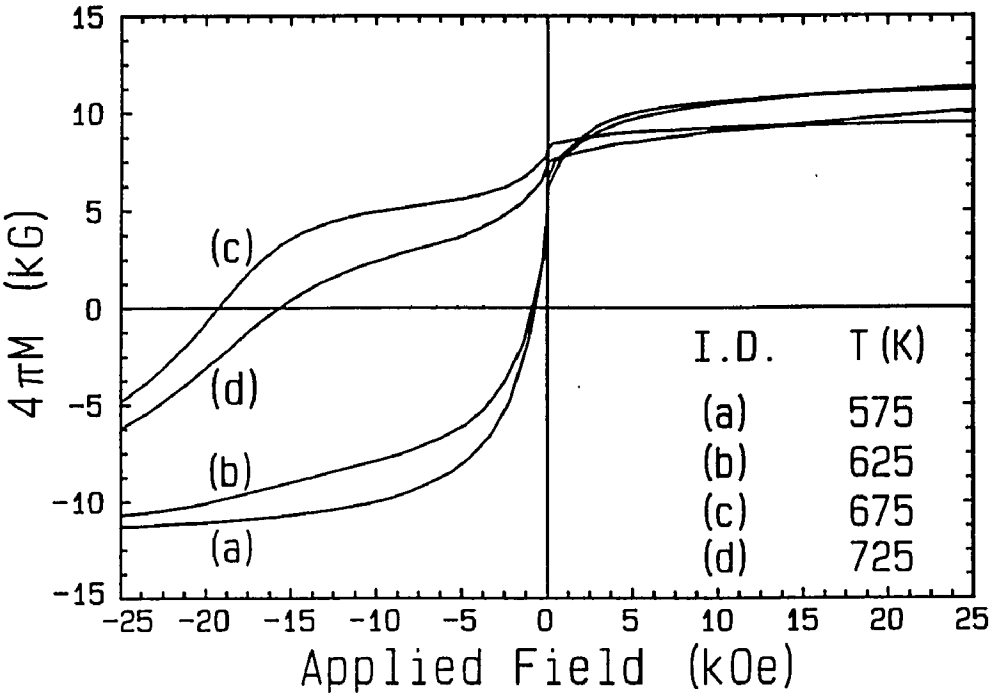

Fig. 18. The effect of nitriding temperature on the magnetic properties of $Sm_2Fe_{17}N_x$ film samples is shown. These Sm_2Fe_{17} film samples were synthesized under the same sputtering conditions, only the nitriding temperature was different, for curves (a) 575 K, (b) 625 K, (c) 675 K, and (d) 725 K respectively. The at% of Sm was approximately 12.2 for all of these samples.

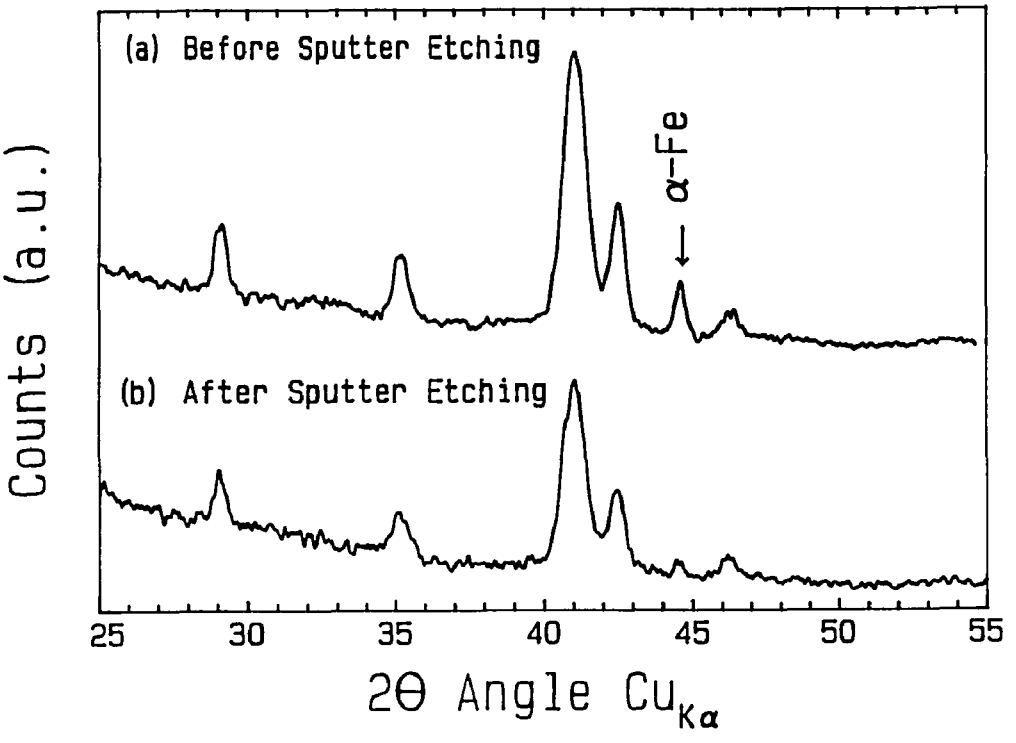

Fig. 19. X-ray diffraction traces, $Cu_{K\alpha}$ radiation, are shown of $Sm_2Fe_{17}N_x$ film samples (a) before, and (b) after sputter etching the film sample by approximately 1.5 μm.

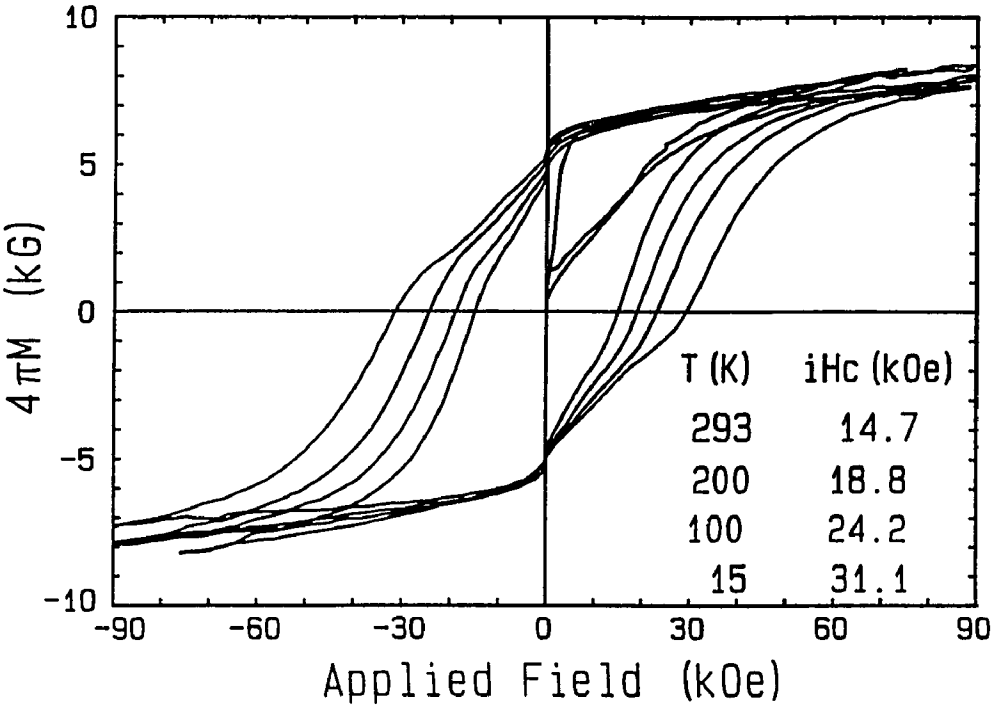

Fig. 20. High field hysterisis loops of Sm_5Fe_{17} at various temperatures. The inplane coercivity, $_iH_c$, increases smoothly from 14.7 kOe at room temperature to 31.1 kOe at 15 kOe.

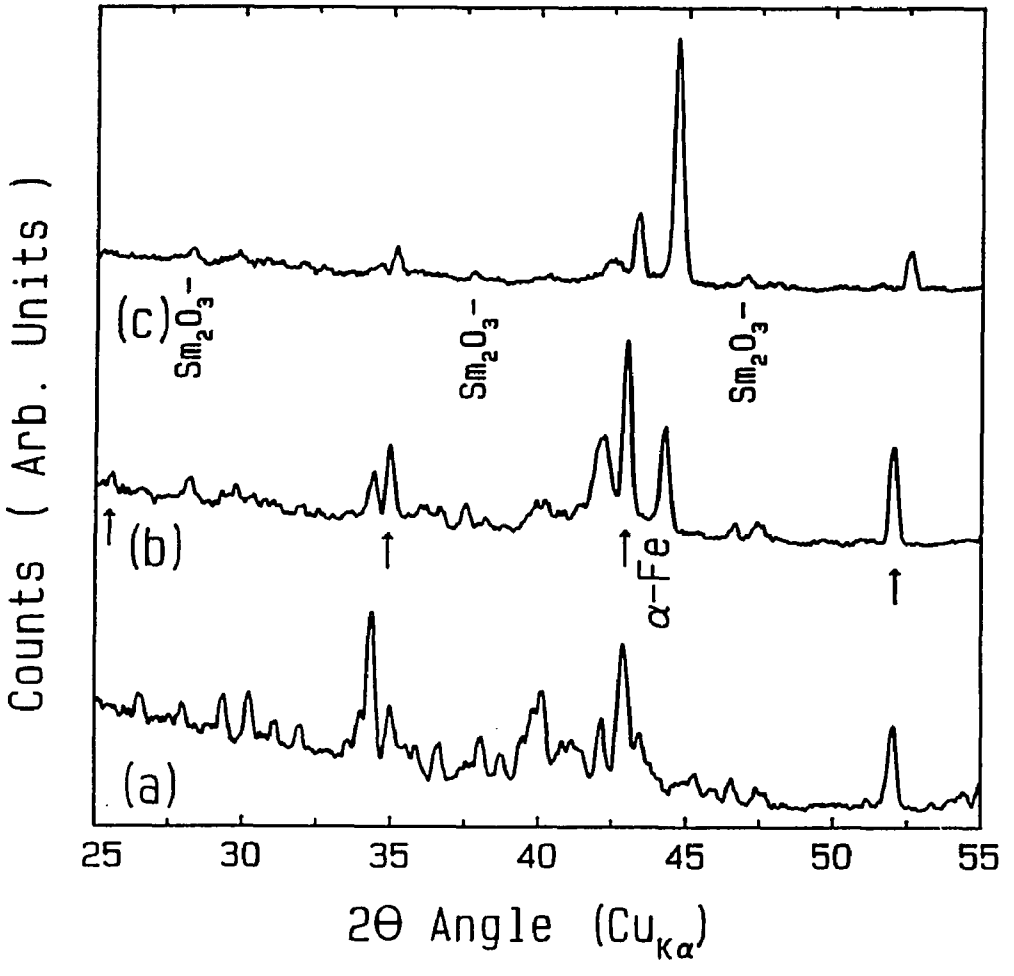

Fig. 21. $Cu_{K\alpha}$ x-ray diffraction traces of films crystallized at 720 K for various crystallization times, C.T. The curves (a), (b), and (c) are respectively for C.T. = 75, 360, and 990 minutes.

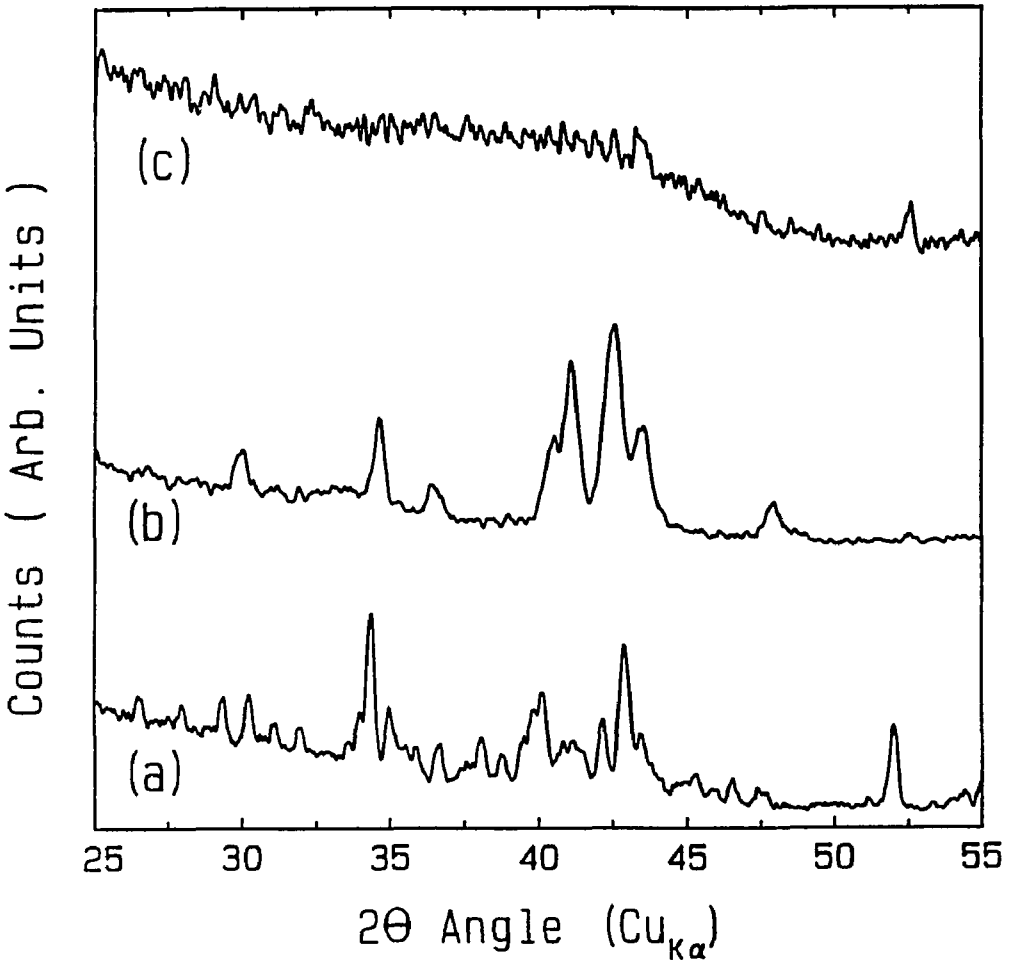

Fig. 22. $Cu_{K\alpha}$ x-ray diffraction traces of films crystallized for 75 minutes at various temperatures; (a) 720 K, (b) 800 K and (c) 600 K.

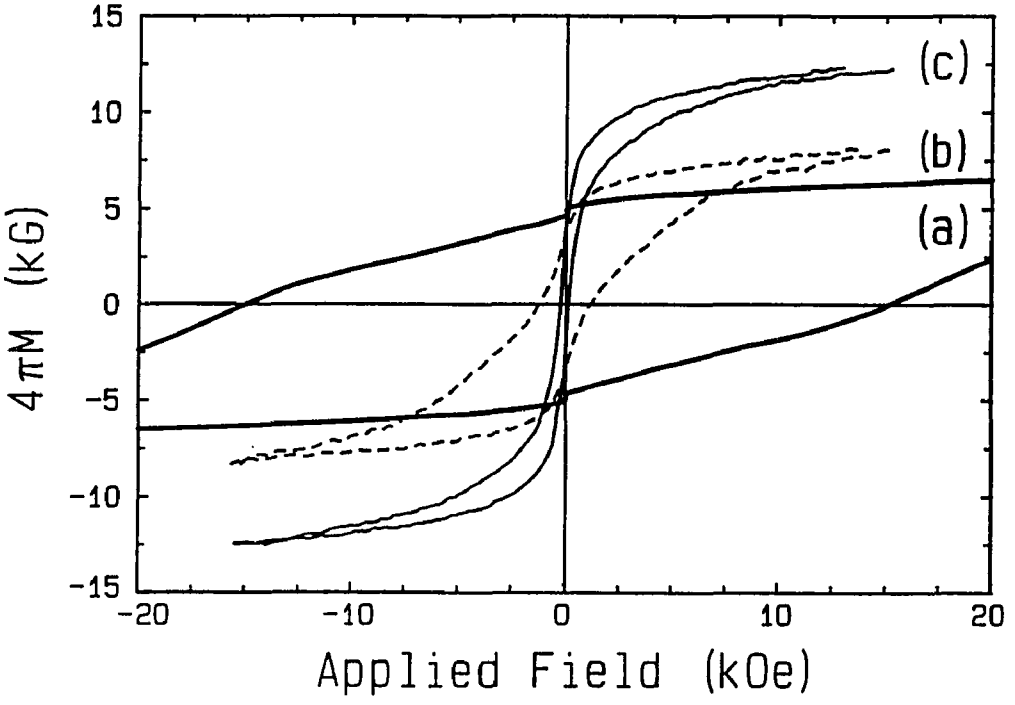

Fig. 23. Hyterisis loops of films crystallized at 720 K for various crystallization times.

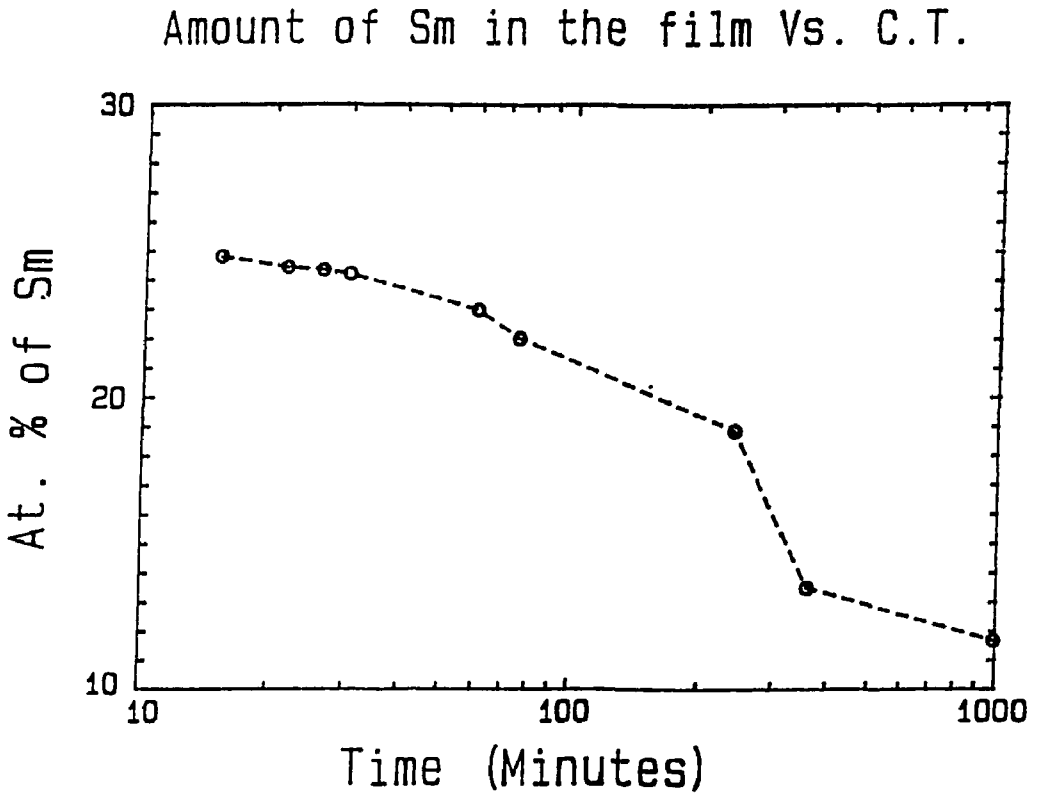

Fig. 24. The at% Sm versus crystallization time, C.T., for two element Sm_5Fe_{17} films that were crystallized in situ from amorphous deposits. All the sputter conditions except crystallization time were kept the same.

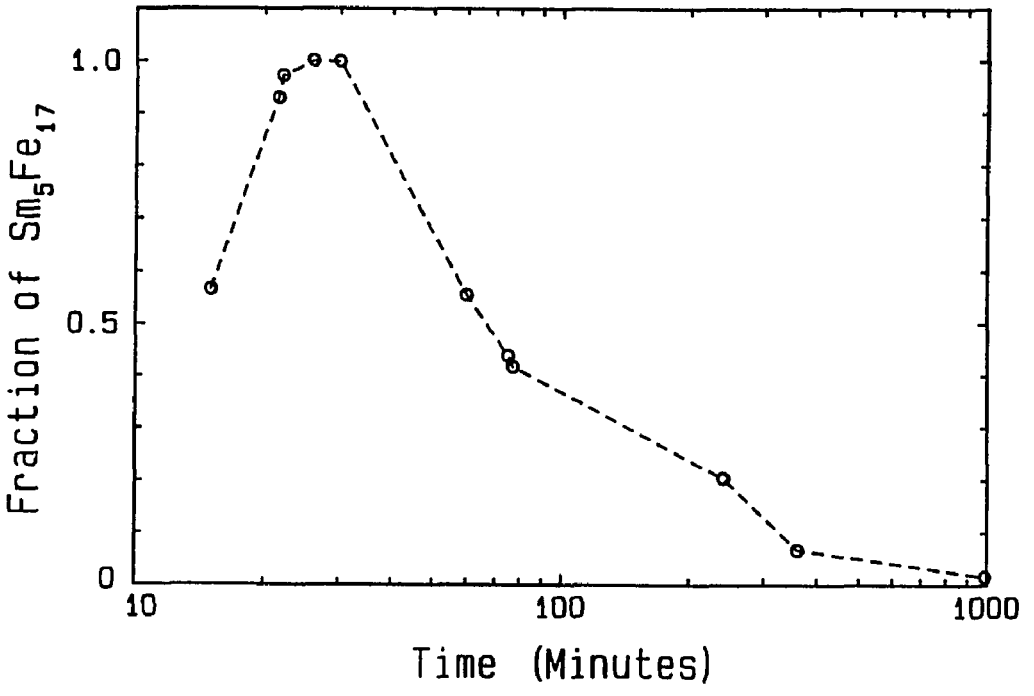

Fig. 25. Fraction, F, of Sm_5Fe_{17} samples made under similar conditions but different crystallization time, F = (width @4πM=0/height 2(4πM))*(1/N_{30min}) where N_{30min} = (width @ 4πM=0/height 2(4πM=0)) of the sample with C.T. = 30 min. and optimum magnetic properties.

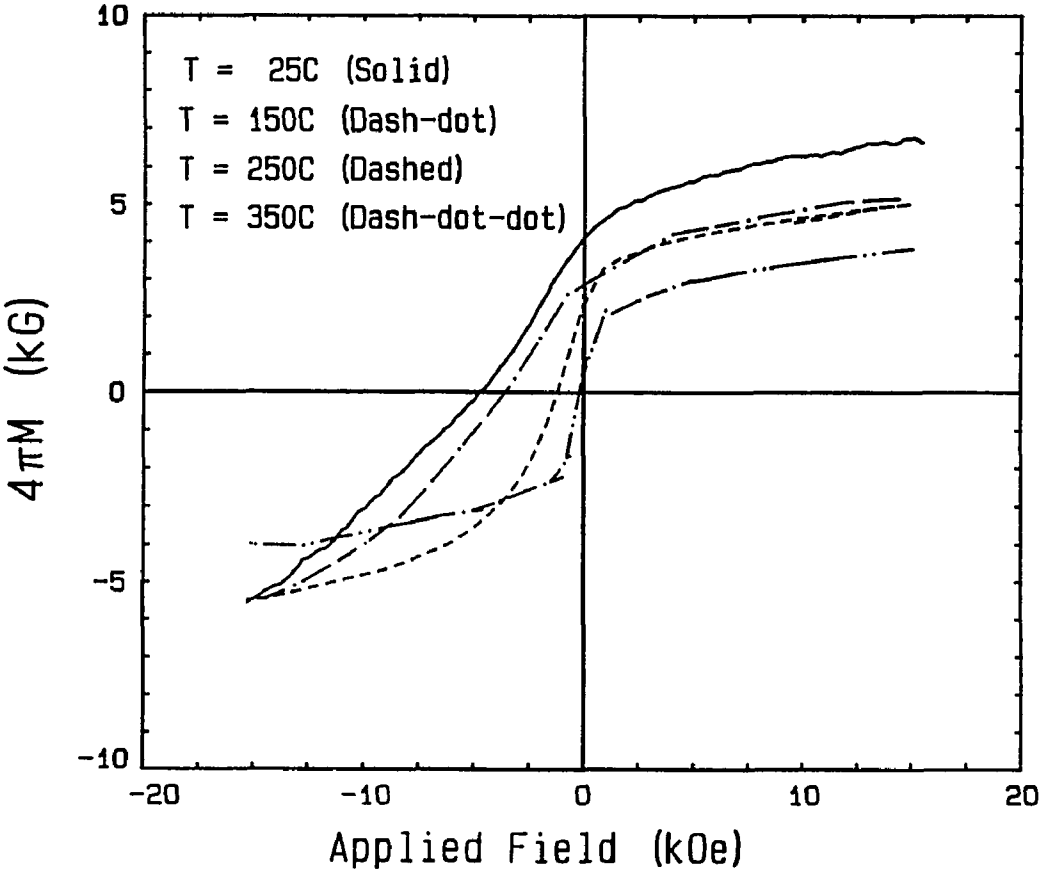

Fig. 26. High temperature hysterisis loops for a Sm_5Fe_{17} sample, T = 25°C (solid), T = 150°C (dash-dot), T = 250°C (dashed), and T = 350°C (dash-dot-dot). Beyond 350°C the phase was found to dissociate quite rapidly indicating that Sm_5Fe_{17} is a metastable phase.

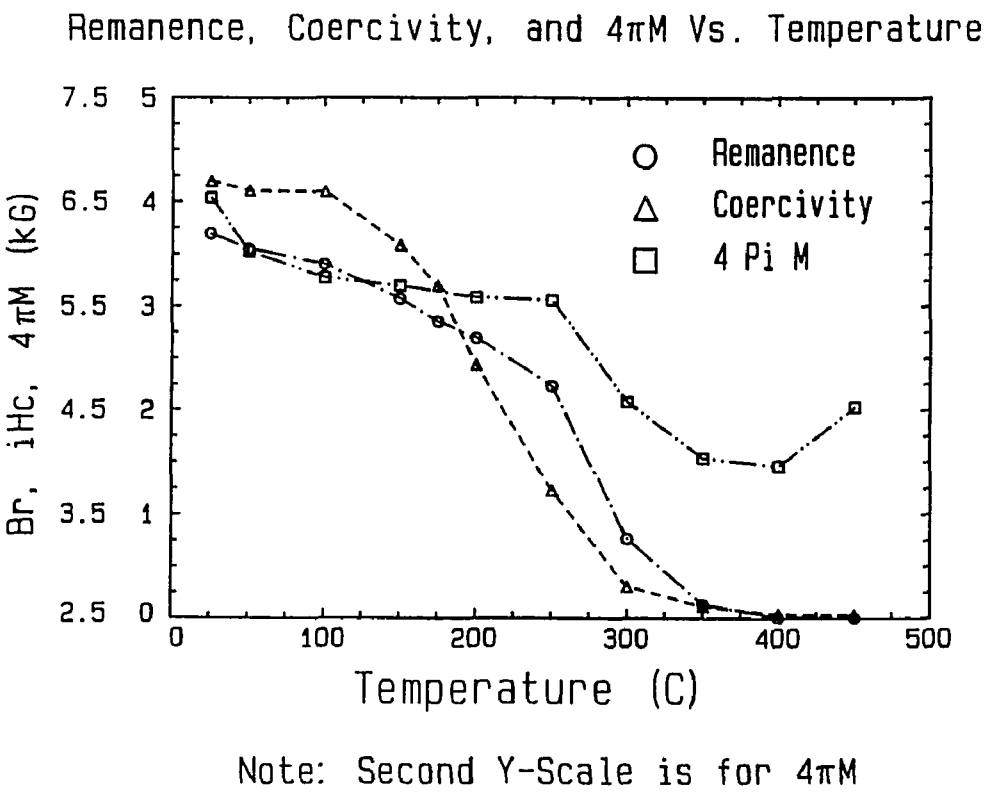

Fig. 27. From high temperature hysterisis loops of Sm_5Fe_{17} sample, magnetization and coercivity were found to decrease monotonically with temperature till the temperature reached 350°C.

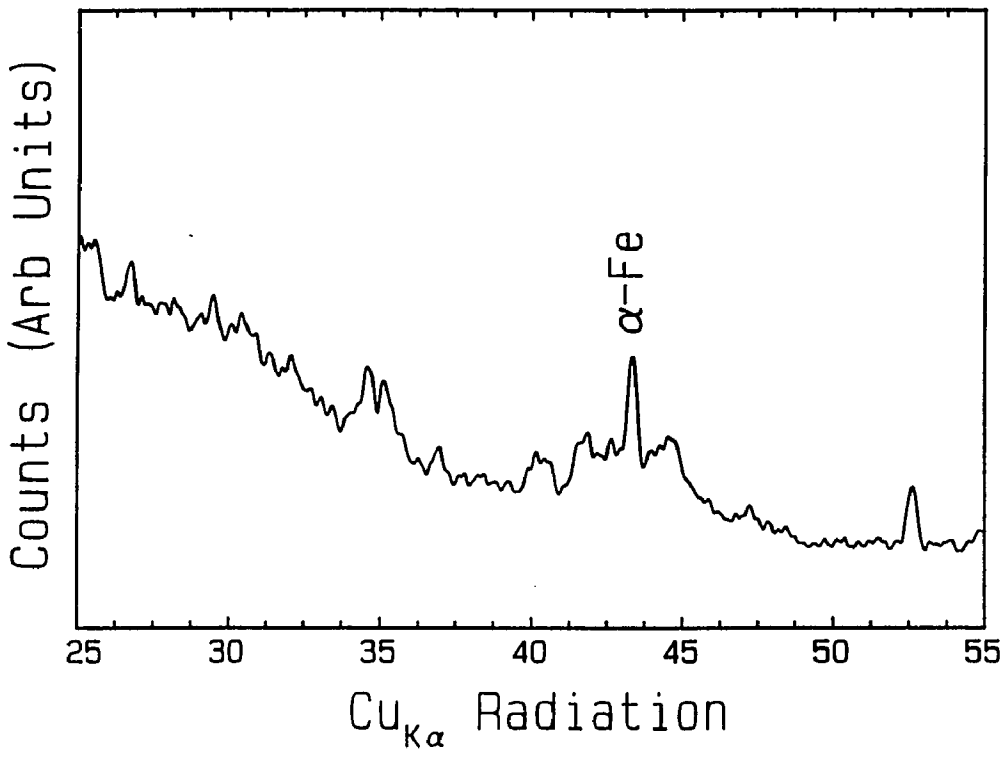

Fig. 28. $Cu_{K\alpha}$ x-ray diffraction trace of films crystallized of a Sm_5Fe_{17} sample subjected to temperatures up to 500°C and then cooled down to room temperature.

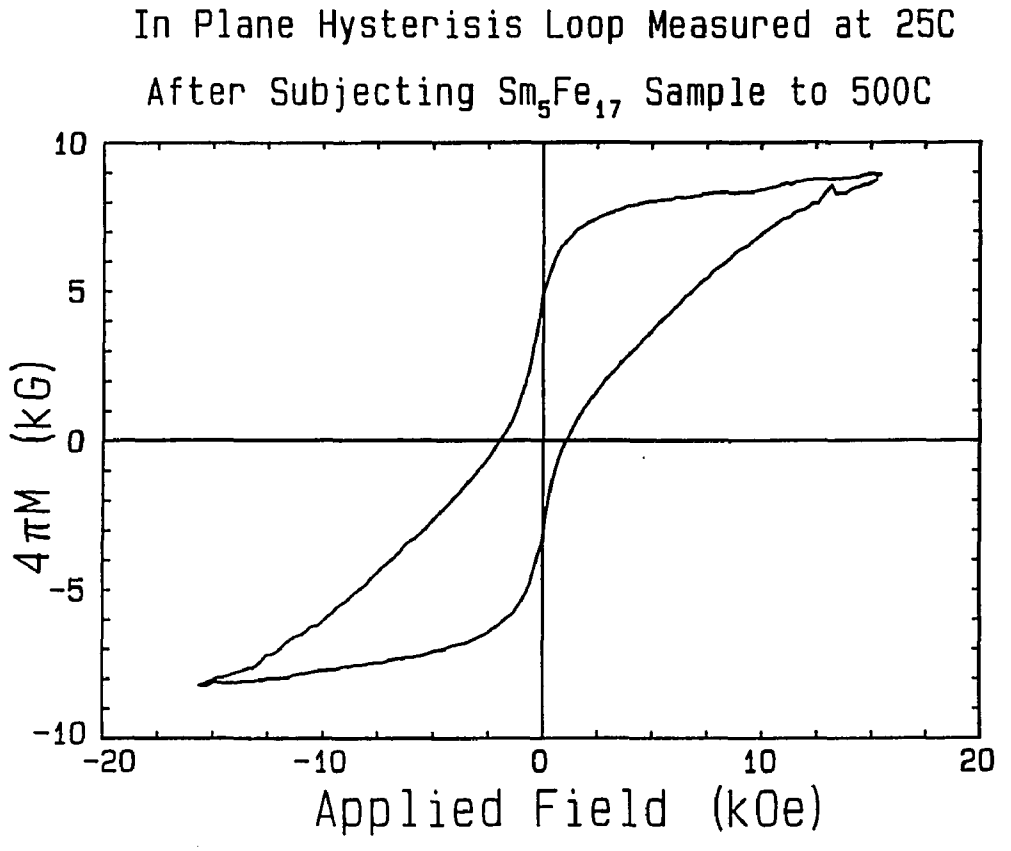

Fig. 29. In plane hysterisis loop measured at room temperature of the sample of Fig. 28. Tailing of the loop in the third quadrant implies the presence of 5-17 phase even when the sample was subjected to high temperatures.

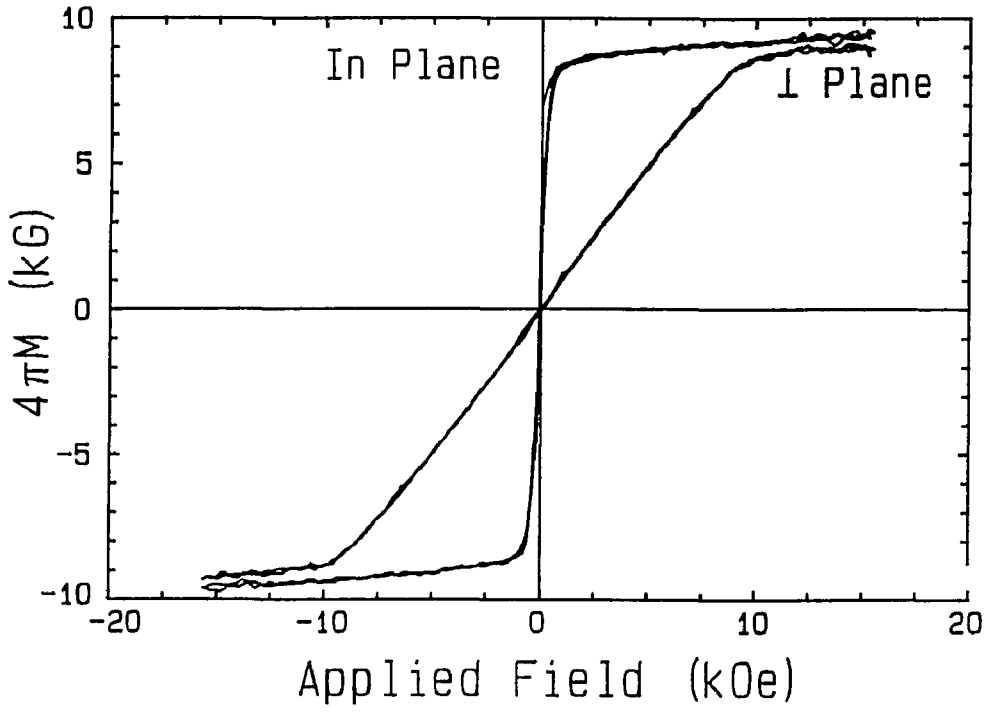

Fig. 30. Hysterisis loops measured at room temperature for a nitrided 5-17 sample. The sample shows soft magnetic properties with easy plane anisotropy.

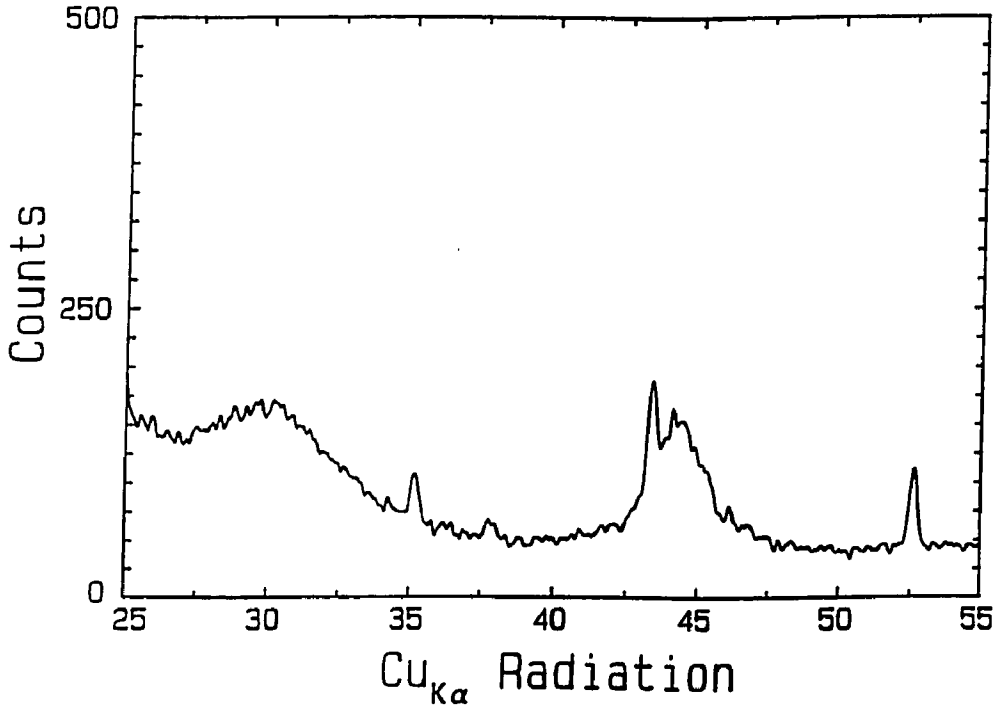

Fig. 31. $Cu_{K\alpha}$ x-ray diffraction traces of nitrided 5-17 film sample. The sharp peaks indicated by arrows are from the substrate. α-Fe seems to be most intense peak.

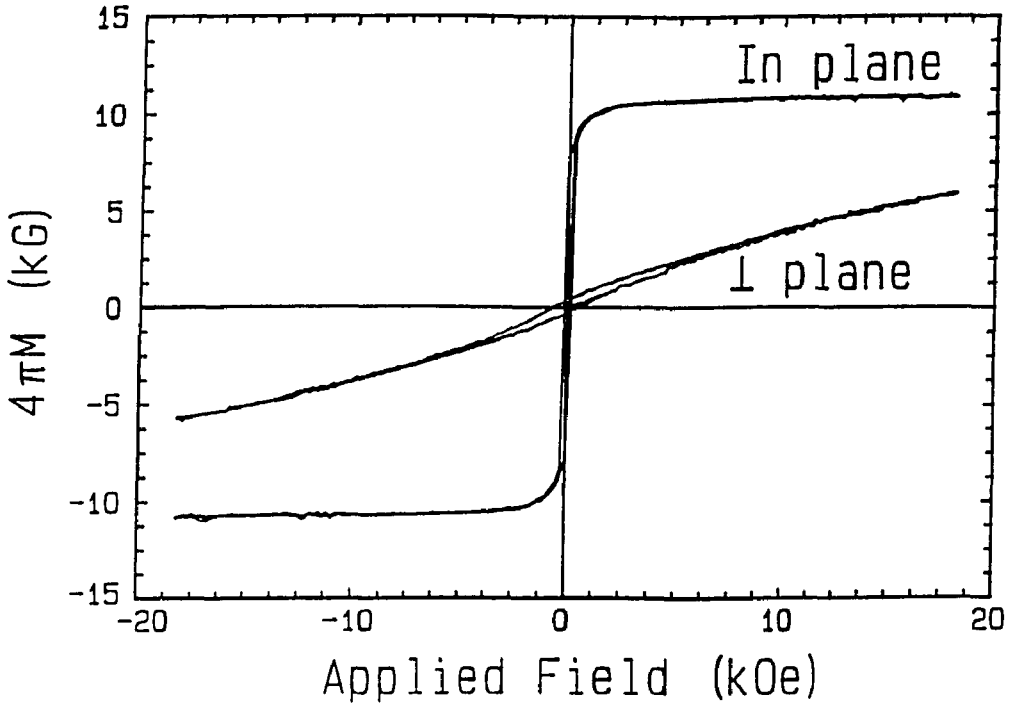

Fig. 32. Hysteresis loops measured at T = 293 K, for $Pr_{1.03}Fe_{10.44}Co_{1.13}Mo_{0.40}$ sample exhibiting easy plane anisotropy are shown. After nitriding the easy plane anisotropy behavior switched to uniaxial behavior.

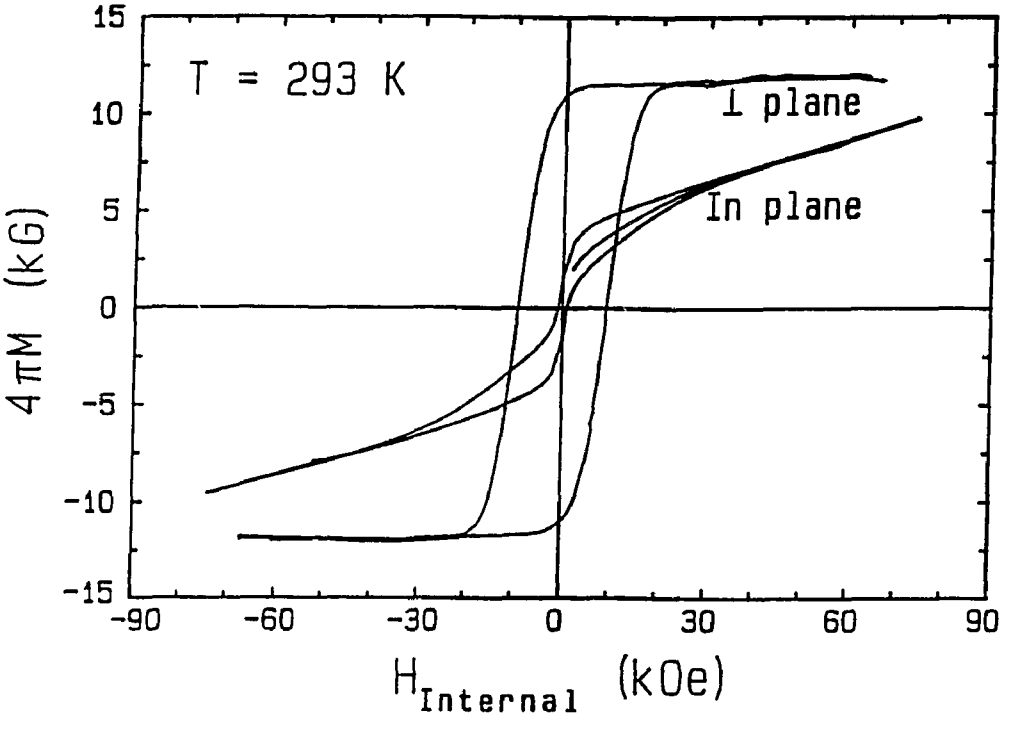

Fig. 33. Hysteresis loops are shown, T = 293 K, for a $Pr_{1.04}Fe_{10.36}Co_{1.16}Mo_{0.44}N$ sample. For the flux density directed perpendicular to the surface, the $4\pi M_s$ was 11.6 ± 0.5 kG, $_iH_c$ was 9.4 kOe, and the static energy product was 23.6 MG-Oe.

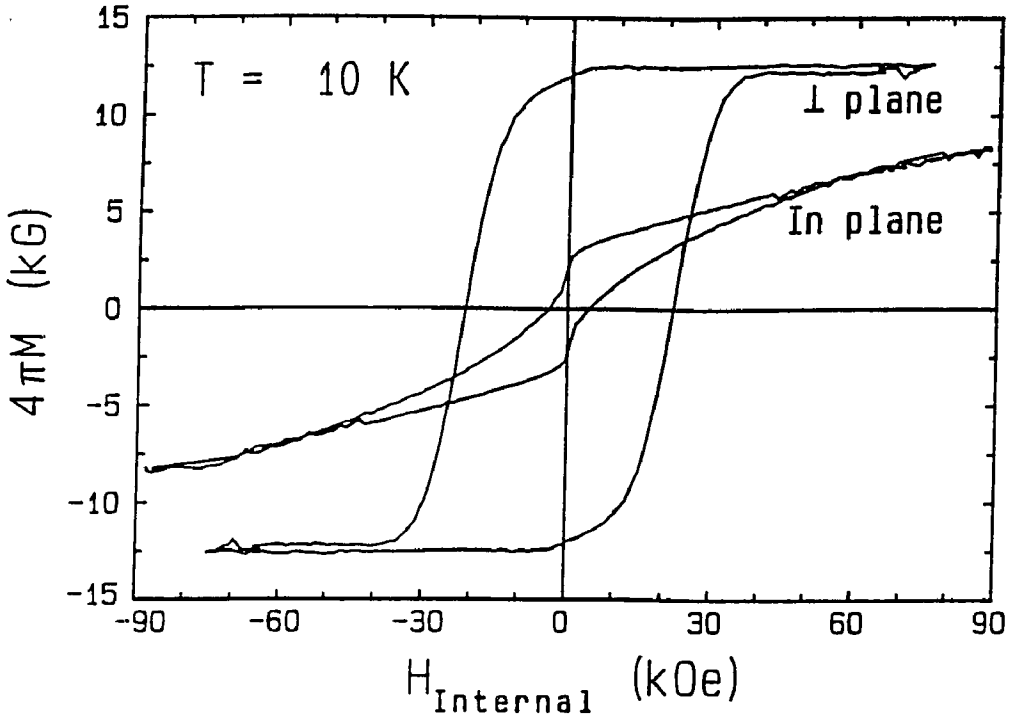

Fig. 34. Hysteresis loops are shown, T = 10 K, for a $Pr_{1.04}Fe_{10.36}Co_{1.16}Mo_{0.44}N$ sample. For the flux density directed perpendicular to the surface, the $4\pi M_s$ was 12.5 ± 0.5 kG, $_iH_c$ was 22.0 kOe, and the static energy product was 32.8 MG-Oe.

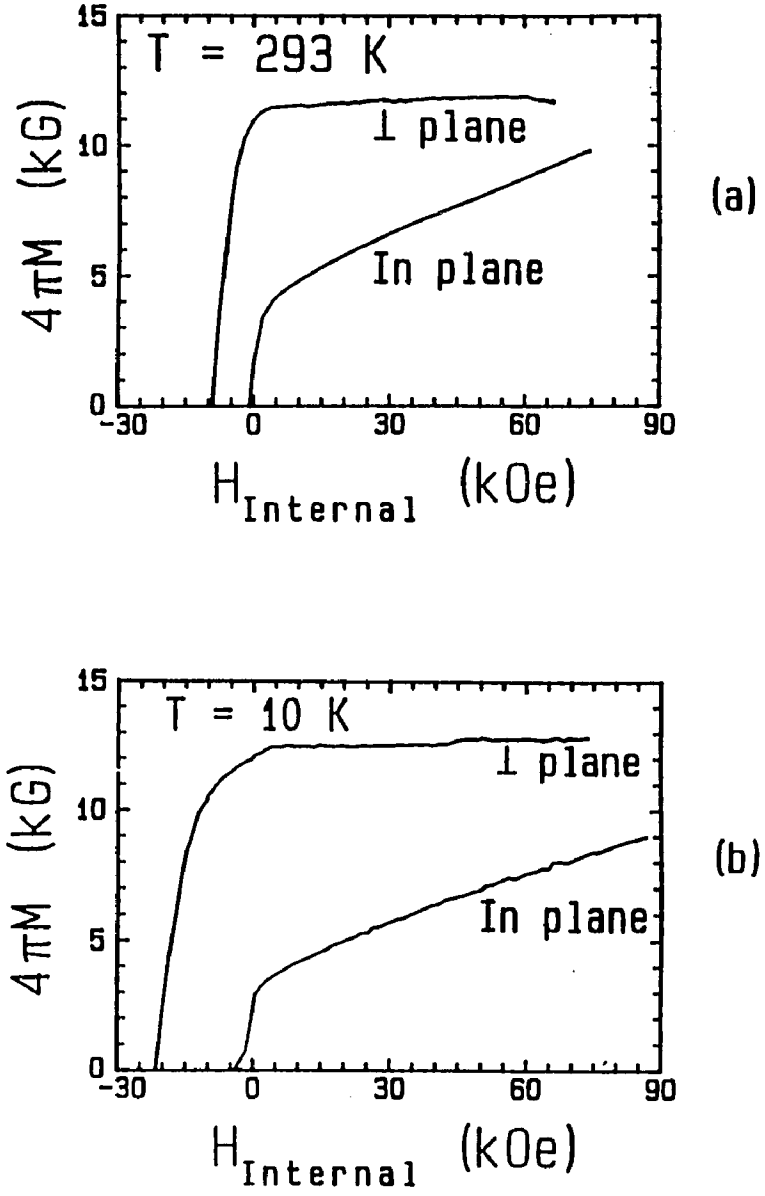

Fig. 35. Demagnetization curves at (a) T = 293 K, and (b) T = 10 K for the samples of Figs. 33, and 34 are shown. The anisotropy field perpendicular to the film plane estimated by extrapolation was 144 and 96.5 kOe at 293 and 10 K respectively. Note that the easy axis of magnetization was perpendicular to the film plane.

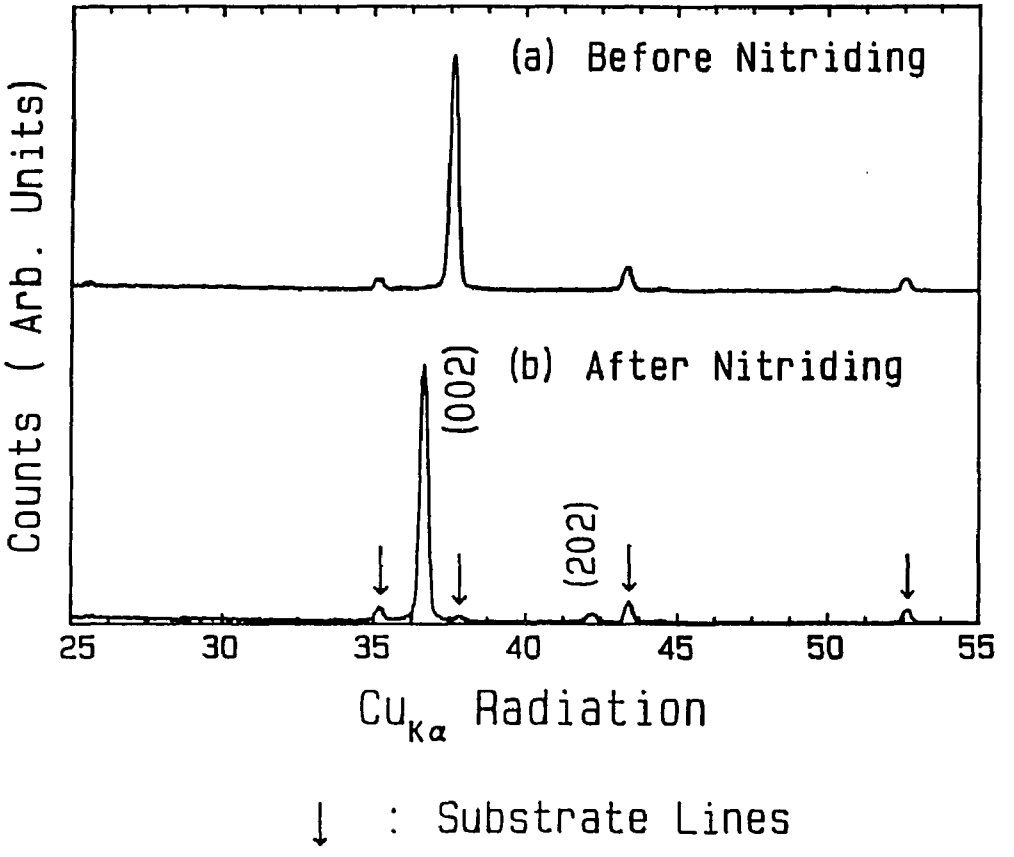

Fig. 36. (a.) An x-ray diffractometer trace, $Cu_{K\alpha}$, for the sample of Fig. 32 is shown before nitriding. (b.) An x-ray diffractometer trace for Figs. 33 and 34 is shown after nitriding. The volume increase upon nitriding was ≈ 6.9%. Both film samples were highly (002) textured.

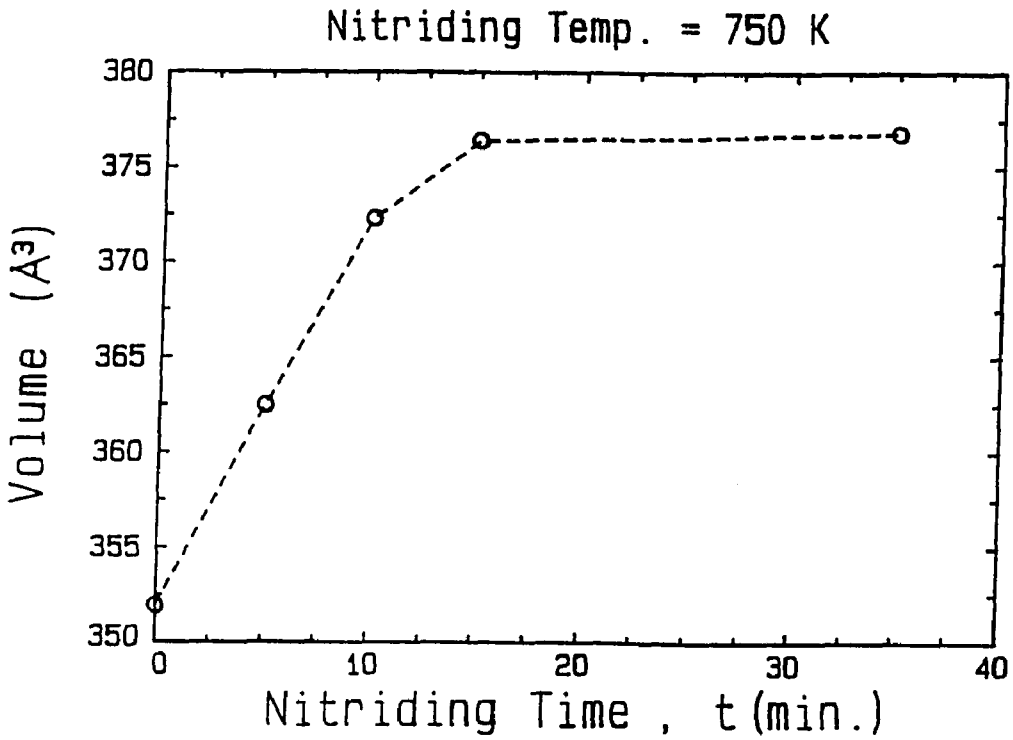

Fig. 37. The cell volume as a function of nitriding time at 750 K is shown for $Pr(Fe,Co,Mo)_{12}$ nitrided in 570 Torr N_2.

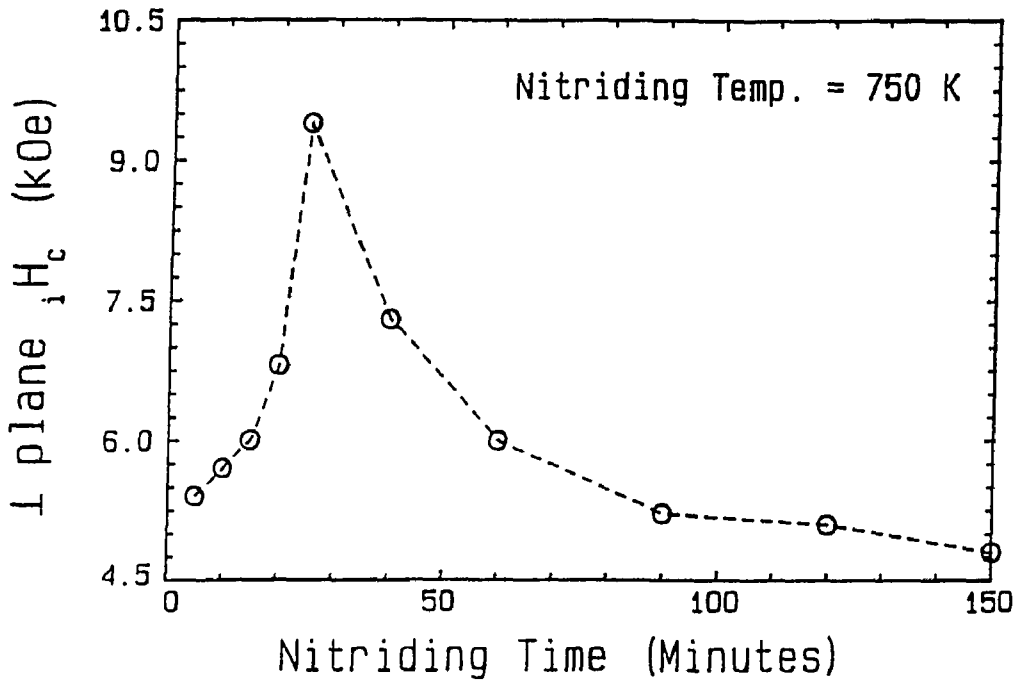

Fig. 38. The variation of room temperature coercivity, $_iH_c$, perpendicular to the film plane is shown as a function of nitriding time at 750 K, 570 Torr N_2, for film samples of nearly the same composition. All films were sputter synthesized under the same conditions except for the nitriding time.

BIBLIOGRAPHY

1. G. Hoffer and K. Strnat, IEEE Trans. Magnetics, 2, 487, 1966.

2. K. Strnat, J. Aplied Phys. 38, 1001, 1967.

3. K. Kumar, J. Appl. Phys., 63, R13, 1988.

4. H. Hegde, P. Samarasekara, R. Rani, A. Navarathna, and F. J. Cadieu, Paper ER-22, 6th Joint MMM-INTERMAG Conference, Albuquerque, June 20-23, 1994.

5. M. Sagawa, S. Fujimura, N. Togawa, H. Yamamoto, and Y. Matsuura, J. Appl. Phys. 55(6), pp 2083-2087, 1984.

6. D. B. Mooij, and K. H. J. Buschow, J. Less-Comm. Metals, pp 349, 142, 1988.

7. A. Navarathna, H. Hegde, R. Rani, F. J. Cadieu, Paper CC-08, 38th Magnetism and Magnetic Materials Conference, Minnesota, November 14-17, 1993. J. Appl. Phys. 75(10), May 15, 1994.

8. A. Navarathna, H. Hegde, R. Rani, K. Chen, F. J. Cadieu, Paper FC-01, INTERMAG'93, IEEE Trans. on Magnetics, 2812, 1993.

9. F. J. Cadieu, and N. Chencinski, IEEE Trans. Magn., MAG - 11, 227, 1975.

10. H. Hegde, Ph. D. Thesis, City University of New York, 1990.

11. J. J. Croat, J. F. Herbst, R. W. Lee, F. E. Pinkerton, Appl. Phys. Lett. 44, 148, 1984.

12. F. J. Cadieu, A. Navarathna, R. Rani, H. Hegde, N. A. Bozarczuk, and R. J. Gambino, Paper DP-07, 37th Magnetism and Magnetic Materials Conference, Houston, December 1-4, 1992, & J. Appl. Phys. 73(10), pp 6124-6126, May 15, 1993.

13. A. Navarathna, H.Hegde, R. Rani, and F. J. Cadieu, Paper EC-01, 37th Magnetism and Magnetic Materials Conference, Houston, December 1-4, 1992, & J. Appl. Phys. 73 (10), pp 6242-6244, May 15, 1993.

14. Hong Sun, Yoshichika Otani, and J. M. D.Coey, J. Appl. Phys. 67(9), p 4659, 1990.

15. F. J. Cadieu, H. Hegde, A. Navarathna, R. Rani, and K. Chen, Appl. Phys. Lett. 59(7), 12 August, 1991.

16. Ruderman, Kittel, Kasuya, and Yosida, Solid State Physics 22, 1, 1968.

17. A. J. Campbell, Phys. F: Met. Phys. 2 L47, 1972.

18. M. S. S. Brooks, O. Erikson, and B. Johansson, J. Phys.: Condens. Matter 1, 5861, 1989.

19. K. H. J. Bushow, Rep. Prog. Phys. 40, 1179, 1977.

20. K. H. J. Bushow, Rep. Prog. Phys. 54, 1123-1213, 1991.

21. Sheng-Chuan Zhu 6th Intern. symp. Pittusburg, pp 351-356, 1990.

22. L. Y. Zhang, F. Pourarian, and W. E. Wallace, J. Magn. Mag. Mater. 74, pp 203, 1988.

23. L. Y. Zhang, E. B. Boltich, V. K. Sinha, and W. E. Wallace, IEEE Trans. Magn. Vol. 25, No 5, Sept. 1989.

24. J. L. Vossen, and Werner Kern, eds., "Thin Film Processes", Academic Press, New York, 1978.

25. B. Chapman, Glow Discharge Processes, Wiley Interscience Publishers, 1980.

26. F. J. Cadieu, L. F. Cooley, and D. H. Douglass, Jr., Rev. Sci. Instr. 42, 587, 1971.

27. F. J. Cadieu, T. D. Cheung, L. Wickramasekara, and S. H. Aly, J. Appl. Phys. 57, 3598, 1985.

28. K. Chen, Ph. D. Thesis, pp.27, 1993.

29. Michael T. Postek, Jr., Scanning Electron Microscope, Ladd Research Industries, Inc., 1980.

30. B. D. Cullity, Elements of x-ray diffraction, 2nd Ed., Addison-Wesley, 1978.

31. W. B. Pearson, The Crystal Chemistry of the Lattice Spacing and Physics of Metals and Alloys, Wiley Interscience, New York, 1972.

32. L. S. Birks, X-ray Spectrochemical Analysis, Interscience Publisher, New York, 1969.

33. P. Villars and L. D. Calvert, Pearson Handbook of Crystallographic Data for Intermetallic Phases Volume 1-4 Materials Park, OH ASM International, 5366pp, 1991.

34. K. H. Buschow, J. Less Common Metals 25(1971) 131. J.strzeszewski, Y.Z. Yang, E.W. Singleton, and G.C. Hadjipanayis, IEEE Trans. on Magnetics 25, 3309, 1989.

35. L. Y. Zhang, E. B. Boltich, V. K. Sinha, and W. E. Wallace, IEEE transaction on Magnetics, Vol. 25, No. 5, September, 1989.

36. H. Hegde, R. Rani, A. Navarathna, K. Chen, and F. J. Cadieu paper submitted for 5th MMM - Intermag, June 1991, Pittsburgh, & J. Appl. Phys. 70, 6345 1991.

37. M. Okada, A. Kojima, K. Yamagishi, and M. Homma, IEEE transaction on Magnetics, Vol. 25, No. 5, September, 1990.

38. H. H. Stadelmaier, F. J. Cadieu, and N. C. Liu, Matl. Letters 6, 80, 1987.

39. H. H. Stadelmaier, G. Schneider, E. Th. Henig, and M. Ellner, Matl. Letters 10, 303, 1991.

40. F. J. Cadieu, Thin Film Physics, Academic, San Diego, Vol. 16, p. 169, 1992.

41. R. A. McCuririe, J. Appl. Phys. 52, 7344, 1981.

42. Proceedings of 6th Int. Symp. of RE magnets pp 423-440, 1990.

43. IEEE Trans. on Mag., 28, 2316, 1992.

44. F. J. Cadieu, H. Hegde, R. Rani, A. Navarathna, and K. Chen, Materials Letters, Volume 11, number 8,9 July 1991.

45. J. Wecker, M. Katter, K. Schnitzke, and L. Schultz,34th MMM- Conference, Boston, 1989.

46. J. M. D. Coey, Hong Sun and Yoshichika Otani, pp36, proceedings of 11th Intl. Workshop and 6th Intl. symposium on Anisotropy and Coercivity in Rare Earth Metal Alloy, Ed. S.G. Sankar, Carnegie Mellon Univ. Press, Pittsburgh, 1990.

47. R. Rani, H. Hegde, A. Navarathna, and F. J. Cadieu, Paper DC-03, 37th Magnetism and Magnetic Materials Conference, Houston, December 1-4, 1992, J. Appl. Phys. 73 (10), pp 6023-6025, May 15, 1993.

48. R. Rani, H. Hegde, A. Navarathna, K. Chen, and F. J. Cadieu, INTERMAG'92, Paper FP-02, IEEE Trans. on Magnetics 28, 2835, 1992.

49. J. M. D. Coey, and H. Sun, Journal of Magnetism and Magnetic Materials, 87, l251, 1990.

50. J. M. D. Coey, J. F. Lawer, H. Sun, and J. E., Allan, J. Appl. Phys. 69, 3007, 1991.

51. M. Katter, J. Wecker, L. Schultz, J.Appl. Phys. 6, 3188, 1991.

52. F. E, Pinkerton, and C. D. Fuerst, Appl. Phys. Lett. 60,(20), May 1992.

53. K. Schnitzke, L. Schultz, J. Wecker, and M. Katter, Appl. Phys. Lett. 57(26), p2853-2855, Dec 1990.

54. J. M. D. Coey, R. Skomski, and S. Wirth, IEEE Trans. Magn. Vol. 28, No. 5, 2332, 1992.

55. M. Katter, J. Magn. Magn. Mater., l14-7, 1992.

56. P. C. M. Gubbens, A. A. Moolenar, G. J. Boender, A. M. van der Kraan, T. H. Jacobs, and K. H. J Buschow, J. Mag. Mag. Mater. 96, 1991; & J. Phys.: Condens. Matter 1, pp755-770, 1989.

57. Hong Sun, J. M. D. Coey, Y. Otani, and D. P. F. Hurley, J. Phys. Condens. Matter 2, pp 6465, 1990.

58. S. S. Jaswal, IEEE Transactions on Magnetism, Vol 28, pp2322-25, 1992.

59. P. Mohn and E. Wohlfarth, J. Phys. F, vol. 16, p2421-2430, 1987.

60. Bao-gen Shen, Fang-wei Wang, Lin-shu Kong, and Leo Cao J. Phys.: Condens. Matter 5, L685, 1993

61. Hu Bo-ping, Li Hong-shuo, Sun Hong, Lawler J. F., and J. M. D. Coey, Solid State Commun. 76, p587, 1991.

62. B. I. Min, J. S. Kang, J. H. Hong, S. W. Jung, J. I. Jeong, Y. P. Lee, S. D. Choi, W. Y. Lee, C. J. Yang, and C. G. Oslon, 6911-6924 J. Phys: Condens. Matter 5, Number 37, 1993.

63. Y. Z. Wang, G. C. Hadjipanayis, and D. J. Sellmyer, Paper SP1, p181, 6th International symposium on Anisotropy and coercivity in Rare Earth Matal Alloys, Ed. S. G. Sankar, Crnegie Mellon Univ. Press, Pittsburgh, Oct. 25, 1990.

64. R. Coehoorn, and G. H. Daalderop J. Magn. Magn. Mat. 1992.

65. M. Q. Huang, L. Y. Zhang, B. M. Ma, Y. Zheng, J. M. Elbicki, W. E. Wallace, and S. G. Sankar, J. Appl. Phys., 70(10), pp 6027-6029, 1991.

66. J. P. Liu, K. Bakker, F. R. de Boer, T. H. Jacobs, D. B. de Mooij, and K. H. J. Buschow, J. Less-Common Metals, 170, 109-19, 1990.

67. Ying-Chang Yang, Xiao-dong Zhang, Lin-Shu Kong, and Qi Pan, Ji-Lian, Yong-Fan Ding, Bai-Sheg Zhang, C-T Ye, and Lan Jin, J. Appl. Phys., 70(10), p6018 -6020, 15 Nov, 1991.

68. R. M. Ibberson, T. H. Jacob, and K. H. J. Buschow, J. Phys.: Condens. Matter 3, 1219-26, 1991.

69. Wang Xiang-Zhong, K. Donnely, J. M. D. Coey, B. Chevalier, , J. Etourneau, and T. Barlureau, J. Mater. Sci. 28, p329, 1988.

70. N. Kamprath, Ph.D. Thesis, City University of New York, 1990.

71. G. Schneider, F. J. G. Landgraph, V. Villas-Boas, G. H. Bezzerra, F.J. Missel, and R. E. Ray, Materials Letters 8, 472, 1989.

72. Hu Bo Jing, J. M. D. Coey. C. J. Cardin, E. J. Devlin, I. R. Harris, J. Less. Comm. Metals 144, L29, 1988.

73. H. H. Stadelmaier, G. Schneider, E.-Th. Henig and Ellner, Matl. Letters 10, 303, 1991.

74. F. J. Cadieu, N. Kamprath, H.Hegde, K. Chen, A. Navarathna, and R.Rani, 35th Magnetism and Magnetic Materials Conference Paper FA-10, 1990, & J. Appl. Phys. 69, 5608, 1991.

75. F. J. Cadieu, H. Hegde, N. Kamprath, K. Chen, A. Navarathna, and R. Rani, Proceedings Sixth International Symposium on Magnetic Anisotropy and Coercivity in RE-TM alloys pp 463-476, Ed. S. G. Sankar, Carnegie Mellon University Press, Pittusburg, October 25, 1990.

76. Y.-C. Yang, X.-D. Zhang, L.-S. Kong, Q. Pan, and S.-L. Ge., Appl. Phys. Lett. 58, 2042, 1991.

77. Y.-C. Yang, Q. Pan, X.-D. Zhang, J. Yang, and M.-H. Zhang, Appl. Phys. Lett. 61, 2723, 1992.

78. F. J. Cadieu, H. Hegde, A. Navarathna, R. Rani, and K. Chen, Appl. Phys. Letters 59, 875, 1991.

79. H. Hegde, R. Rani, A. Navarathna, K. Chen, F. J. Cadieu, J. Appl. Phys. 70, 6345, 1991.

80. Ying-chang Yang, et al., Solid State Commun. 78, 313, 1991.

81. Z.W. Li, X.Z. Zhou, and A.H. Morrish, J. Phys. Condens. Matter 4, 10409, 1992.

82. Qi-nian Qi, Hong Sun, R. Skomski, and J. M. D. Coey, Physical review B 45, number 21, 12278-12286, 1992.

83. R. Rani, H. Hegde, A. Navarathna, F. J. Cadieu, Paper CC-07, 38th Magnetism and Magnetic Materials Conference, Minnesota, November 14-17, 1993. J. Appl. Phys. 75(10), May 15, 1994.